Distance-Based Microfluidic Paper Analytical Devices for Portable, Low-Cost, and Rapid Analyses

by

Mohammad Rahbar
(BSc, MSc)

A thesis submitted in fulfilment of the requirements for the degree of
Doctor of Philosophy

Australian Centre for Research on Separation Science
School of Natural Sciences

University of Tasmania

June 2019

Declaration

This thesis contains no material which has been accepted for a degree or diploma by the University or any other institution, except by way of background information and duly acknowledged in the thesis, and to the best of my knowledge and belief no material previously published or written by another person except where due acknowledgement is made in the text of the thesis, nor does the thesis contain any material that infringes copyright. The publishers of the papers comprising Chapters 2 to 5 hold the copyright for that content, and access to the material should be sought from the respective journals. The remaining non-published content of the thesis may be made available for loan and limited copying and communication in accordance with the Copyright Act 1968.

Mohammad Rahbar

June 2019

Acknowledgements

I would like to express my gratitude toward all who assisted me throughout my PhD with their precious advices and comments. Firstly, I would like to deeply thank all my PhD supervisors Prof. Mirek Macka, Prof. Brett Paull, and Prof. Pavel Nesterenko for all their valuable guidance and continual support. In particular, I'm extremely grateful for Mirek who spent a lot time mentoring me and teaching me how to do fundamental scientific research and also providing me with a remarkable freedom to research and explore new ideas in my own way. Thanks heaps to Brett for always correcting me an keeping me on the right track. I also would like to express my thankfulness for Prof. Aaron Wheeler for all his support, supervision, and feedback while I was working at the Department of Chemistry, University of Toronto as a visiting student in the last year of my PhD. Many thanks to Prof. Michael Breadmore for all his kindness and generous concern. I also appreciate all my colleges and friends during my PhD both in UTAS and U of T for their friendship, assist, and inspiration. Special thanks to ACROSS for providing such an amazing environment to grow and learn. Finally, and most importantly, I'm so grateful for my family (Mom, Dad, and brother) and my cousins for all their support and attention throughout my whole life.

Statement of co-authorship

The following people and institutions have contributed to the publication of work undertaken as a part of this thesis:

Mohammad Rahbar, ACROSS, School of Natural Sciences, UTAS: Candidate

Mirek Macka, ACROSS, School of Natural Sciences, UTAS

Brett Paull, ACROSS, School of Natural Sciences, UTAS

Pavel Nesterenko, ACROSS, School of Natural Sciences, UTAS

Aaron Wheeler, Department of Chemistry, University of Toronto

Author contributions

Paper 1: Rahbar, M., Nesterenko, P. N., Paull, B., & Macka, M. Geometrical alignment of multiple fabrication steps for rapid prototyping of microfluidic paper-based analytical devices. Analytical chemistry, 89(22) (2017) 11918-11923.

Presented in Chapter 2: Candidate was the primary author and performed all the experiments. MM, BP, and PN helped with the formation of the idea, refinement, and presentation.

Paper 2: Rahbar, M., Nesterenko, P. N., Paull, B., & Macka, M. High-throughput deposition of chemical reagents via pen-plotting technique for microfluidic paper-based analytical devices. Analytica chimica acta, 1047 (2019) 115-123.

Presented in Chapter 3: Candidate was the primary author and performed all the experiments. MM, BP, and PN helped with the formation of the idea, refinement, and presentation.

Paper 3: Rahbar, M., Paull, B., & Macka, M. Instrument-free argentometric determination of chloride using trapezoidal distance-based microfluidic paper devices. Analytica chimica acta, 1063 (2019) 1-8.

Presented in Chapter 4: Candidate was the primary author and performed all the experiments. MM and BP helped with the formation of the idea, refinement, and presentation.

Paper 4: Rahbar, M., Macka, M., Wheeler, A. & Paull, B. Ion-Exchange Based Immobilization of Chromogenic Reagents on Microfluidic Paper Analytical Devices. Analytical chemistry (https://doi.org/10.1021/acs.analchem.9b01288).

Presented in Chapter 5: Candidate was the primary author and performed all the experiments. MM, BP, and AW helped with the formation of the idea, refinement, and presentation.

Signed:

Prof. Brett Paull
Supervisor
School of Natural Sciences
University of Tasmania
Date: 20/06/2019

Prof. Mark Hunt
Dean
School of Natural Sciences
University of Tasmania
Date: 24.6.2019

Abstract

The work presented in this thesis describes research towards design, and novel means of fabrication of distance-based microfluidic paper-based analytical devices (µPADs), and development of selected applications for (bio)chemical point-of-care analysis. Chapter 1 provides insights into the principles and evolution of µPADs, particularly those based on the distance-based detection method. Chapter 2 introduces a new facile fabrication technique for (distance-based) µPADs using a low-cost desktop electronic craft plotter/cutter. This simple approach enabled rapid prototyping of µPADs by coupling a wax printer with a plotter/cutter, enabling the desired cutting and reagent deposition steps being performed in a fully integrated and geometrically aligned manner along with the wax-printing step. Chapter 3 extends the development of this fabrication method and further investigates the deposition characteristics and performance of this novel approach, demonstrating its capability for deposition of in-house formulated reagents upon µPADs with various designs, while the deposition volume could be precisely quantified gravimetrically. Chapter 4 demonstrates the effect of the µPAD device geometry on the distance signal obtained from the fabricated distance-based µPADs. It is shown that implementation of asymmetrical geometry microfluidic paper channels (varying width instead of the typical rectangular channels) improved analytical parameters significantly. This is demonstrated with the instrumentation-free determination of chloride via trapezoidal distance-based µPADs from as little as 5 µL sample volume, a key requirement for analysis of chloride in sweat as a basis of diagnosis of cystic fibrosis. In chapter 5, the stable immobilization of chromogenic reagents upon paper, being a significant issue in regard to distance-based detection, is addressed. Herein, anion exchange filter paper is introduced as a new substrate for fabrication of µPADs, providing immobilization of water-soluble anionic reagents upon the paper surface and consequently

allowing the development of distance-based assays without being compromised by the sample fluid washing away effect, otherwise limiting the choice of reagents to only water-insoluble ones. This extends the applicability of the distance-based detection method to assays which involve water-soluble anionic chromogenic reagents, not readily immobilized on the standard filter paper. Finally, Chapter 6 of this thesis discusses the limitations of (distance-based) µPADs and provides further insight and direction for future research.

Table of contents

List of Abbreviations

AAS	Atomic absorption spectroscopy
BSA	Bovine serum albumin
^{o}C	Degree centigrade
3D	Three dimensional
DIC	Digital image colorimetry
DEAE	Diethylaminoethyl
DNA	Deoxyribonucleic Acid
EDTA	Ethylene diamine tetraacetic acid
HRP	Horseradish peroxidase
ICP-MS	Inductively coupled plasma mass spectrometry
IC	Ion chromatography
IE	Ion exchange
GSH	Glutathione
LED	Light-emitting diode
LOC	Lab-on-a-chip
LOQ	Limit of quantitation
LOD	Limit of detection
µPADs	Microfluidic paper-based analytical devices
MW	Molecular weight
µL	Microliter
nL	Nanoliter
pL	Picoliter
POC	Point-of-care
PDMS	Poly(dimethylsiloxane)
PCR	Polymerase chain reactions
PMMA	Poly(methyl methacrylate)
RSD	Relative standard deviation
SEM	Scanning electron microscope
SD	Standard deviation
SERS	Surface-enhanced Raman spectroscopy
STH	Soil-transmitted helminth
UV	Ultraviolet
WHO	World Health Organization

Chapter 1- Introduction to Microfluidic Paper Analytical Devices

1-1- Point-of-care testing

Over the past few decades, the scientific research community has shown extensive interest in the development of point-of-care (POC) testing platforms in order to facilitate traditional (bio)chemical assays, opening new windows toward rapid, portable, low-cost, and real-time analyses. POC platforms also make healthcare, environmental, food, and water safety monitoring accessible and affordable for resource-limited regions by enabling on-site testing and eliminating the need for bulky and expensive bench-top instruments, which usually rely on skilled operators [1,2]. It is obvious that miniaturization is a key point and a significant challenge in the development of POC platforms, so the microfluidics approach has been developed as a viable solution to enable conventional bench-top analyses be performed in a micro-scale format and in a miniaturized manner. This challenge has been addressed in different formats using various materials (e.g. silicon, glass, PDMS, poly(methyl methacrylate) (PMMA), and other polymers) as the base substrates for fabrication of the microfluidic-based analytical devices. Each of these materials presents some particular advantages and disadvantages [3].

In 2007, the Whitesides group expanded the concept of microscale analysis further and introduced microfluidic paper-based analytical devices (µPADs) as a new platform for POC analyses [4]. They demonstrated that the natural capillary-driven fluid flow through the cellulose fibers makes paper a viable alternative to the conventional materials, typically used as substrates for the fabrication of microscale analytical systems, as it eliminates the need for any external pumps or power sources. They used photolithography to create patterned paper

in order to bring the microfluidic feature to the surface of the paper, and applied µPADs to the multiplexed determination of glucose and protein levels in urine samples (Figure 1). Since that initial report, there have been significant efforts directed to the development of µPADs for a variety of applications such as medical, environmental, food, and water analyses.

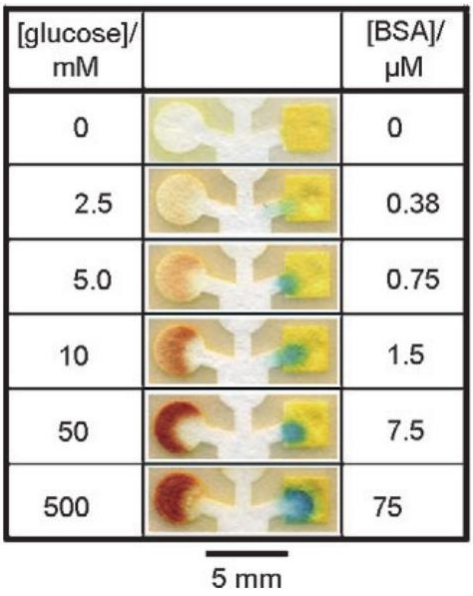

Figure 1. The first reported µPAD demonstrated for the determination of glucose and protein levels in urine sample (Adapted from Ref. [4]).

1-2- Microfluidic paper-based analytical devices

In addition to its common applications, paper, as a low-cost, accessible, and disposable material has been extensively used in (bio)chemical analyses. There are several paper-based analytical devices which have been well established and commercialized such as traditional dipsticks, pH paper, glucose urinary tests, and pregnancy test lateral flow strips. Despite the advantages of these traditional paper devices, they mainly provide a qualitative measurement (i.e. yes or no answer) of the target analyte, typically with poor sensitivity and selectivity [5]. However, the emerging µPADs, using patterned paper as a platform for POC testing, provide semi-quantitative or quantitative measurements in a multiplexed manner, which is a major

strength of these types of POC devices [6]. The existing patterned pathways in µPADs deliver complex (bio)chemical assays, involving various complicated sample-preparation and reaction steps all on one device (e.g. in 3D µPADs), eliminating the need for conventional time-consuming and tedious benchtop-based assay operations [7]. Figure 2 illustrates an example of a µPAD fabricated using patterned paper for the multiplexed determination of different analytes in a single sample [8]. The relatively simple fabrication techniques, and compatibility with a wide variety of detection methods, makes the µPAD a versatile platform for different POC-based applications [7].

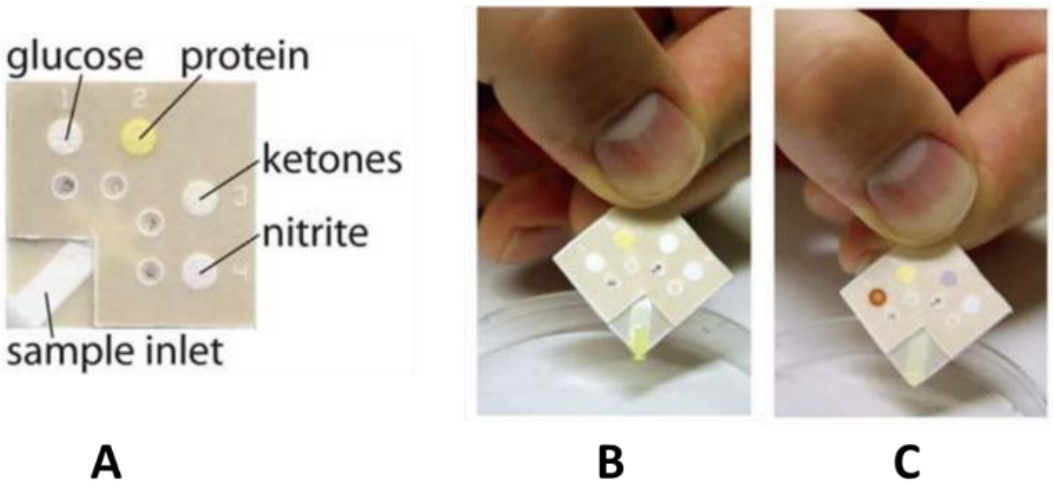

Figure 2. An example of a µPAD programed for the multiplexed determination of different analytes (glucose, protein, ketones, and nitrite) in a urine sample (adapted from Ref. [8]).

1-3- Fabrication

The simplicity of the fabrication process for µPADs is one the most important advantages of these devices, allowing low-cost and easy prototyping with various shapes and forms, targeting a wide variety of applications. In the past decade there have been numerous methods introduced for µPAD fabrication. Despite some differences in detail, all of these methods involve some common steps [10,11]. The primary step is to create hydrophilic microfluidic pathways upon the paper surface in order to direct the sample into the detection

zones. This has been achieved using various techniques; however, wax printing using commercial wax-printers has been the most popular and reliable method in this regard [12]. The desired patterns are designed using computer software and then printed upon the filter paper surface. This is followed by a wax melting step using a hot plate, oven, or hot lamination, causing the wax to penetrate through the thickness of the paper, forming hydrophobic barriers which later will confine the liquid sample inside the hydrophilic paper areas [13]. Figure 3 illustrates the different steps of the wax printing method for producing hydrophobic boundaries on the paper. Some alternative approaches for making hydrophilic channels include laser or craft cutting of paper patterns, and patterning hydrophobic materials upon the paper surface using ink-jet printing, pen-plotting, or screen-printing techniques [12].

Figure 3. Schematic representation of the wax printing method for creating the hydrophobic boundaries (adapted from Ref. [13]).

After creating the hydrophilic zones on the paper, the fabrication process is continued by deposition of the required (bio)chemical reagents (inks) into the hydrophilic areas for further analyses. This deposition has been addressed using different methods, such as manual pipetting, hand drawing with reagent pens, pen-plotting with technical pens, and inkjet printing. Among these methods, inkjet printing has gained the most popularity as it offers good accuracy and reproducibility in terms of the volume (i.e. pL or nL) and shape of the

deposited patterns of the reagents in a high-throughput manner [14,15]. Figure 4A shows a representation of the inkjet printing (deposition) of chemical reagents (inks) inside the detection zones of a µPAD. A photograph of the detection zones of a µPAD printed with chemical inks (yellow color) in various patterns is also shown in Figure 4B. Despite the above-mentioned advantages, the inkjet printing technique presents some drawbacks such as the time-consuming and tedious cleaning of the printhead and cartridges of the printers. In addition, the printheads and cartridges have a very limited shelf life when they are modified and used for chemical ink deposition multiple times. This makes it difficult to use them for rapid and low-cost benchtop prototyping of µPADs.

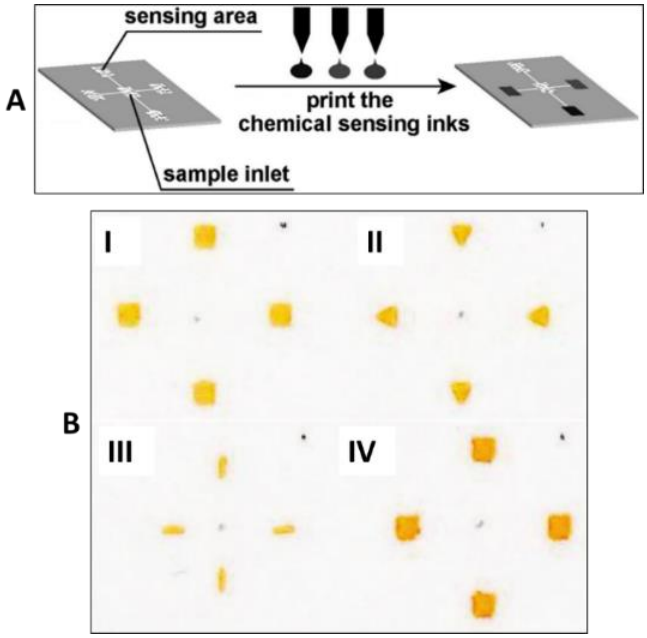

Figure 4. (A) Schematic representation of inkjet deposition of chemical reagents onto µPADs. (B) Photograph showing the detection zones of a µPAD with different geometries printed with chemical inks. (I) Squares (II) Triangles (III) Lines (IV) Triplicate ink amount (compared to I) (Adapted from Ref. [16]).

On occasion the fabrication process requires cuts to be created upon the surface of the paper or protective polymeric layers (e.g. laminating films), which is usually done manually by hand. However, recently there have been several approaches to performing the cuts in a more reproduceable and reliable manner. For example, laser cutters [17] and craft cutters [18] have

been shown to cut the paper with the desired resolution in an automated manner; however, laser cutters are relatively expensive and are not compatible with typical paper wax-printed patterns, causing misalignment issues. Craft cutters also have similar difficulty aligning cuts with wax-printed patterns.

In the final fabrication step, the µPADs are usually laminated in order to prevent sample evaporation and cross contamination, and to provide higher mechanical stability for the fabricated devices [19]. Lamination also protect unstable reagents from direct exposure to ambient air.

1-4- Detection techniques

One of the most important strengths of µPADs, compared to traditional paper test strips, is the capability for semi-quantitative and quantitative signal measurements, using various detection methods such as colorimetric [20], electrochemical [21], chemiluminescent [22], electrochemiluminescent [23], fluorescent methods [24], and surface-enhanced Raman spectroscopy (SERS) [25]. Among these methods, colorimetric detection has been the most widely implemented due to its simplicity, and also its compatibility with conventional imaging devices such as smartphones and desktop scanners [26].

Colorimetric methods are based on the development of a color pattern in the detection zone of the µPAD, resulting from a colorimetric reaction between the analyte present in the applied sample and the chromogenic reagents, which are usually pre-deposited on the paper surface. The generated color pattern is then analyzed in order to quantify the concentration of the target analyte in the tested sample. This analysis is usually performed using digital image colorimetry (DIC) by quantifying the intensity of the color pattern using image-

processing software (e.g. ImageJ) and then correlating the measured intensity to the analyte concentration [27]. Figure 5 illustrates the different steps of the DIC detection method using µPAD-based analyses.

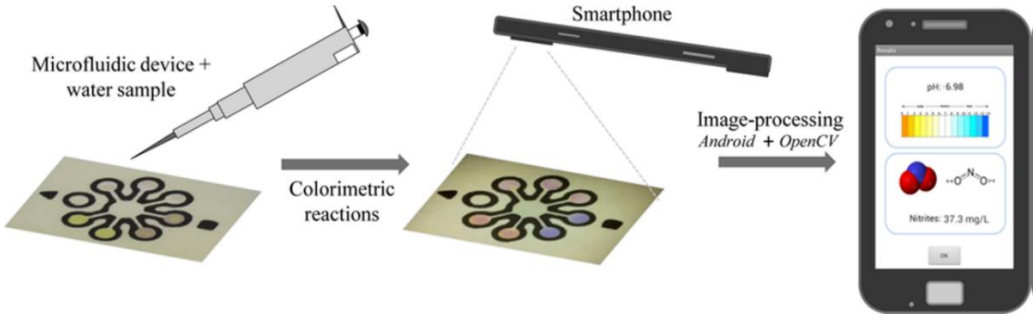

Figure 5. Schematic representation of digital image colorimetry (DIC) for quantitative measurements of analytes using µPADs (Adapted from Ref. [27]).

Beside the DIC-based detection, instrument-free measurements have also been introduced with µPADs, which do not rely on any kind of external reader or detector, enabling equipment-free measurements in a sample-in/answer-out manner [28]. Examples of such instrument-free readout techniques include counting-based, time-based, and distance-based detection methods. In the counting-based method, several detection zones are designed and impregnated with varying concentrations of the corresponding chromogenic reagents which will produce a color change after reacting with the target analyte in the sample [29]. After the reaction is complete, the number of detection zones showing the color pattern can be counted, representing the analyte concentration. Figure 6A shows an example of a counting-based µPAD, developed for instrument-free acid-base titration.

The time-based measurements rely on measuring the amount of time needed to obtain a particular color pattern in the detection zone of the µPAD. The time required to attain the desired color pattern can be correlated to the analyte concentration [30]. Figure 6B illustrates a time-based µPAD, determining the concentration of the target analyte (hydrogen peroxide)

by measuring the time required for the green color development in the detection zone. Both counting-based and time-based detection methods are extremely prone to human error as users are supposed to recognize the formation of a color pattern with a specific hue and intensity and then compare that with standard color charts.

The distance-based detection method, which is the core concept of the present thesis, has been shown to be the most attractive and viable instrument-free detection technique for µPADs [31]. Here the intensity or hue of the developed color pattern is not considered, and instead the length of a colored band formed along a microfluidic detection channel is utilized, which can be measured using a simple scale. This makes reading of the color signal with the naked eye more reliable and easier for end-users, while being less affected by possible human error. The following section will provide more details regarding the distance-based detection technique.

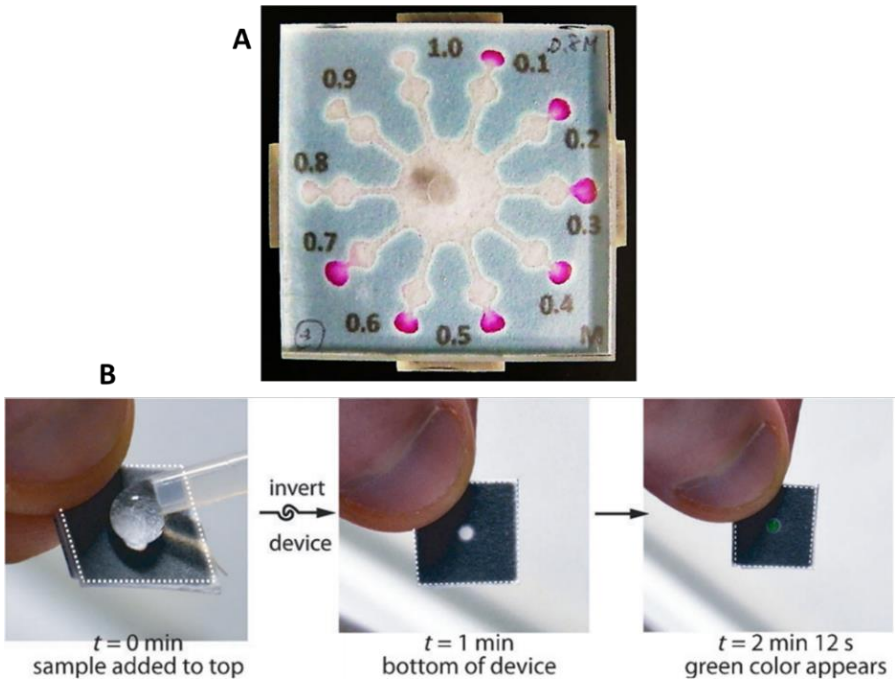

Figure 6. (A) A counting-based µPAD for instrument-free acid-base titration upon paper (Adapted from Ref. [29]). The higher the number of the colored detection circles, the higher the concentration of the analyte. (B) A time-based µPAD for determination of hydrogen

peroxide. The time required for development of the green pattern is correlated to the analyte concentration (Adapted from Ref. [30]).

1-4-1- Distance-based detection

In analytical devices based on a distance-based (length-based) measurement, typically a colored band is generated along the designed detection zones (usually in channel format), the length of which can be correlated to the concentration of the target analyte present in the sample [31]. This concept was initially implemented for POC applications in the 1980s (Figure 7), where an immunoassay was performed on a paper strip impregnated with capture antibodies along with the corresponding chromogenic substrate, resulting in the formation of a colored band after the application of the sample, which contained HRP (horseradish peroxidase)-labeled target analyte [32,33]. The length of the colored band was measured and correlated to the concentration of the target analyte, where the longer the length of the band, the higher the concentration of analyte. This is a simple, straight-forward, rapid, and user-friendly readout approach, especially favorable for POC purposes, which can be implemented for low-cost and on-site (bio)chemical testing. Later, distance-based detection was also employed in different microfluidic platforms such as glass, PDMS, and thread, where the color band formation was based on various principles such as volumetric expansion and stop-flow [31].

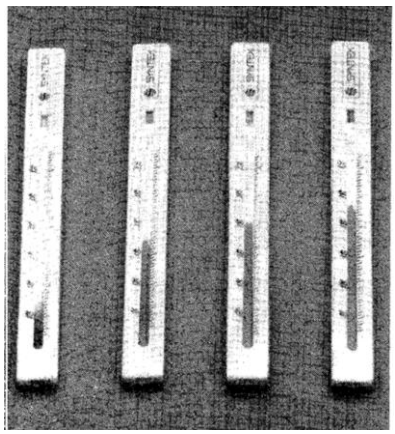

Figure 7. The primary distance-based POC device used for determination of theophylline (Adapted from Ref. [33]).

In 2013, the Henry group brought this concept into the space of µPADs by performing a distance-based measurement upon paper microfluidic channels [34]. They developed distance-based µPADs for the measurement of glucose, nickel, and glutathione (GSH) where colored bands (distance signals) were formed along the paper microfluidic channels representing the analyte concentration. The colored-band formation was based on different mechanisms (Figure 8) such as an enzymatic reaction (for glucose detection), a complexometric reaction (for nickel detection), and an aggregation of nanoparticles (for GSH detection) indicating the applicability of distance-based detection for a wide variety of chemistries. Since this initial report, distance-based µPADs have gained extensive attention and have been developed for the determination of a diverse range of chemical and biological analytes.

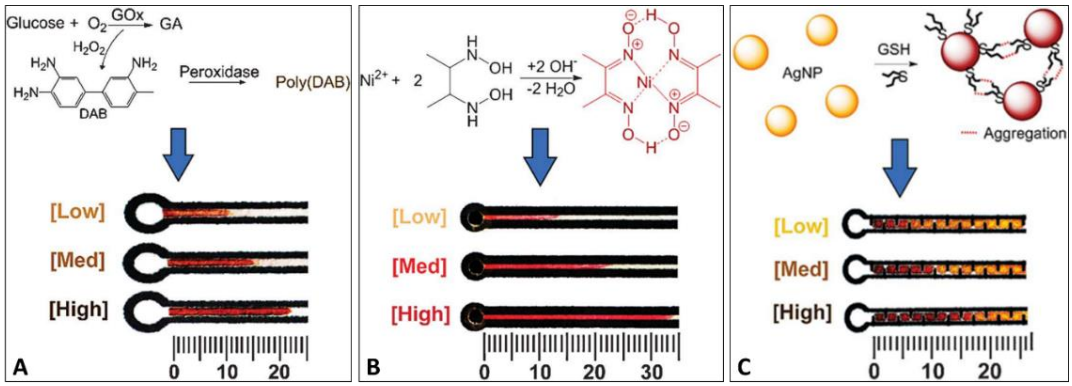

Figure 8. The first reported distance-based µPADs for the determination of (A) glucose, based on an enzymatic reaction, (B) nickel, based on a complexometric reaction, and (C) GSH, based on the aggregation of silver nanoparticles. (Adapted from Ref. [34]).

Distance-based µPADs are typically thermometer shaped and usually consist of a circular sample zone connected to a rectangular detection channel, providing a platform for the formation of a colored band. The chromogenic reagents are deposited (immobilized) over these detection channels, and consequently react with the target analyte present in the

sample loaded into the sample zone, resulting in the formation of a colored band the length of which is proportional to the analyte concentration. Finally, the length of the generated band can be measured simply using a scale (typically printed next to the detection channel) indicating the amount of target analyte. Figure 9 represents the working principle of distance-based µPADs. The key point here is that in order to obtain a stable distance signal, the chromogenic reagents or the colored product of the colorimetric reaction must somehow be immobilized on the surface of the paper in the detection channels. Otherwise, the colored product will be washed away by the sample flowing along the detection channel, preventing the formation of a colored band (distance-signal) on the µPADs [35-40]. This fact limits the applicability of the distance-based detection method to those assays or chemistries involving water-insoluble reagents (or colored products) which will not be eluted by the sample flow, allowing formation of a colored band.

The sample flow is an important parameter in distance-based measurements since the liquid sample is supposed to travel along the detection channel to deliver the target analyte to the reacting sites. In distance-based µPADs, using paper as the substrate for the fabrication of the microfluidic platforms is advantageous as it provides a natural fluid flow based on capillary action, eliminating the need for any external instrument for fluid manipulation.

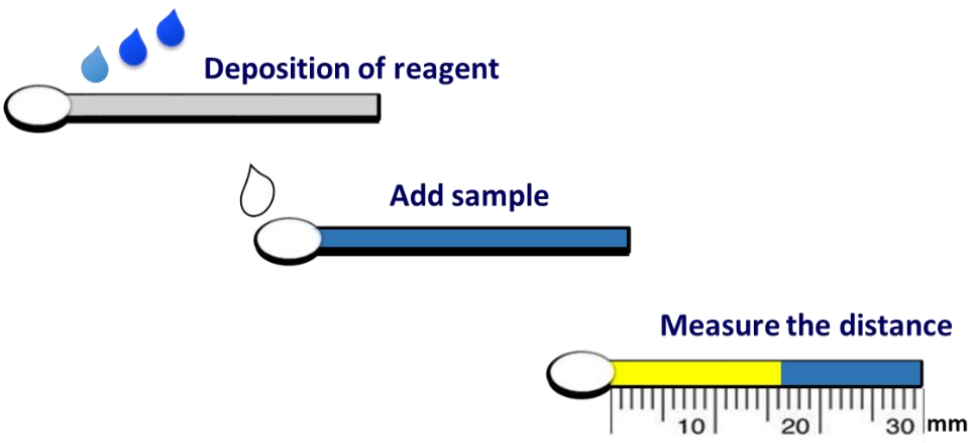

Figure 9. A schematic representation of the working principle of distance-based µPADs.

Henry et al. extended their work on distance-based µPADs by benefiting from another significant strength of µPADs, which is the capability for multiplexed analyses. They demonstrated the instrument-free multiplexed determination of metals using distance-based µPADs where one single device was designed to measure the concentrations of three different metals (Fe, Ni, Cu) in an aliquot of the tested sample [41].

The distance-based method has been also demonstrated for the quantification of other significant analytes in different biological, environmental, food, and water samples (Figure 10). The level of lactoferrin in human tear samples was measured via distance-based µPADs, producing fluorescent distance signals over the detection channels [42]. Here, the microfluidic feature allowed testing tiny volumes of tear samples, as small as 2 µL, which is crucial when it comes to the analysis of analytes in samples of limited volume (e.g. tears, sweat, and plasma). Distance-based µPADs were coupled with a portable solid-phase extraction system for naked-eye on-site measurement of trace amounts of copper in drinking water [43]. A distance-based paper DNA reader was developed for equipment-free quantification of soil-transmitted helminth (STH) infections at the molecular level. Here, the distance-based µPAD detection was integrated with a portable smart-phone-based PCR (polymerase chain reactions) cycler for DNA amplification, providing a POC platform for on-site detection of STH infections — a serious global health issue [44]. In another work, Salmonella — one the most prevalent foodborne bacterial pathogens, was measured using distance-based µPADs incorporating an immunomagnetic separation approach [45]. All these examples indicate the flexibility, compatibility, and integrability of the distance-based detection technique with various external sample treatment systems for a wide variety of applications.

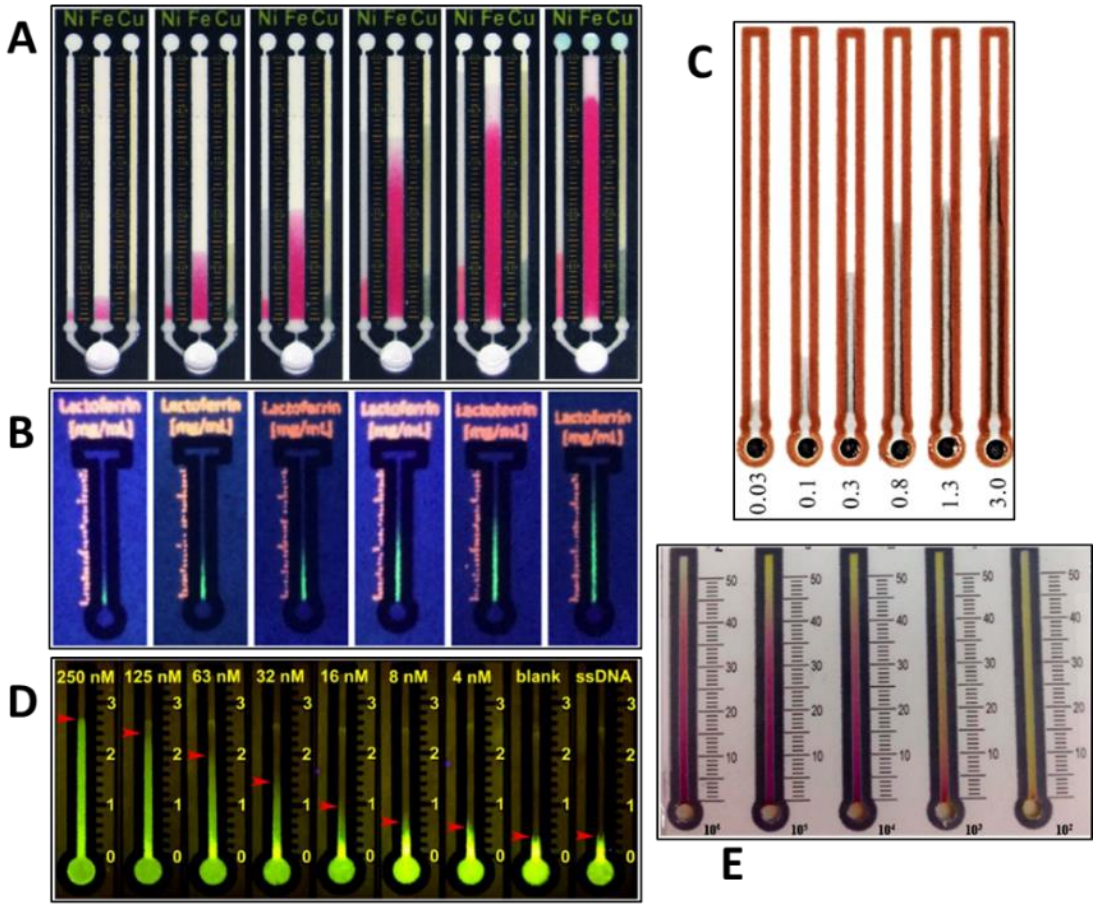

Figure 10. Some examples of distance-based µPADs for the testing of various chemical and biological samples. (A) Multiplexed determination of metals (Fe, Ni, Cu) (Adapted from Ref. [41]). (B) Fluorescent-based determination of lactoferrin in human tears (Adapted from Ref. [42]). (C) Copper detection in drinking waters (Adapted from Ref. [43]). (D) Distance-based DNA reader for measurement of soil-transmitted helminth (STH) (Adapted from Ref. [44]). (E) µPADs for instrument-free determination of foodborne bacterial pathogens (Salmonella) (Adapted from Ref. [45]).

1-5- Conclusions and Aims

In the last decade, the interest in development of µPADs as potential POC platform has grown remarkably, and considerable progress has been made in different aspects of this concept. A diverse range of fabrication and detection methods has been introduced, making µPADs a viable and versatile approach for POC applications, while offering improved sensitivity and selectivity for the operation of various biological and chemical assays [46-49]. Despite the recent advances in µPAD analyses, there are still several challenges and

drawbacks in this field which need to be addressed. One of the main advantages of µPADs claimed over other types of POC devices is the facile fabrication procedure, which has been realized to some extent by implementing a robust and simple wax-printing technique for the creation of the microfluidic features. However, as mentioned earlier, the fabrication process includes some other steps such as chemical deposition and cutting, performed best using inkjet printing and laser cutting, respectively, where both have their limitations. In order to avoid using these methods, the deposition and cutting have been performed easily by manual pipetting and cutting, which then generates reproducibility issues. Thus, there is a lack of a comprehensive, easy-to-perform, low-cost, reliable, and robust fabrication techniques for the rapid prototyping of µPADs. This issue will be addressed in the second and third chapters of this thesis by looking for a novel fabrication approach which can be used for the prototyping of all types of µPADs, particularly those that are distance-based.

In terms of the detection principles, the distance-based detection method is an emerging, attractive, and viable detection approach for µPADs, being capable of the equipment-free determination of a variety of biological and chemical analytes in different medical and environmental samples. In addition, the World Health Organization (WHO) provides some criteria for effective POC devices, which are known by the "ASSURED" acronym, standing for "**a**ffordable, **s**ensitive, **s**pecific, **u**ser-friendly, **r**apid and robust, **e**quipment-free, and **d**eliverable (accessible) to end-users" [50]. Distance-based µPADs meet the majority of these requirements, although the sensitivity and specificity might be a challenge for some particular assays (but this can be improved by implementing some proper optimization strategies). Despite the previously demonstrated advantages of the distance-based detection method, there are still some limitations such as poor sensitivity and also the mentioned sample

washing away effect, limiting its applicability for a wide range of assays. The fourth and fifth chapters of this thesis will study the distance-based detection method further in order to push the boundaries of this practical readout technique for µPAD applications. The fourth chapter will investigate the effect of device geometry on the improvement of the analytical performance (particularly the sensitivity) of distance-based µPADs. The fifth chapter will investigate the immobilization of the water-soluble chromogenic reagents upon the surface of paper, resolving the issue of reagents washing away, and consequently extending the applicability of distance-based detection to a wider range of (bio)chemical assays.

1-6- References

[1] P. Yager, G.J. Domingo, J. Gerdes, Point-of-care diagnostics for global health, Annual Review of Biomedical Engineering, 10 (2008) 107–144.

[2] R.W. Peeling, D. Mabey, Point-of-care tests for diagnosing infections in the developing world, Clinical Microbiology and Infection, 16 (8) (2010) 1062–1069.

[3] P.N. Nge, C.I. Rogers, A.T. Woolley, Advances in microfluidic materials, functions, integration, and applications, Chemical Reviews, 113 (2013) 2550-2583.

[4] A.W. Martinez, S.T. Phillips, M.J. Butte, G.M. Whitesides, Patterned paper as a platform for inexpensive, low-volume, portable bioassays, Angewandte Chemie International Edition, 46 (2007) 1318-1320.

[5] A.K. Yetisen, M.S. Akram, C.R. Lowe, Paper-based microfluidic point-of-care diagnostic devices, Lab on a Chip - Miniaturisation for Chemistry and Biology, 13 (2013) 2210-2251.

[6] D.R. Ballerini, X. Li, W. Shen, Patterned paper and alternative materials as substrates for low-cost microfluidic diagnostics, Microfluidics and Nanofluidics, 13 (2012) 769-787.

[7] D.M. Cate, J.A. Adkins, J. Mettakoonpitak, C.S. Henry, Recent developments in paper-based microfluidic devices, Analytical Chemistry, 87 (2015) 19-41.

[8] A.W. Martinez, S.T. Phillips, Z. Nie, C.M. Cheng, E. Carrilho, B.J. Wiley, G.M. Whitesides, Programmable diagnostic devices made from paper and tape, Lab on a Chip - Miniaturisation for Chemistry and Biology, 10 (2010) 2499-2504.

[9] J. Hu, S. Wang, L. Wang, F. Li, B. Pingguan-Murphy, T.J. Lu, F. Xu, Advances in paper-based point-of-care diagnostics, Biosensors and Bioelectronics, 54 (2014) 585-597.

[10] Y. He, Y. Wu, J.Z. Fu, W.B. Wu, Fabrication of paper-based microfluidic analysis devices: a review, RSC Advances, 5 (2015) 78109-78127.

[11] X. Jiang, Z.H. Fan, Fabrication and Operation of Paper-Based Analytical Devices, Annual Review of Analytical Chemistry, 2016, pp. 203-222.

[12] Y. Xia, J. Si, Z. Li, Fabrication techniques for microfluidic paper-based analytical devices and their applications for biological testing: A review, Biosensors and Bioelectronics, 77 (2016) 774-789.

[13] E. Carrilho, A.W. Martinez, G.M. Whitesides, Understanding wax printing: A simple micropatterning process for paper-based microfluidics, Analytical Chemistry, 81 (2009) 7091-7095.

[14] N. Komuro, S. Takaki, K. Suzuki, D. Citterio, Inkjet printed (bio)chemical sensing devices, Analytical and Bioanalytical Chemistry, 405 (2013) 5785-5805.

[15] K. Yamada, T.G. Henares, K. Suzuki, D. Citterio, Paper-based inkjet-printed microfluidic analytical devices, Angewandte Chemie - International Edition, 54 (2015) 5294-5310.

[16] K. Abe, K. Suzuki, D. Citterio, Inkjet-printed microfluidic multianalyte chemical sensing paper, Analytical Chemistry, 80 (2008) 6928-6934.

[17] M.A. Mahmud, E.J.M. Blondeel, M. Kaddoura, B.D. MacDonald, Creating compact and microscale features in paper-based devices by laser cutting, Analyst, 141 (2016) 6449-6454.

[18] X. Fang, S. Wei, J. Kong, Paper-based microfluidics with high resolution, cut on a glass fiber membrane for bioassays, Lab on a Chip - Miniaturisation for Chemistry and Biology, 14 (2014) 911-915.

[19] L. Ge, J. Yu, S. Ge, M. Yan, Lab-on-paper-based devices using chemiluminescence and electrogenerated chemiluminescence detection, Analytical and Bioanalytical Chemistry, 406 (2014) 5613-5630.

[20] P. Teengam, W. Siangproh, A. Tuantranont, T. Vilaivan, O. Chailapakul, C.S. Henry, Multiplex paper-based colorimetric DNA sensor using pyrrolidinyl peptide nucleic acid-induced AgNPs aggregation for detecting MERS-CoV, MTB, and HPV oligonucleotides, Analytical Chemistry, 89 (2017) 5428-5435.

[21] S. Nantaphol, A.A. Kava, R.B. Channon, T. Kondo, W. Siangproh, O. Chailapakul, C.S. Henry, Janus Electrochemistry: Simultaneous Electrochemical Detection at Multiple Working Conditions in a Paper-based Analytical Device, Analytica Chimica Acta, 1056 (2019) 88-95.

[22] W. Li, S. Ge, S. Wang, M. Yan, L. Ge, J. Yu, Highly sensitive chemiluminescence immunoassay on chitosan membrane modified paper platform using TiO2 nanoparticles/multiwalled carbon nanotubes as label, Luminescence, 28 (2013) 496-502.

[23] W. Li, L. Li, S. Li, X. Wang, M. Li, S. Wang, J. Yu, 3D origami electrochemiluminescence immunodevice based on porous silver-paper electrode and nanoporous silver double-assisted signal amplification, Sensors and Actuators B: Chemical, 188 (2013) 417-424.

[24] Y. Chen, X. Guo, W. Liu, L. Zhang, based fluorometric immunodevice with quantum-dot labeled antibodies for simultaneous detection of carcinoembryonic antigen and prostate specific antigen, Microchimica Acta, 186 (2019) 112.

[25] J. Zhu, Q. Chen, F.Y. Kutsanedzie, M. Yang, Q. Ouyang, H. Jiang, Highly sensitive and label-free determination of thiram residue using surface-enhanced Raman spectroscopy (SERS) coupled with paper-based microfluidics, Analytical Methods, 9 (2017) 6186-6193.

[26] G.G. Morbioli, T. Mazzu-Nascimento, A.M. Stockton, E. Carrilho, Technical aspects and challenges of colorimetric detection with microfluidic paper-based analytical devices (μPADs) - A review, Analytica Chimica Acta, 970 (2017) 1-22.

[27] N. Lopez-Ruiz, V.F. Curto, M.M. Erenas, F. Benito-Lopez, D. Diamond, A.J. Palma, L.F. Capitan-Vallvey, Smartphone-based simultaneous pH and nitrite colorimetric determination for paper microfluidic devices, Analytical Chemistry, 86 (2014) 9554-9562.

[28] Y. Yang, E. Noviana, M.P. Nguyen, B.J. Geiss, D.S. Dandy, C.S. Henry, Paper-Based Microfluidic Devices: Emerging Themes and Applications, Analytical Chemistry, 89 (2017) 71-91.

[29] S. Karita, T. Kaneta, Acid-base titrations using microfluidic paper-based analytical devices, Analytical Chemistry, 86 (2014) 12108-12114.

[30] G.G. Lewis, M.J. DiTucci, S.T. Phillips, Quantifying Analytes in Paper-Based Microfluidic Devices Without Using External Electronic Readers, Angewandte Chemie, 124 (2012) 12879-12882.

[31] T. Tian, J. Li, Y. Song, L. Zhou, Z. Zhu, C.J. Yang, Distance-based microfluidic quantitative detection methods for point-of-care testing, Lab on a Chip, 16 (2016) 1139-1151.

[32] R. Zuk, V. Ginsberg, T. Houts, J. Rabbie, H. Merrick, E. Ullman, M. Fischer, C.C. Sizto, S. Stiso, D. Litman, Enzyme immunochromatography--a quantitative immunoassay requiring no instrumentation, Clinical Chemistry, 31 (1985) 1144-1150.

[33] R. Chen, T.M. Li, H. Merrick, R.F. Parrish, V. Bruno, A. Kwong, C. Stiso, D.J. Litman, An internal clock reaction used in a one-step enzyme immunochromatographic assay of theophylline in whole blood, Clinical Chemistry, 33 (1987) 1521-1525.

[34] D.M. Cate, W. Dungchai, J.C. Cunningham, J. Volckens, C.S. Henry, Simple, distance-based measurement for paper analytical devices, Lab on a Chip - Miniaturisation for Chemistry and Biology, 13 (2013) 2397-2404.

[35] W. Dungchai, Y. Sameenoi, O. Chailapakul, J. Volckens, C.S. Henry, Determination of aerosol oxidative activity using silver nanoparticle aggregation on paper-based analytical devices, Analyst, 138 (2013) 6766-6773.

[36] Y.-T. Chen, J.-T. Yang, Detection of an amphiphilic biosample in a paper microchannel based on length, Biomedical Microdevices, 17 (2015) 1-8.

[37] X. Wei, T. Tian, S. Jia, Z. Zhu, Y. Ma, J. Sun, Z. Lin, C.J. Yang, Target-responsive DNA hydrogel mediated “stop-flow” microfluidic paper-based analytic device for rapid, portable and visual detection of multiple targets, Analytical Chemistry, 87 (2015) 4275-4282.

[38] X. Wei, T. Tian, S. Jia, Z. Zhu, Y. Ma, J. Sun, Z. Lin, C.J. Yang, Microfluidic Distance Readout Sweet Hydrogel Integrated Paper-Based Analytical Device (μDiSH-PAD) for Visual Quantitative Point-of-Care Testing, Analytical Chemistry, 88 (2016) 2345-2352.

[39] Y. Zhang, D. Gao, J. Fan, J. Nie, S. Le, W. Zhu, J. Yang, J. Li, Naked-eye quantitative aptamer-based assay on paper device, Biosensors and Bioelectronics, 78 (2016) 538-546.

[40] R. Pratiwi, M.P. Nguyen, S. Ibrahim, N. Yoshioka, C.S. Henry, D.H. Tjahjono, A selective distance-based paper analytical device for copper (II) determination using a porphyrin derivative, Talanta, 174 (2017) 493-499.

[41] D.M. Cate, S.D. Noblitt, J. Volckens, C.S. Henry, Multiplexed paper analytical device for quantification of metals using distance-based detection, Lab on a Chip - Miniaturisation for Chemistry and Biology, 15 (2015) 2808-2818.

[42] K. Yamada, T.G. Henares, K. Suzuki, D. Citterio, Distance-Based Tear Lactoferrin Assay on Microfluidic Paper Device Using Interfacial Interactions on Surface-Modified Cellulose, ACS Applied Materials and Interfaces, 7 (2015) 24864-24875.

[43] C.W. Quinn, D.M. Cate, D.D. Miller-Lionberg, T. Reilly III, J. Volckens, C.S. Henry, Solid-Phase Extraction Coupled to a Paper-Based Technique for Trace Copper Detection in Drinking Water, Environmental Science & Technology. 52(6) (2018) 3567-3573.

[44] A.G. Wang, T. Dong, H. Mansour, G. Matamoros, A.L. Sanchez, F. Li, Based DNA Reader for Visualized Quantification of Soil-Transmitted Helminth Infections, ACS Sensors, 3 (2018) 205-210.

[45] M. Srisa-Art, K.E. Boehle, B.J. Geiss, C.S. Henry, Highly Sensitive and Rapid Detection of Salmonella typhimurium Using a Colorimetric Paper Based Analytical Device Coupled with Immunomagnetic Separation, Analytical Chemistry, 90(1) (2017) 1035-1043.

[46] M.M. Gong, D. Sinton, Turning the Page: Advancing Paper-Based Microfluidics for Broad Diagnostic Application, Chemical Reviews, 117(12) (2017) 8447-8480.

[47] K. Yamada, H. Shibata, K. Suzuki, D. Citterio, Toward practical application of paper-based microfluidics for medical diagnostics: state-of-the-art and challenges, Lab on a Chip, 17(7) (2017) 1206-1249.

[48] G. Zhu, X. Yin, D. Jin, B. Zhang, Y. An, Y. Gu, Paper-based immunosensors: Current trends in the types and applied detection techniques, TrAC Trends in Analytical Chemistry, 111 (2018) 100-117.

[49] Y. Song, B. Lin, T. Tian, X. Xu, W. Wang, Q.A. Ruan, J. Guo, Z. Zhu, C.J. Yang, Recent Progress in Microfluidics-based Biosensing, Analytical Chemistry, 91(1) (2018) 388-404.

[50] D. Mabey, R.W. Peeling, A. Ustianowski, M.D. Perkins, Tropical infectious diseases: diagnostics for the developing world, Nature Reviews Microbiology, 2 (2004) 231.

Chapter 2- Simple, Rapid, and Low-Cost Prototyping of µPADs, Section 1: Integration of Wax-Printer and Plotter/cutter

This chapter has been published as a research article in “Analytical Chemistry, 89(22) (2017) 11918-11923.” It is produced here with permission of the American Chemical Society.

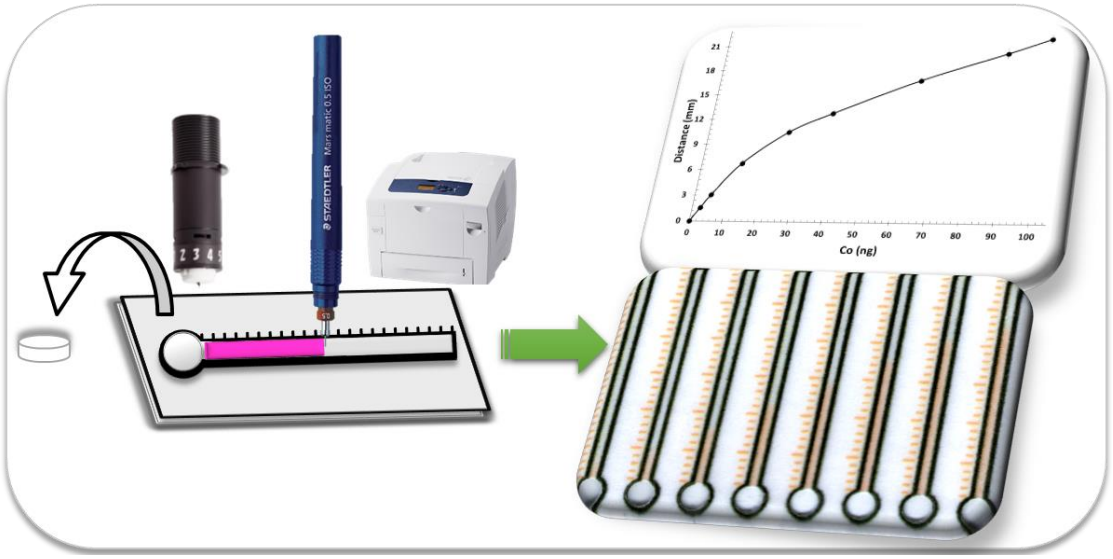

2-1- Overview

Three main fabrication steps for microfluidic paper-based analytical devices (µPADs) were fully integrated with accurate geometrical alignment between the individual steps in a simple and rapid manner. A wax printer for creating hydrophobic barriers was integrated with an inexpensive (ca. $300) electronic craft plotter/cutter for paper cutting, followed by colorimetric reagent deposition using technical pens. The principal shortcoming in the lack of accurate and precise alignment of the features created by these three individual fabrication steps was addressed in this work by developing appropriate alignment procedures during the multistep fabrication process. The wax printing step was geometrically aligned with the following cutting and plotting (deposition) steps in a highly accurate and precise manner using optical scanning function of the plotter/cutter based on registration marks printed on the paper using the wax printer and scanned by the plotter/cutter. The accuracy and precision of alignment in a two-dimensional plane were quantified by cutting and plotting cross shaped features and measuring their center coordinates relative to wax printed reference lines. The average accuracy along the X- and Y-axis was 0.12 mm and 0.16 mm for cutting, and 0.19 mm and 0.17 mm for plotting, respectively. The potential of this approach was demonstrated by fabricating µPADs for instrument-free determination of cobalt in waters using distance-based readout, with excellent precision (%RSD = 5.7) and detection limit (LOD) of 2.5 ng and 0.5 mg/L (mass and concentration LODs, respectively).

2-2- Introduction

In the last decade, microfluidic paper-based analytical devices (µPADs) have gained attention due to their unique advantages of low-cost, ultimate portability, ease of use, and disposal. µPADs are easy-to-use miniaturized analytical devices which are simply fabricated by demarcating defined hydrophilic channels on paper by creating hydrophobic barriers using wax printing or other techniques. The channels then guide liquids such as sample moving by capillary forces, to react with particular chemical reagents deposited into detection zones [1,2].

In spite of all the advances, fabrication of µPADs still have some limitations. For instance, fabrication methods are still either tedious or can pose challenges in relation to their facile and reproducible fabrication. These impediments hinder the advance of µPADs in broad areas of analytical chemistry. So far, many varieties of µPADs with different designs and applications have been reported fabricated by different methods [3]. These fabrication methods have several (usually three) main steps including creating confined hydrophilic patterns on paper, cutting the required shapes and areas, and deposition of colorimetric reagents on the paper [4,5]. Each of these steps is usually realized with different techniques. Thus, for creating hydrophilic patterns, several methods have been reported including wax printing, paper cutting and shaping, ink stamping, laser treatment, photolithography, and plotting [4,5]. Among those various methods, wax printing has been most widely used due to its inherent advantages of low-cost, simplicity, easy and rapid fabrication (only one heating step is needed after printing), and suitability for mass production [6].

The cutting step has also been accomplished by different devices such as handheld cutters, handheld punchers, laser cutters, and electronic craft cutters [4]. We reported cutting using an electronic craft cutter equipped with standard blades, which offered much more reproducible fabrication compared to hand cutting, and less costly compared to laser cutting [7]. When it comes to reagent deposition, a few methods have been used for this purpose, including pipetting, brushing, inkjet printing, dipping, and spraying [8]. We reported deposition of colorimetric reagents on paper using technical pens in an electronic craft plotter/cutter showing great promise due to automated and reproducible deposition [7]. The use of the craft plotter/cutters in fabrication process of microfluidic devices has increased recently, which is due to the low-cost, flexibility, automated deposition, and simplicity of these instruments. It should be noted that in most of the reported works [9-16] only the cutting feature of the plotter/cutters has been implemented rather than the plotting. In other words, the craft plotter/cutter has been used to perform very simple cuts upon the paper, vinyl, or other materials without particular demands on precision. The plotting feature has been used only a few times so far for creating hydrophobic barriers on paper by deposition of inks filled in special pens [4,7,17].

As the three major fabrication tools, namely wax printing, plotting and cutting with a plotter/cutter, offer different advantages, they could be used together for fabrication of µPADs based upon their combined use. However, there is no comprehensive method comprising all these three steps accomplished in a simple, low-cost, flexible, reproducible, and rapid way, and importantly, accurately geometrically aligned. In other words, at least one of these three main steps is usually done either by hand or other unreliable ways, which impact the reproducibility and robustness of the whole fabrication process and affects the

final results. The paper media has to be moved from one instrument to the next one during the fabrication process which makes it difficult to keep the features fabricated in different steps precisely geometrically aligned.

In this work we show for the first time that a combination of wax printing for making fluidic barriers, digital craft cutter for cutting, and also plotting with the technical pens for reagent deposition, can be accurately aligned to provide a low-cost, simple, rapid, reproducible, and comprehensive fabrication method for prototyping of µPADs. Further, we show that the geometrical alignment of this combination of different fabrication steps can be assured by utilizing an optical scanner function of the plotter/cutter. The accuracy and precision of the alignment (deviation in coordinates of fabricated features from theoretical coordinates) were quantified using purposely designed fabrication experiments. As for an analytical demonstration of the developed fabrication method, distance-based µPADs were designed, fabricated and implemented for instrument-free determination of cobalt in water samples, which in itself presents a novel analytical use of µPADs as quantitative determination of cobalt using µPADs has not been reported.

2-3- Experimental section

2-3-1- Chemicals and materials

All chemicals were of analytical reagent grade. Citric acid monohydrate, 1-nitroso-2-naphthol, sodium phosphate dibasic dihydrate, rhodamine 6G, and ethylenediaminetetraacetic acid (EDTA) disodium salt dihydrate were purchased from Sigma-Aldrich. Standard Co(II) solutions were produced by diluting a stock solution of 1000 mg/L of the nitrate salt of the element supplied by Sigma-Aldrich. Water was treated with a Millipore

(Bedford, MA, USA) Milli-Q water purification system. Whatman grade 1 qualitative filter paper with a pore size of 11 µm and thickness of 180 µm (GE Healthcare Australia Pty. Ltd, NSW, Australia) was used to fabricate the µPADs. Transparent laminating film (thickness of 125 µm, GBC, NSW, Australia) was used to laminate the µPADs.

2-3-2- Fabrication of the distance-based µPADs

As shown in Figure S-1, the distance-based microfluidic patterns composed of a straight channel (1.9 × 29 mm) and a circular sample zone (3.7 mm outer diameter) along with scale bars (drawn at 1.0 mm intervals next to the channel for naked eye measurement of the color change length) were pre-designed using the Silhouette Studio® software (Figure S-2) and printed on paper by the wax printer. The patterns were printed on both sides of the paper to let the wax penetrate throughout the paper thickness from two sides (top and bottom) after the heating step to prevent any leakage of the sample from the µPADs [6,21]. After that, the sheet was loaded on the adhesive surface of a reusable cutting mat and was placed on the plotter/cutter for cutting out the sample zone as a circular hole in the paper of diameter 3 mm. In the next step, the technical pens were filled with the colorimetric reagents and then inserted in the plotter/cutter to deposit the reagents on the straight channels. Afterward, the sheet was laminated from both sides to give a higher mechanical stability to the final µPAD and also to prevent contamination of the detection areas. Circles (diameter = 4 mm) were cut out in the top lamination film (before lamination) by the same cutting as where the filter paper was cut out for introducing sample. The lamination was performed at a temperature of 165 °C to melt the wax entirely through the thickness of the paper to create consistent hydrophobic barriers. Finally, the fabricated µPADs were cut into separate segments with

desired sizes using the same cutting system and stored for further use in a sealed plastic bag. Figure S-3 represents the paper media undergoing different fabrication steps.

2-4- Results and discussion

2-4-1- Alignment of multiple fabrication steps

The here presented alignment of multiple fabrication method for prototyping of µPADs was composed of three main steps including wax printing of the hydrophobic barriers, cutting out the sample zone and deposition of the colorimetric reagents (Figure 1). As the wax printing was performed by the wax printer while the other two steps were accomplished by the plotter/cutter, it was crucial to keep all the three steps aligned. These two separate devices have different working principles which make it difficult to couple them during the multiple fabrication steps, while keeping all these steps geometrically aligned. Specifically, for fabrication of the distance-based µPADs, it was essential to perform the cutting and deposition precisely, since we were dealing with very small dimensions during the cutting (circles, inner diameter = 3.3 mm) and the deposition (narrow channels, inner width = 1.4 mm) steps (Figure S-4). Thus, any misalignment could lead to the cutting or reagent deposition outside of the desired areas. In addition, each of these functions had to be replicated in high numbers (e.g. 170 times for 170 µPADs printed on an A4 size paper) for minimal consumption of paper, as desirable in the case of mass production.

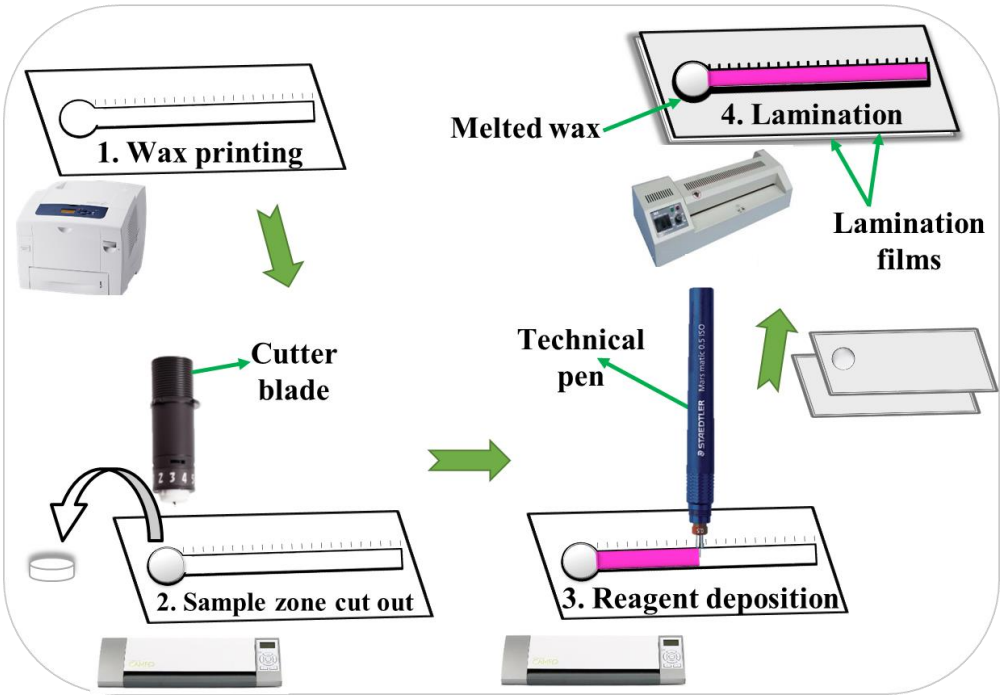

Figure 1. Schematic illustration of the overall fabrication process with geometrically aligned steps for distance-based µPADs.

2-4-2- Optical scanner and "Registration Marks"

The working principle of the plotter/cutter is based on electromechanically driven movements along the X/Y-axes defined by the device (Figure S-5). It is obvious that the X/Y-based operation of the machine cannot be reliable enough for such challenging tasks demanding accurate alignment while transferring the paper media from one instrument (wax printer) to another one (plotter/cutter). Fortunately, the latest models of plotter/cutters such as the Silhouette CAMEO possess an optical scanning feature which is available for highly accurate and precise cutting or plotting, but does not however appear to have been used to date for fabricating µPADs or in fact any research purpose. Under normal conditions, the optical scanner is deactivated so the machine will function merely based on the X/Y-axes, as explained earlier. However, there is an option in the Silhouette Studio software called "Registration Marks" which can be selected while designing the microfluidic patterns and this is how the scanner function can be activated. These marks are some default patterns which

would be printed on the paper media around the workspace border and later will be read by the optical scanner (Figure S-6). Then according to the location of the marks, the software can triangulate the exact position of the lines which are already defined to be cut or plotted. In other words, we can have a very precise control over the performance of the plotter/cutter and so can instruct the instrument to do a task exactly at the locations where desired. Activating the optical scanner by using the "Registration Marks" in the design was the most important action regarding the alignment issue although there were still some other necessary actions and considerations (explained in further details in Supplementary Information) which should be taken into account. By applying the optical scanning function along with all those considerations, we could manage to perform the cutting and deposition with a high accuracy and precision in good alignment with the wax printed features. The overall cutting and deposition steps in fabrication of distance–based µPADs, are demonstrated in the Supplementary Information Movies S1 and S2, respectively.

2-4-3- Accuracy and precision of the alignment

To demonstrate the reliability of the new method for fabrication of µPADs, the alignment accuracy of the wax printer with plotter/cutter was investigated. A graphical pattern similar to a simple two-dimensional coordinate system was designed with the Silhouette Studio software to simulate a fabrication process of µPADs. As shown in Figure 2A, this pattern is composed of two reference lines (black lines, X/Y-axes, 40×40 mm) perpendicular to each other, which were designed to be printed by the wax printer. There are also crosses in this pattern on all four possible areas of a plane which were supposed to be cut (gray color, 3×3 mm) and plotted (pink color, 5×5 mm) by the plotter/cutter. After performing all these three steps, we measured the coordinates (i.e. centers) of the cut and plotted crosses. The distance

of the experimental coordinates from the reference lines compared to the pre-designed (theoretical) values provided a numerical representation of the accuracy and precision of the alignment and compatibility of the wax printer with the plotter/cutter. The cutting coordinates (e.g. $C_2(x_2, -y_2)$ in Figure 2A) were measured using a distance-calibrated microscope since the cut lines made by the blade were narrow enough resulting in obvious centers for each cross. The x and y values for each coordinate were obtained by measuring the distance between the centers and the edge of corresponding reference lines (printed X or Y-axis). However, for the plotted crosses we had to determine the center point of cross sections of relatively wide lines. To find out the plotting coordinates (e.g. $P_1(-x_1, y_1)$ in Figure 2A), we used a simple equation (eq S1) to compensate for the distance which the ink penetrates into the paper. Further details in this regard can be found in Supplementary Information.

The graph depicted in Figure 2B was obtained from the pre-designed pattern undergoing those three steps one after another (n = 8). The black lines (× shape) in this plot are the expected values for cutting and deposition performances. Gray dots are the cutting and the pink dots are the deposition coordinates obtained after performing either of these steps. All the measured coordinates are well located on the expected lines indicating a highly accurate whole process. Numerical values for the slight deviations of the measured coordinates from the theoretical ones represent the accuracy. The average of these values for 16 coordinates (n = 8) was reported as overall accuracy, which was calculated to be 0.12 mm and 0.16 mm for cutting, and 0.19 mm and 0.17 mm for plotting, along the X- and Y-axis, respectively. The fabrication precision as an average standard deviation of individual coordinates was also reported separately along the X- and Y-axes, representing the overall precision of the cutting

and deposition process (Table 1). Since the number of repetitions for obtaining each coordinate was the same (n = 8), this average can be regarded as a reliable estimation of the overall standard deviation. As anticipated, the standard deviation along the Y-axis was almost two times more than that along the X-axis for both cutting and deposition steps. This is to be expected due to the fact that the Y-axis is defined by the movement of the whole media via the twisting pinch rollers which can cause some minor drifting during operation. However, the X-axis is the result of movement of the pen holder (media is static) over a rail which is likely to be more consistent. These results show that the proposed idea of integrating the wax printer with the plotter/cutter as described in this paper is reliable, highly accurate and can be implemented for a variety of applications including prototyping of miniaturized analytical devices such as µPADs.

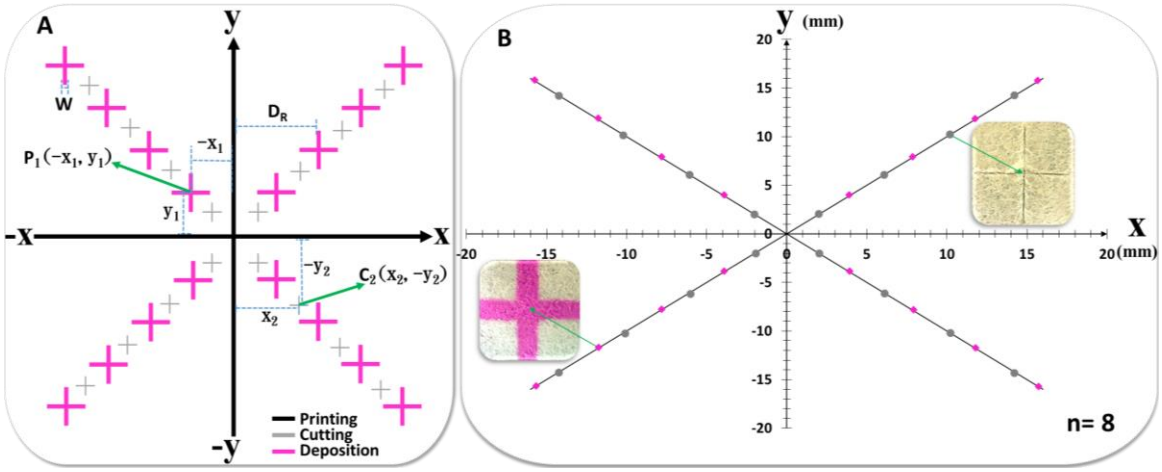

Figure 2. Accuracy and precision of geometrical alignment in multiple fabrication steps. (A) Graphical pattern simulating different fabrication steps of µPADs, where the black lines ((+), reference lines, X/Y-axes) represent the wax printing step, gray crosses (+) represent the cutting step, and pink crosses (+) represent the deposition step. D_R is the distance measured by microscope between the edge of plotted lines and the edge of corresponding reference lines, and W is the width of plotted lines. (B) Experimentally determined coordinates of the cut and plotted crosses obtained from the pre-designed pattern undergoing (n = 8) the corresponding fabrication steps, where the black lines (× shape) are the expected values for cutting and deposition performances, (●) cutting, and (◆) deposition coordinates (e.g. C_2 and P_1 in Figure 2A) obtained after performing either of these steps. Insets are the actual photographs of cut and plotted crosses. For detailed description of the coordinate determination procedures see Supplementary Information.

Table 1. Accuracy and precision values for alignment of the cut and plotted crosses performed by the plotter/cutter relative to the wax printed reference lines

Alignment factors (mm)	Cutting	Deposition
Accuracy X-axis	0.12	0.19
Accuracy Y-axis	0.16	0.17
[a]S X-axis	0.04	0.05
S Y-axis	0.08	0.12

[a]S is average of standard deviations.

2-4-4- Distance-based determination of cobalt in waters

In the distance-based measurement, the sample moves forward through straight microfluidic channels and reacts with the deposited colorimetric reagent resulting in a color change that is observed as a boundary between the reagent alone and the reagent reacted with the analyte [18]. The length of the color change to that boundary can be related to the concentration of the analyte present in the sample. It has been demonstrated that the distance-based µPADs have the potential to be applied for portable, instrument-free and rapid analysis of a variety of analytes [19-24]. Cobalt is one of the inorganic contaminants the determination of which in natural waters is very important since its excess can cause some serious health problems for humans, animals, plants, and microorganisms [25,26]. According to the Australian and New Zealand guidelines for fresh and marine water quality, the concentration of cobalt in irrigation waters should not be more than 0.1 mg/L (short-term use) or 0.05 mg/L (long-term use) [27]. Conventional analytical methods for determination of cobalt are costly and time-consuming, and they also need complex equipment and trained operators which are not suitable for on-site analysis [28]. However, the distance-based µPADs

can be applied for rapid, low-cost, instrument-free, and portable analysis of the water samples.

The developed distance-based µPADs fabricated by this facile method were successfully applied for instrument-free quantification of cobalt in water samples using 1 nitroso-2 naphthol as the metallochromic ligand. The detection chemistry is detailed in the Supplementary Information. Determination of standard solutions of Co was investigated in the range of 2.5-100 ng (0.5-20 mg/L) and the calibration curves were obtained using different distances of color change formed on the µPADs for various concentrations of analytes. The detection limit (LOD), which in distance-based µPADs is considered as the lowest distinguishable length [20] (usually 0.5 mm) of color change along the channel, was 2.5 ng and 0.5 mg/L of Co as mass and concentration LODs, respectively.

In this work, the unnecessary paper area of the sample zone was cut out (Figure S-7) to improve analytical parameters such as sensitivity and LOD, based on rationale as follows. Even though paper is conventionally considered as a neutral material, but the overall surface charge of the cellulose is negative due to the presence of the carboxyl groups formed by the addition of oxidative reagents to the fibers during papermaking process. The surface of paper will acquire a relatively low cation-exchange capacity and can retain metal cations through the electrostatic interactions [29,30]. Therefore, a portion of the analyte can be adsorbed on the surface of the paper normally available at the sample zone of other µPADs without even reaching to the detection area. This issue will be more considerable when very low concentrations of the metals are being monitored. Removing the sample zone has also been reported in very few previous works [20,21] with µPADs while the cutting was done by handheld punching which is not suited for high throughput fabrication and of limited

reproducibility. Here we performed this job in a very simple and rapid way with very high precision and speed. This concept was further investigated by comparing two different types of µPADs (with and without cutting the sample zone) for determination of cobalt (Figure S-8). As expected, the µPADs without paper in the sample zone exhibited a lower LOD as well as a lower RSD value, and higher sensitivity for detection of cobalt. These results show the importance of sample zone cutting.

Figure 3 represents the performance of the µPADs and associated response curves for detection of Co, after introducing 5 µL of standard samples into the inlets of the devices. As illustrated in the corresponding figures, these results represent excellent reproducibility as noted by the standard deviations and error bars. The effect of possible interferences on determination of cobalt was also investigated by applying water samples containing Co (5 ppm) and different metal ions (Al, Ca, Cu, Fe, Mg, Mn, Ni, K, Na, Pb, and Zn) in Co:metal ratio of 1:1. Under these conditions, the co-existing metals did not have any significant impact on the distance of the color band formed. As a validation study of the distance-based µPADs, some irrigation water samples were collected (Scottsdale, Tasmania, Australia) and spiked with known concentration (5 ppm) of standard Co solution and then analyzed both with the µPADs and atomic absorption spectroscopy (AAS). The results obtained from both these techniques (Table S-1) were in a very good agreement (within 10 % error). On the other hand, the non-spiked water samples (blank) did not produce any distance signal on the µPADs which showed these samples were at levels below LOD of the target metal. These results were confirmed by the AAS analysis, where the concentrations of the metals in blanks were measured to be at trace levels (≈ 5 ppb) which were below the LOD of the µPADs.

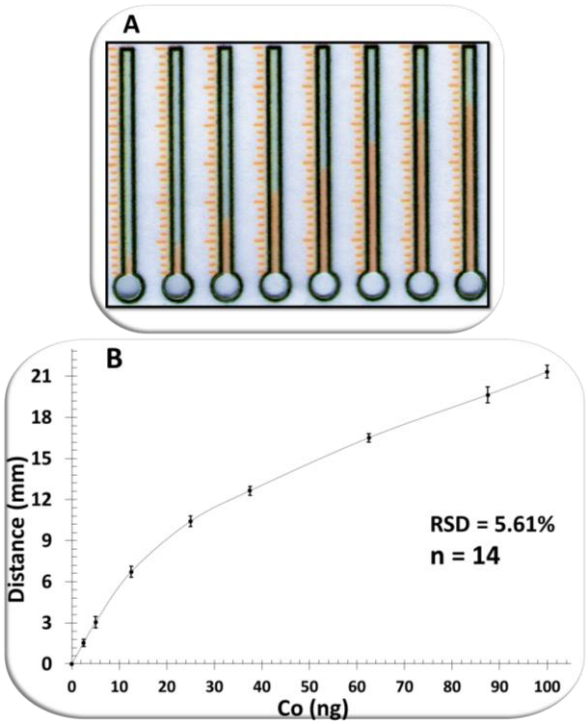

Figure 3. (A) Photograph of distance-based µPADs after pipetting 5 µL of Co standard solutions. Contrast and brightness are modified for the sake of better observation. (B) Response curve of different concentrations (2.5-100 ng) of Co to distance-based µPADs. Markers reflect the average of 14 repetitive measurements. The error bars represent the standard deviations from the average values.

2-5- Conclusions

Several fabrication steps of µPADs can be integrated in a simple manner by coupling a wax printer and an electronic craft plotter/cutter. Wax printing as the most popular technique for creating hydrophobic barriers for µPADs is performed by a wax printer and then followed by the cutting and deposition steps done by the plotter/cutter. Optical scanning function of the plotter/cutter is used to assure the geometrical alignment of the multiple fabrication steps. The accuracy and precision of alignment of wax printing relative to cutting and plotting could be quantified in purposely designed fabrication experiments measuring coordinates of cut and plotted cross-shaped features. Cutting and deposition can be fully automated and be done exactly inside the user-selected spots minimizing misalignment issues and allowing a computerized fabrication process. This approach is illustrated by fabrication of distance-

based µPADs which need high precision for cutting and deposition steps. The RSD (5.61%) obtained for determination of cobalt in water samples, indicates the high reliability of this method for fabrication of µPADs. The newly developed method can be readily implemented for rapid, low-cost, simple, robust, and reproducible prototyping of different types of µPADs which include multiple steps (e.g. wax printing, cutting, and deposition). However, the fabrication process does not necessarily have to include the combination of steps in a particular order such as here (Figure 1). In other words, any order of these steps can be performed in an equally aligned manner for various applications. For instance, integration of only two steps from the three shown in this work can be used either separately or along with other possible techniques in fabrication of µPADs or other types of miniaturized analytical devices.

2-6- References

[1] D.M. Cate, J.A. Adkins, J. Mettakoonpitak, C.S. Henry, Recent developments in paper-based microfluidic devices, Analytical Chemistry, 87 (2015) 19-41.

[2] N.A. Meredith, C. Quinn, D.M. Cate, T.H. Reilly, J. Volckens, C.S. Henry, Paper-based analytical devices for environmental analysis, Analyst, 141 (2016) 1874-1887.

[3] Y. Yang, E. Noviana, M.P. Nguyen, B.J. Geiss, D.S. Dandy, C.S. Henry, Paper-Based Microfluidic Devices: Emerging Themes and Applications, Analytical Chemistry, 89 (2017) 71-91.

[4] Y. He, Y. Wu, J.Z. Fu, W.B. Wu, Fabrication of paper-based microfluidic analysis devices: a review, RSC Advances, 5 (2015) 78109-78127.

[5] Y. Xia, J. Si, Z. Li, Fabrication techniques for microfluidic paper-based analytical devices and their applications for biological testing: A review, Biosensors and Bioelectronics, 77 (2016) 774-789.

[6] K. Tenda, R. Ota, K. Yamada, T.G. Henares, K. Suzuki, D. Citterio, High-resolution microfluidic paper-based analytical devices for sub-microliter sample analysis, Micromachines, 7 (2016) 80.

[7] N. Nuchtavorn, M. Macka, A novel highly flexible, simple, rapid and low-cost fabrication tool for paper-based microfluidic devices (μPADs) using technical drawing pens and in-house formulated aqueous inks, Analytica Chimica Acta, 919 (2016) 70-77.

[8] K. Yamada, T.G. Henares, K. Suzuki, D. Citterio, Paper-based inkjet-printed microfluidic analytical devices, Angewandte Chemie - International Edition, 54 (2015) 5294-5310.

[9] R.A.G. de Oliveira, F. Camargo, N.C. Pesquero, R.C. Faria, A simple method to produce 2D and 3D microfluidic paper-based analytical devices for clinical analysis, Analytica Chimica Acta, 957 (2017) 40-46.

[10] A.C. Glavan, R.V. Martinez, E.J. Maxwell, A.B. Subramaniam, R.M. Nunes, S. Soh, G.M. Whitesides, Rapid fabrication of pressure-driven open-channel microfluidic devices in omniphobic RF paper, Lab on a Chip, 13 (2013) 2922-2930.

[11] E.T.S.G. Da Silva, M. Santhiago, F.R. De Souza, W.K.T. Coltro, L.T. Kubota, Triboelectric effect as a new strategy for sealing and controlling the flow in paper-based devices, Lab on a Chip - Miniaturisation for Chemistry and Biology, 15 (2015) 1651-1655.

[12] Y. Koo, V.N. Shanov, Y. Yun, Carbon Nanotube Paper-Based Electroanalytical Devices, Micromachines, 7 (2016) 72.

[13] D. T. Phan, S.A.M. Shaegh, C. Yang, N.-T. Nguyen, Sample concentration in a microfluidic paper-based analytical device using ion concentration polarization, Sensors and Actuators B: Chemical, 222 (2016) 735-740.

[14] A.S. Afonso, C.V. Uliana, D.H. Martucci, R.C. Faria, Simple and rapid fabrication of disposable carbon-based electrochemical cells using an electronic craft cutter for sensor and biosensor applications, Talanta, 146 (2016) 381-387.

[15] S. Oyola-Reynoso, A.P. Heim, J. Halbertsma-Black, C. Zhao, I.D. Tevis, S. Çınar, R. Cademartiri, X. Liu, J.-F. Bloch, M.M. Thuo, Draw your assay: Fabrication of low-cost paper-based diagnostic and multi-well test zones by drawing on a paper, Talanta, 144 (2015) 289-293.

[16] W.Y. Li, Z.Z. Shi, C. Fang, Y. Lu, L. Yu, C.M. Li, Integration of paper and micropipette tip to build a “sample-in, answer-out” point-of-care device, Microfluidics and Nanofluidics, 21 (2017).

[17] R. Amin, F. Ghaderinezhad, L. Li, E. Lepowsky, B. Yenilmez, S. Knowlton, S. Tasoglu, Continuous-Ink, Multiplexed Pen-Plotter Approach for Low-Cost, High-Throughput Fabrication of Paper-Based Microfluidics, Analytical Chemistry, 89(12) (2017) 6351-6357.

[18] T. Tian, J. Li, Y. Song, L. Zhou, Z. Zhu, C.J. Yang, Distance-based microfluidic quantitative detection methods for point-of-care testing, Lab on a Chip, 16 (2016) 1139-1151.

[19] D.M. Cate, W. Dungchai, J.C. Cunningham, J. Volckens, C.S. Henry, Simple, distance-based measurement for paper analytical devices, Lab on a Chip - Miniaturisation for Chemistry and Biology, 13 (2013) 2397-2404.

[20] D.M. Cate, S.D. Noblitt, J. Volckens, C.S. Henry, Multiplexed paper analytical device for quantification of metals using distance-based detection, Lab on a Chip - Miniaturisation for Chemistry and Biology, 15 (2015) 2808-2818.

[21] R. Pratiwi, M.P. Nguyen, S. Ibrahim, N. Yoshioka, C.S. Henry, D.H. Tjahjono, A selective distance-based paper analytical device for copper (II) determination using a porphyrin derivative, Talanta, 174 (2017) 493-499.

[22] K. Yamada, T.G. Henares, K. Suzuki, D. Citterio, Distance-Based Tear Lactoferrin Assay on Microfluidic Paper Device Using Interfacial Interactions on Surface-Modified Cellulose, ACS Applied Materials and Interfaces, 7 (2015) 24864-24875.

[23] X. Wei, T. Tian, S. Jia, Z. Zhu, Y. Ma, J. Sun, Z. Lin, C.J. Yang, Microfluidic Distance Readout Sweet Hydrogel Integrated Paper-Based Analytical Device (μDiSH-PAD) for Visual Quantitative Point-of-Care Testing, Analytical Chemistry, 88 (2016) 2345-2352.

[24] Y. Zhang, D. Gao, J. Fan, J. Nie, S. Le, W. Zhu, J. Yang, J. Li, Naked-eye quantitative aptamer-based assay on paper device, Biosensors and Bioelectronics, 78 (2016) 538-546.

[25] Sarkar, B. Heavy metals in the environment, CRC Press, 2002.

[26] Underwood, E. Trace elements in human and animal nutri-tion, 4th ed.; Elsevier, 2012.

[27] ANZECC, ARMCANZ. (Australian and New Zealand Envi-ronmental and Conservation Council, Agriculture and Resource Management Council of Australia and New Zealand,

Canberra) Aus-tralian and New Zealand guidelines for fresh and marine water quality. no. 4. Volume 3, Chapter 9, 2000.

[28] Safavi, A.; Abdollahi, H.; Nezhad, M. H.; Kamali, R. Spectrochim. Acta, Part A 2004, 60, 2897-2901.

[29] Barbosa, L. C., Maltha, C. R., Demuner, A. J., Cazal, C. M., Reis, E. L., & Colodette, J. L.. A rapid method for quantification of carboxyl groups in cellulose pulp. BioResources, 8(1) (2013) 1043-1054.

[30] Murphy, A., B. Gorey, K. De Guzman, N. Kelly, E. P. Nesterenko, and A. Morrin, Microfluidic paper analytical device for the chromatographic separation of ascorbic acid and dopamine." RSC Advances, 5 (2015) 93162-93169.

2-7- Supplementary information for chapter 2

2-7-1- Instrumentation

A wax printer (Colorqube 8870, Xerox, Norwalk, CT, USA) was used to print the microfluidic patterns on paper. A desktop electronic craft plotter/cutter (Silhouette CAMEO®, Kuluin, QLD, Australia) connected via a USB cable was implemented for the cutting and deposition steps. The cutting was done by the Silhouette replacement cutting blade (SILH-BLADE-3) which can be inserted in the pen holder of the plotter/cutter and be adjusted for cutting different substrates with various thicknesses. The deposition was performed using Mars®matic 700 technical pens (STAEDTLER Mars GmbH & Co. KG, Nuernberg, Germany, line width= 0.5 mm) filled with colorimetric reagents. Silhouette Studio® free software was used to design the microfluidic patterns for the µPADs and also for manipulation of both the wax printer and the plotter/cutter. Silhouette Cameo reusable cutting mat (12"X12" Cut12) was used for proper loading of the paper media in the plotter/cutter machine with high precision. An A3 laminator (LM330, Laminating Wholesalers, VIC, Australia) with adjustable lamination temperature was used to laminate the devices from both sides. Dino-Lite EDGE digital microscope (AM4115T-GFBW, SCINET, WA, Australia) with a magnification range of 20x-220x and controlled by DinoCapture 2.0 software was used for all required measurements.

2-7-2- Further experimental details for alignment of the fabrication steps

In addition to the optical scanning function which was explained earlier, some other actions were also found to be important in assuring optimal alignment of the fabrication steps including using a compound graphical design for operating of the plotter/cutter, calibration of the plotter/cutter prior to use, proper loading of the paper media into both the wax printer

and Cameo plotter/cutter, and precise cutting of the paper media to the desired sizes (A4, A5, etc.). Each of these steps is explained in further details in the next sections.

2-7-2-1- Media cutting

Accurate and reproducible cutting of the paper media in desired sizes (A4, A5, etc.) is very important for alignment of the fabrication steps. The filter paper sheet was inserted into the plotter/cutter machine and papers with exact sizes were pre-cut for further usage. The same procedure was used to cut the laminating films in required sizes. The optimum sharpness level of the blade was 1 for paper and 5 for laminating film which was adjusted using the blade ratchet prior to cutting. The optimum sharpness level should be set in the software as well. A blade ratchet was used to adjust the sharpness of the blade to the optimum level for cutting either the paper or the laminating film. If the blade sharpness level is too high, the cutting mat beneath the paper media will be cut as well and, consequently, the blade might get obstructed while swiveling in the paper to cut out the circular sample zone.

2-7-2-2- Compound graphical design for operating of the plotter/cutter

One of the main advantages of the wax printers is their flexibility in terms of being compatible with most of the computer graphics editor programs, including the Silhouette Studio®, a vector-based software operating the Cameo plotter/cutter. Using one single software for manipulation of both the wax printer and the plotter/cutter prevents any possible misalignment likely occurring if using different software for each instrument. Additionally, using the compound graphical design is very helpful in minimizing any possible misalignment, since all the required graphical patterns are integrated into one single design instead of having separate designs for each fabrication step. One of the most important

features of the Silhouette Studio® software is that it enables us to select which part of a compound graphical design to be sent either to the wax printer or plotter/cutter. Here we used elaborate compound graphical designs (Figure 2A and Figure S-1) composed of three different parts including the printing pattern, cutting line and deposition line without any need for separate designs for each step. The line width of the printing patterns was set by the software to be 0.4 mm which will be increased after wax melting step. However, the line width of the cutting or deposition line was set on 0 mm which caused the printer not to be able to read them while doing the printing step. The plotter/cutter can recognize all lines with any width (even 0 mm) and perform the cutting or plotting on them. Thus, the cutting and deposition lines were not printed and were used only to manipulate the plotter/cutter. An image of the workspace of the software showing the compound graphical designs used for fabrication of distance-based µPADs, is depicted in Figure S-2. In the computer designing step, all either the cutting or deposition lines were grouped together to facilitate the operation of plotter/cutter machine during the fabrication process. The grouped lines could be easily selected, put in "Cut" mode, and sent to the Silhouette for further corresponding either cutting or deposition actions while the rest of the design was kept in "No Cut" mode. The desired patterns should be inside the area defined by the registration marks and anything outside the area will result in further misalignment issues.

The same cutting procedure was also used to cut out the circles (4 mm) in the top lamination films to create the holes for introducing sample to the µPADs (Figure S-7). In order to cut the holes on the lamination film, from the mentioned compound design used for fabrication of distance-based µPADs (Figure S-1), only the cutting lines where copied into another separate file, ungrouped and then were only enlarged (3 mm to 4 mm) without changing the position

of the circles. Then they were grouped again and sent to the cutter to cut out the circles on the film. After preforming the cutting on the lamination film, the cut circles were aligned (observed by the optical microscope) with the circles already cut on the filter paper. Moreover, as explained in the previous section, prior to cutting the sample inlets, both the paper media and lamination film were cut precisely and reproducibly in desired sizes (A4, A5, etc.) with the plotter/cutter which further contributes to precise alignment of these two media. Therefore, simply by placing the cut lamination film on top of the filter paper matching the edges of the paper and lamination film, the circles from these two separate layers are precisely matched.

2-7-2-3- Media loading

The proper loading of the media into both the wax printer and plotter/cutter is another important point which should be taken into account. Firstly, the filter paper which was already cut exactly into the desired sizes was fed into wax printer through the manual feed tray. After printing, it is very important not to make any further adjustments to the designed patterns in the software workspace since any alteration will result in cutting or plotting on the wrong place. After patterning the hydrophobic lines on both sides, the paper had to be replaced and be introduced to the plotter/cutter for the cutting and deposition steps. The standard replacement cutting mat was used for accurate introduction of the paper media into Cameo machine and also to avoid any kind of drifting during the cutting operation. Additionally, the proper cutting mat (Cameo 12"X12") and also the correct page size should be selected in design page settings window of the software. The other very important point here was that the page settings be set exactly the same for both the printing and cutting steps. Thus, in the page setting window, the “Current Printer” option was selected as the page size. The paper

media was precisely placed and lined up on the sticky side of the mat and then the mat was placed exactly next to the last left guideline (Figure S-5) on the machine. The pinch rollers (Figure S-5) in the machine also need to be aligned correctly to grip the paper media tightly during the cutting process. Since here a standard Cameo mat was used, the pinch rollers were adjusted to be all the way out as the default settings. The “Load Mat” button on the machine was pressed to feed in the mat. The blade and pen should also be inserted into the machine in the correct way. The blades were inserted into the machine’s default pen holder but for the technical pens, a standard pen holder (Silhouette, PEN-HOLDER2-3T) was used to keep the pens firm during the deposition process.

2-7-2-4- Calibration of the plotter/cutter

Calibrating the Cameo prior to the cutting/plotting was crucial since we were using the registration marks to perform an accurate “Print & Cut” job. Firstly, the calibration test page was printed using the wax printer without any extra adjustment and then the paper media was introduced into the machine with careful loading (as explained in the previous section). Later, the standard blade was used to test the performance of the machine. The required adjustments were done according to how far the cut was performed from the expected lines. The detailed Information about the calibration procedure can be found in Silhouette Studio® user’s manual [1].

2-7-3- Coordinate determination of the center points of plotted crosses

We used eq S1 to figure out the plotting coordinates (i.e. center of plotted crosses in Figure 2B),

$$D_M = D_R + \left(\frac{W}{2}\right) \qquad (S1)$$

Where D_M is the final measured distance for each coordinate (i.e., x or y value), D_R is the distance read by microscope between the edge of plotted lines and the edge of corresponding reference lines, and W is the width of plotted lines. The W value (line width = 645±0.04 μm) was the average of line widths measured at one random point along the plotted lines (128 points) and the low standard deviation indicates that this average value can be reliably considered as the width of all plotted lines. The detailed information about microscopic measurements of line widths is given in the following sections.

2-7-4- Cobalt detection

Determination of cobalt was carried out using a 0.3% solution of 1-nitroso-2-naphthol (NN) in ethanol (%50) which gives a colored complex with cobalt in a pH range (4-5) where there is a minimum of interference from other metals. Normally in aqueous solutions, the formed complex of Co(III)-NN is a stable reddish-brown precipitate. In this reaction the reagent functions as an oxidizing agent which converts Co(II) to Co(III). Some metals such as Cu(II), Fe(II), Fe(III), and Ni(II) also give an insoluble precipitate with this reagent and may interfere with the cobalt test. However, by adjusting the pH and also using proper masking agents, the interferences can be reduced. The buffer-masking solution composed of citric acid-phosphate buffer (citric acid 0.2 M and sodium phosphate 0.4 M) and EDTA (0.3 M) with the mixed ratio of 7:3, was deposited on the straight channels using the technical pens. After drying, the NN reagent solution was deposited on the channels for further analysis. The amount of colorimetric reagents and buffer-masking solutions deposited on the channels were optimized (by changing the reagent concentration) to create the best color contrast while the

lowest possible LOD can also be achieved. In order to further improve the LOD, µPADs with narrower detection channels or lower concentration of the deposited reagent might be helpful. The deposition line (Figure S-1) was intentionally designed to be shorter (28 mm) than the length of the microfluidic channel (29 mm) to prevent any possible penetration of the colorimetric reagent into the sample zone during the deposition step. In other words, the deposition was done starting from the end of the channel and ending to a point which was 1 mm above the sample zone. The overall time of analysis from the introduction of the sample until the arrival of the sample front to the end of the channels, was about twenty-five minutes.

2-7-5- Microscopic measurements

Dino-Lite EDGE digital microscope has the capability of switching the light source from blue LED (has a 510nm emission filter) to the white LED. All the measurements were done using the white LED of the microscope while the blue LED was switched off. DinoCapture 2.0 software has some practical features which allow measurement of a variety of shapes and areas with a high accuracy and precision. When it comes to the line width, the edges of the plotted lines in micro scale are not smooth enough along the lines to be detected by naked eyes. However, we used a useful feature in the software namely “Auto Distance Measurement” (Figure S-9), which can be used to detect edges of the plotted lines. This feature allows us to create a detection path by setting the edge detection criteria (R, G, B color threshold in the range of 0-255) where the line widths can be easily determined [2].

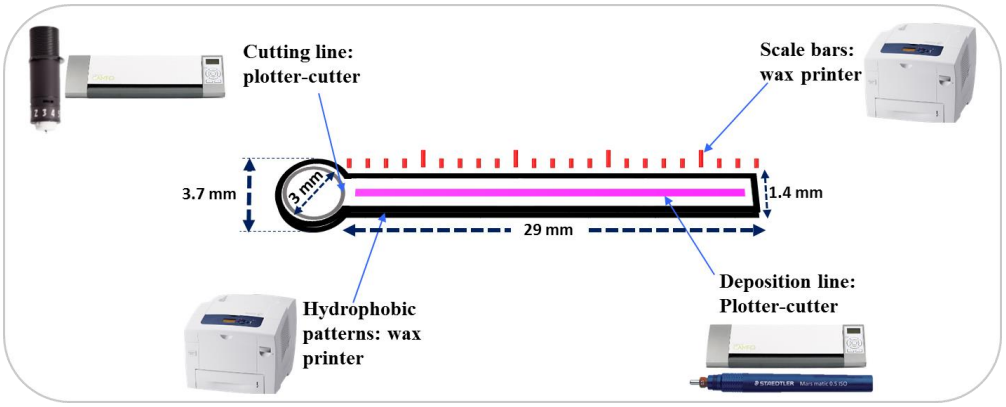

Figure S-1. Compound graphical design for manipulation of plotter/cutter. The outline of a single microfluidic pattern with the corresponding dimensions is also presented. Obviously, these dimensions represent the computer designs which will be widened after the heating step and melting of the wax. The size of both the sample zone and the channels were optimized for the storage of the least volume of sample (5 µL), and at the same time having a stable fluid flow and obvious color change.

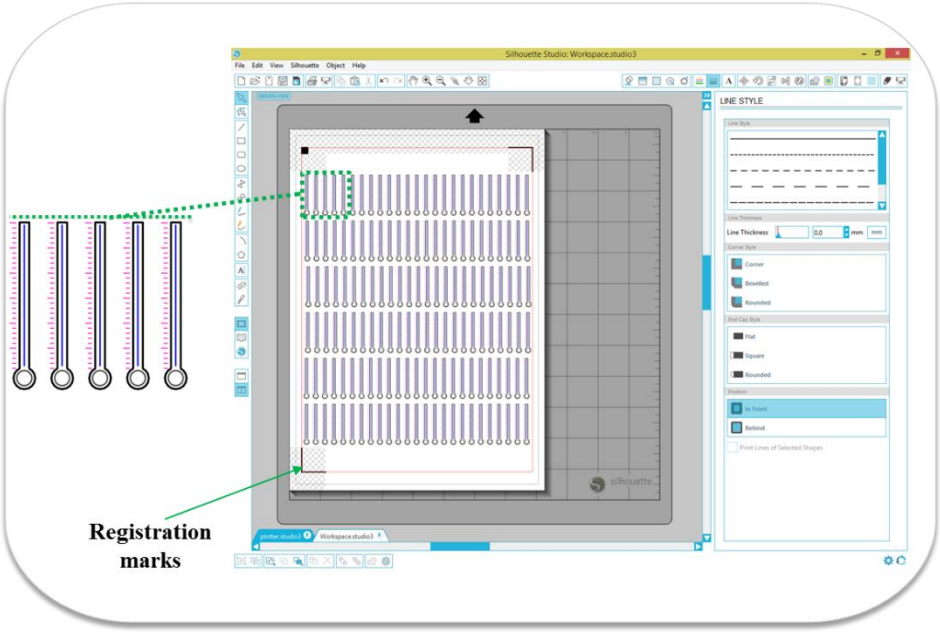

Figure S-2. Workspace of the Silhouette Studio® software showing the designed distance-based µPADs' graphical patterns. The "registration marks" are also indicated around the borders of the workspace.

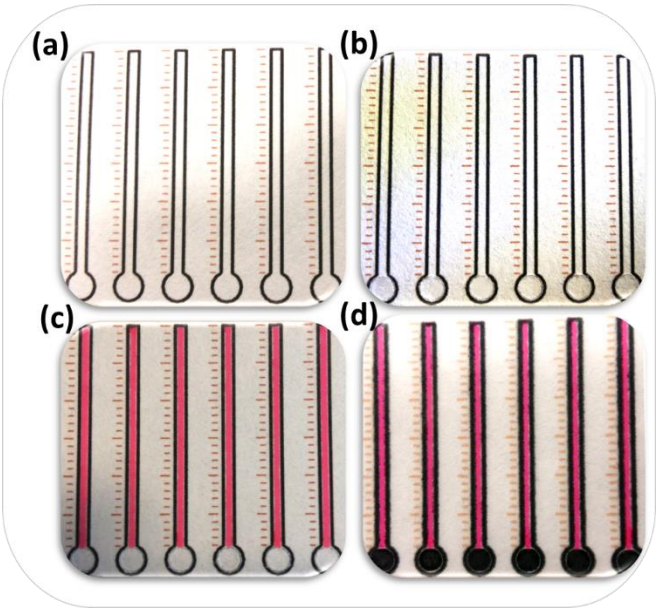

Figure S-3. Demonstration of the paper media undergoing four different stages of the fabrication process. (a) Wax printing of microfluidic patterns. (b) Sample zone cutting. (c) Reagent deposition. (d) Lamination and wax melting.

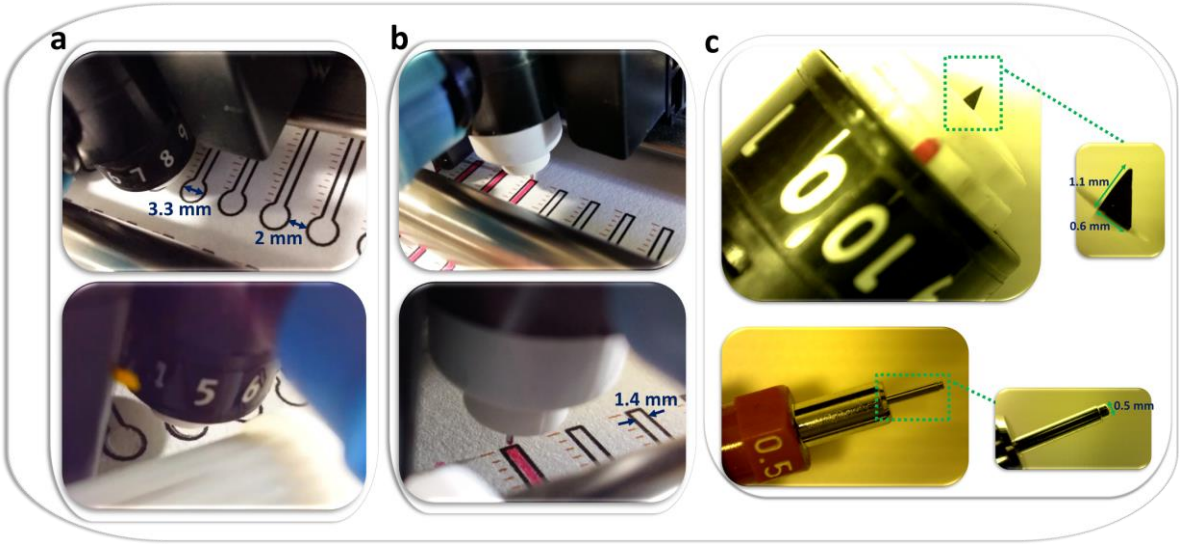

Figure S-4. Dimensions of the desired (A) cutting, and (B) deposition areas on the paper in comparison to the (C) blade and pen tip sizes. The cutting and deposition steps are geometrically aligned with the printed features.

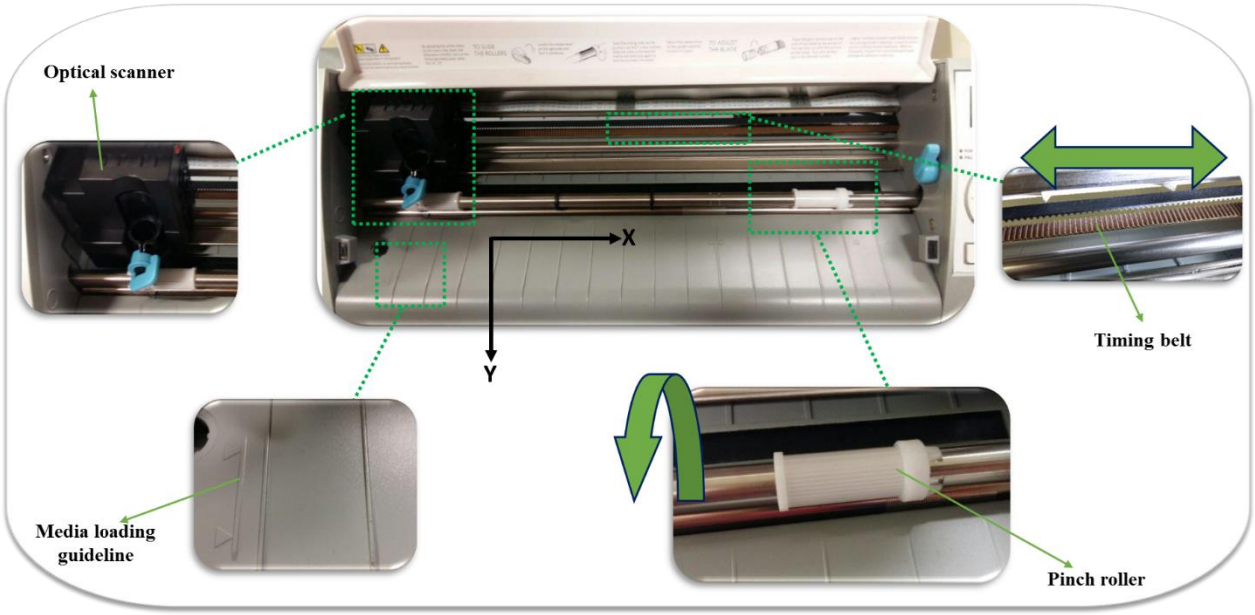

Figure S-5. Front view of the Silhouette Cameo plotter/cutter. Different parts of the machine including optical scanner, loading guideline, timing belt, and pinch rollers are depicted. The X-axis is defined by movement of the blade or pen holder on the rail with the timing belt and the Y-axis is defined by twisting pinch rollers which can feed in and out the paper media. Green arrows indicate the moving direction of the corresponding parts.

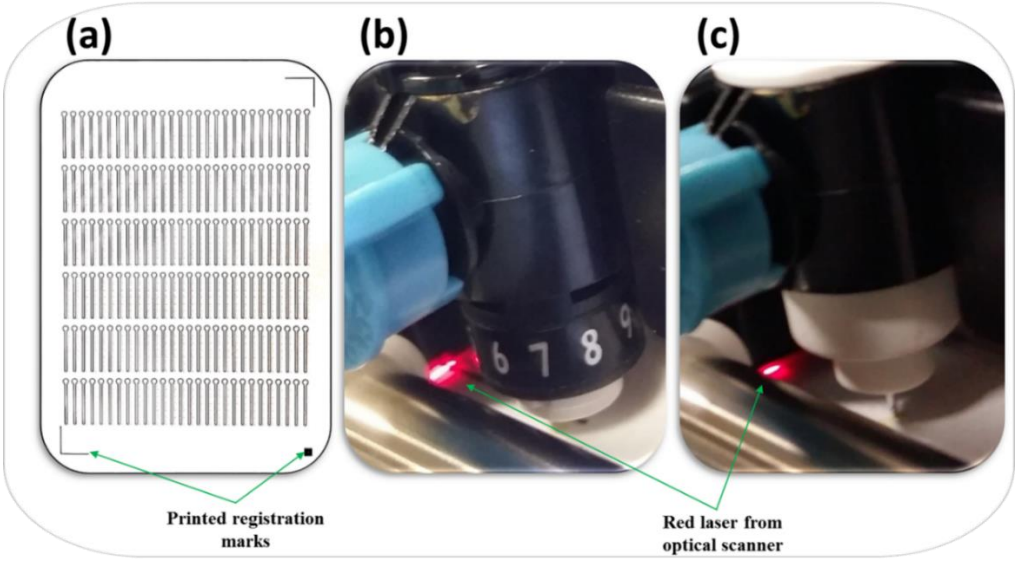

Figure S-6. Registration marks and optical scanner. (a) Microfluidic patterns along with the registration marks printed on an A4 size paper sheet. Optical scanner detecting the registration marks before (b) cutting, and (c) plotting. These marks will not be cut or plotted during the cutting or plotting steps and they are only to aid the Cameo with locating the cutting or plotting lines.

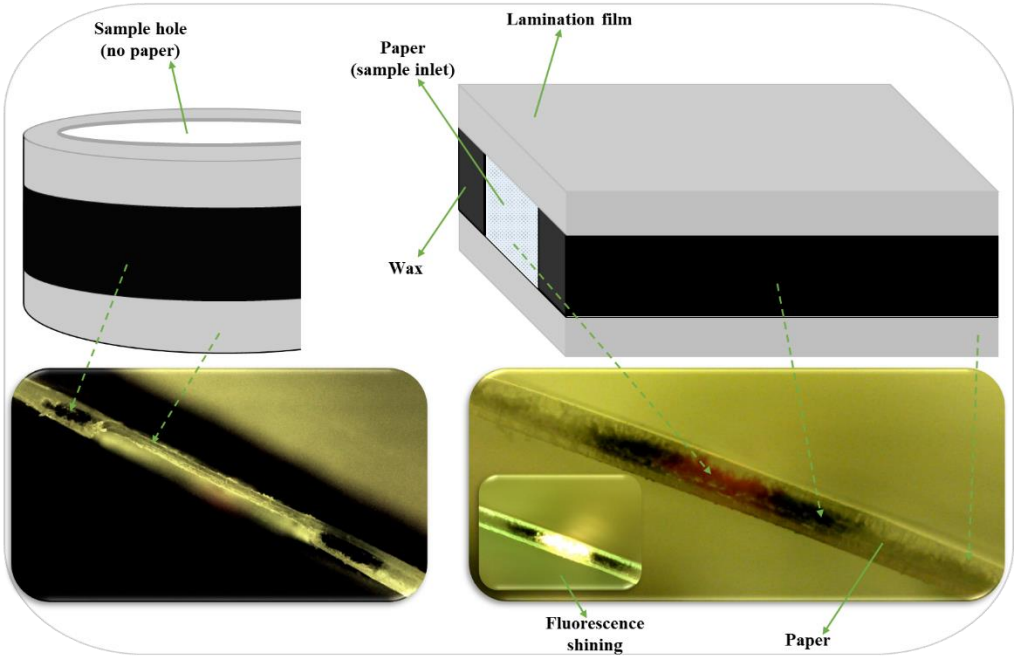

Figure S-7. Demonstration of the sample zone and sample inlet configuration after cutting out the paper from that area. There is no paper (sample hole) in the sample zone after cutting. The rectangle shape inlet is the only source of sample for the detection channel which allows a more uniform flow pattern. Photographs also show the cross-sectional view of the sample zone and inlet; no paper in the sample zone but the paper contained fluorescent dye (rhodamine 6G) in the sample inlet is indicated after illumination by the microscope (blue LEDs on).

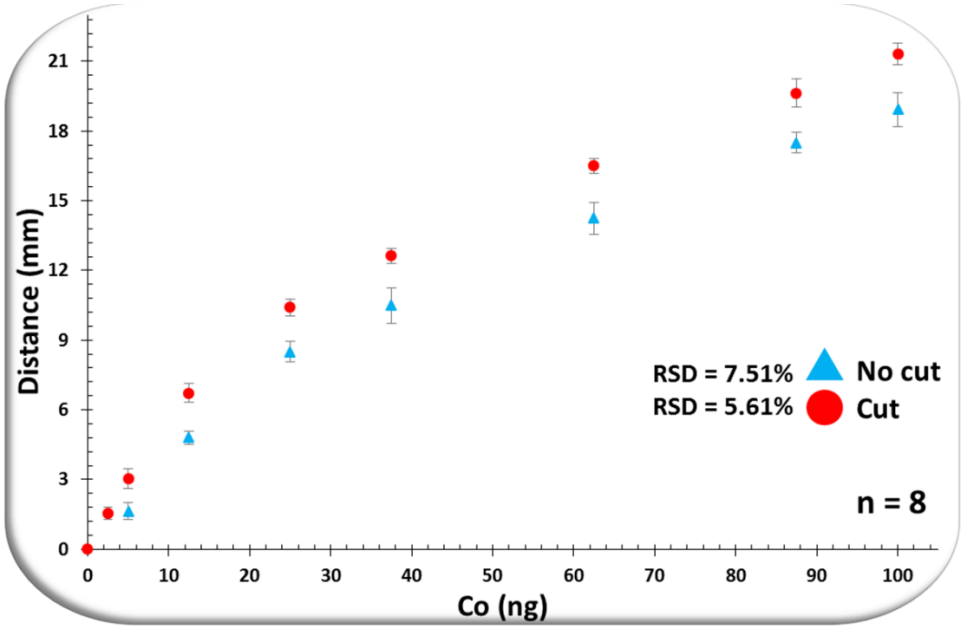

Figure S-8. Effect of paper available in the sample zone in determination of cobalt. Cutting out the sample zone (●) improves analytical parameters including detection limit (i.e. from 5 ng (no cut) to 2.5 ng (cut)), sensitivity, and also RSD compared to un-cut paper (▲). We associate the better RSD with the fact that in the case of µPADs with cut sample zone at the inlet of the µPAD active area, the sample enters the active area of the µPAD with a sharper boundary (Figure S-7) thus resulting in a more uniform flow pattern and more reproducible determination with lower RSD values. In addition, the already mentioned electrostatic interactions between any residual anionic sites of the paper and the metal cation can affect the reproducibility of the distance-based signal.

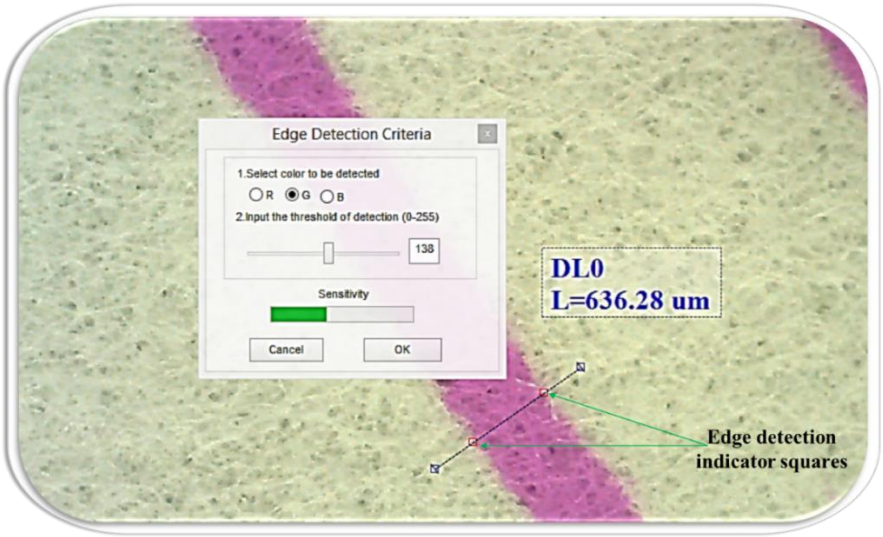

Figure S-9. Using the "Auto Distance Measurement" of DinoCapture 2.0 software for line width measurement of plotted lines on the paper.

Table S-1. Recovery test of spiked water sample determined by AAS and distance-based µPADs (n = 3).

Cobalt	AAS	µPADs
Added (ppm)	5	5
Found (ppm)	4.96 ± 0.12	5.31±0.32
Recovery (%)	99.4	106.3

Movie S-1. Demonstration of the cutting step in fabrication process of distance-based µPADs.

https://pubs.acs.org/doi/suppl/10.1021/acs.analchem.7b03796/suppl_file/ac7b03796_si_002.mpg

Movie S-2. Demonstration of the deposition step in fabrication process of distance-based µPADs. For a better demonstration of the deposition step, the technical pens were filled with rhodamine 6G solution (1% in 50% ethanol) and deposited on the narrow straight microfluidic channels.

https://pubs.acs.org/doi/suppl/10.1021/acs.analchem.7b03796/suppl_file/ac7b03796_si_003.mpg

References for the supplementary information

[1] Silhouette Studio® V3 user's manual, https://cdn.silhouetteamerica.com/m/d/manual_silhouette-studio_v5.pdf, (accessed July 2017).

[2] DinoCapture 2.0 Users Guide, http://www.dino-lite.com/download03.php, (accessed July 2017).

Chapter 3- Simple, Rapid, and Low-Cost Prototyping of µPADs, Section 2: High-throughput Deposition of Chromogenic Reagents with Quantified Volume

This chapter has been published as a research article in "Analytica Chimica Acta, 1047 (2019) 115-123." It is produced here with permission of the Elsevier.

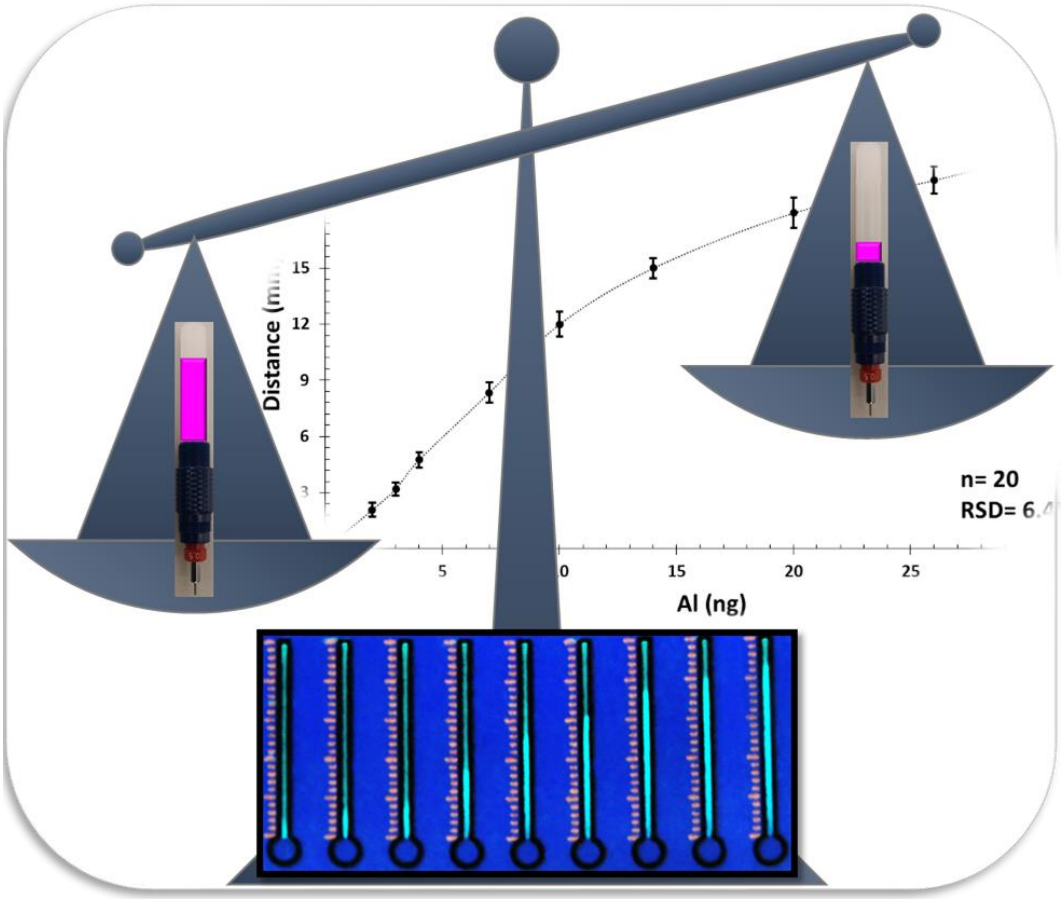

3-1- Overview

The deposition of chemical reagent inks on paper is a crucial step in the development and fabrication of microfluidic paper-based analytical devices (µPADs). A pen-plotting approach, delivering chemical ink deposition using technical pens filled with reagents and inserted into a desktop electronic plotter, is shown herein to be a versatile, low-cost, simple, rapid, reproducible, and high-throughput solution. The volume of the deposited ink was quantified gravimetrically, confirming that nanoliter volumes of reagents can be deposited reproducibly (e.g. 7.55 ± 0.37 nL/mm for a plotting speed of 10 cm/s) in detection zones of µPADs, typically spatially defined using wax printing. This approach was further investigated with regard to deposition of reagents in different geometrical forms (circular and linear), so demonstrating its applicability for preparation of µPADs with flexible design and application. By adjusting the plotting speed for linear deposition, lines with a relatively large range of widths (≈ 628-1192 µm) were created. Circular deposition was also demonstrated via delivery of reagents within wax printed circular fluidic barriers of a range of diameters (inner diameter = 1.5-7 mm). These capabilities were practically demonstrated via the fabrication of µPADs, based upon differing detection principles for determination of aluminum in natural waters using Morin as the fluorescent reagent. Traditional µPADs based on digital image colorimetry (DIC) were produced using circular deposition, whilst distance-based µPADs exploited linear deposition. Both types of µPADs developed using this method showed excellent precision for determination of trace concentrations of aluminum (average RSDs = 3.38% and 6.45%, and LODs = 0.5 ng (0.25 ppm) and 2 ng (0.5 ppm), for traditional and distance-based detection, respectively).

3-2- Introduction

In the last decade, there has been significant interest in the development of microfluidic paper-based analytical devices (µPADs) in order to meet the increasing demands of low-cost, rapid, portable, and disposable technologies, in the fields of environmental, biomedical and industrial analysis [1-3]. µPADs are easy-to-use miniaturized analytical devices, which are fabricated by creating fluidic barriers defining confined hydrophilic areas on a paper substrate, using wax printing or another related technique [4,5]. The fabrication process then involves the deposition of chemical reagents (e.g. colorimetric reagents, buffers, conductive inks, etc. depending on the detection principles and applications) upon the paper [6-8].

Obviously homogeneous and reproducible deposition of the reagents is a crucial element in µPAD preparation, especially in the case of distance-based µPADs, where the sample should have a uniform, reproducible and unrestricted flow through the microfluidic channels to react with the colorimetric reagents. Distance-based µPADs rely on measurement of the length of a color band formed on a straight microfluidic channel resulting from colorimetric reactions taking place between the analyte (present in the sample) and pre-deposited chemical reagents [9-14]. Even in traditional µPADs, which are based on color intensity measurements, having a homogenously deposited reagent leads to improved quantitative performance [15].

To-date this deposition step has been carried out using various methods, including manual pipetting, dipping, spraying, brushing, pneumatic dispensing, screen printing, photolithography, and inkjet printing. Each of these techniques has their inherent advantages and disadvantages, however some of them are more reliable and efficient than others. Inkjet printing has been shown to be one of the most successful approaches, providing deposition

of reagents with high resolution and accuracy, and precise control over volumes of deposited material (picoliter-sized droplets) [16-22]. Inkjet printing does however suffer from tedious modification steps, and time-consuming print head and cartridge washing steps for different reagents. Additionally, inkjet printers can also be incompatible with certain biological reagents (e.g. inks containing proteins), as they either apply a heat pulse (thermal printers) or shear force (piezoelectric printers) to the corresponding inks [17].

Recently we reported upon the deposition of reagents using technical pens inserted into a low-cost electronic desktop plotter, as a simpler, quicker, more flexible, and also more convenient approach to µPAD formation [23]. The alignment of the plotting step with the wax printed microfluidic features, which was the main concern associated with the pen-plotting technique, was also addressed in a follow-up study [24]. The chemical reagents were deposited exactly in user-selected spots (detection zones defined via wax printing) on the paper by activating the optical scanner of the Cameo plotter/cutter, along with some other required commands.

Pen-plotting offers many advantages over the above techniques, including inkjet printing. With pen-plotting there is no need for modification and the pen cartridge can be easily and quickly (≤3 minutes) opened, washed, dried and refilled with new reagents. It is also flexible in terms of substrate material, as plotting can be carried out with numerous substrates such as filter paper, nitrocellulose membranes, etc., and contrary to inkjet printers, pen-plotting is non-destructive, as no kind of pulse or force is applied to the reagents. The technical pens are also compatible with most organic solvents, which may be used in the formulation of the chemical reagent inks. Finally, they are also more flexible in terms of the viscosity of the

reagent inks used, as a variety of inks can be plotted on paper without the need for viscosity modifiers, surfactants, etc.

However, in spite of all these advantages, currently there is still a high degree of uncertainty in terms of the ink deposition volume on the substrate using the pen-plotting technique. Also, apart from the very basic and simple linear deposition mode, the applicability of the pen-plotting approach for more complex designs and geometries has not yet been demonstrated. Therefore, in this work, we used an accurate gravimetric method to quantify the amount of deposited ink on paper as volume per length (nL/mm, for linear deposition) or per area (nL/mm^2, for circular deposition). The performance of the pen-plotting approach was also further characterized by investigating its coverage capability for ink deposition on µPADs with various shapes and designs (e.g. straight lines or circles). Further, the effect of plotting speed on the width of the plotted lines and the diameter of plotted circles was investigated. The versatility of the pen-plotting deposition approach was demonstrated via the determination of aluminum in natural water samples using µPADs based upon two different detection principles, specifically a traditional color intensity-based analysis, and also a distance-based detection method. In this regard, a fluorescence-based determination of aluminum using a Morin complexing agent was performed on the surface of paper.

3-3- Experimental section

3-3-1- Chemicals and materials

All chemicals were of analytical reagent grade. Morin, acetic acid, sodium acetate, 1,10-phenanthroline, hydroxylamine hydrochloride, and rhodamine 6G, were purchased from Sigma-Aldrich. Standard solutions of Na(I), K(I), Pb(II), Ni(II), Zn(II), Mg(II), Mn(II), Ca(II), Co(II),

Cd(II), Cr(II), Fe(II), Hg(II), Fe(III), and Al(III) metal ions were prepared in deionised water by diluting a stock solution of 1000 mg/L (in 5% nitric acid) of the nitrate salt of each element supplied by BDH Chemicals (Queensland, Australia). All the solutions were used immediately after preparation. Deionised water was obtained with a Millipore (Bedford, MA, USA) Milli-Q water purification system. Whatman grade 1 qualitative filter paper with a pore size of 11 μm and thickness of 180 μm (GE Healthcare Australia Pty. Ltd, NSW, Australia) was used to fabricate the μPADs. Transparent film (125 μm thickness, GBC®, NSW, Australia) was used to laminate the μPADs.

3-3-2- Instrumentation

A wax printer (Colorqube 8870, Xerox, Norwalk, CT, USA) was used to print the microfluidic designs on the filter paper. A desktop electronic craft plotter/cutter (Silhouette CAMEO®, Kuluin, QLD, Australia) was used to deposit chemical inks on the detection zones of the μPADs. The deposition was performed using Mars®matic 700 technical pens (STAEDTLER Mars GmbH & Co. KG, Nuernberg, Germany, line width = 0.5 mm) filled with the desired reagents and inserted into the pen holder of the Cameo plotter. We have previously reported that these pens are compatible with most organic solvents [23]. Silhouette Studio® (V4.1.156) free software was used to design the desired patterns for both characterization experiments and also fabrication of μPADs. A Silhouette Cameo reusable cutting mat (12"X12" Cut12) was used for the precise loading of the paper media into the plotter. An A3 laminator (LM330, Laminating Wholesalers, VIC, Australia) with adjustable lamination temperature was used to laminate the devices from the bottom side to prevent any possible leakage of solutions. A Dino-Lite EDGE digital fluorescence microscope (AM4115T-GFBW, SCINET, WA, Australia) with a magnification range of 20x-220x, controlled by DinoCapture 2.0 free software, was

used for all required optical measurements. The digital image colorimetry (DIC) experiments were also accomplished by the same microscope and corresponding software. A UV viewing cabinet (Spectroline®, CM-10, NY, USA, UV light source = 254nm) was used for observation of the fluorescence emission from the Al-Morin complex developed over the straight microfluidic channels of the distance-based µPADs. A Nikon digital DSLR camera (D90 with AF-S DX NIKKOR lens, Nikon Australia Pty Ltd) was used to capture the photographs of the distance-based µPADs after fluorescence emission under UV illumination. A Sartorius analytical balance (MC 210 S, readability: 0.01 mg) was used for all gravimetric measurements.

3-3-3- Design and fabrication of µPADs

The overall fabrication process of µPADs is depicted in Figure S-1. The required microfluidic designs (Figure S-2) for both traditional and distance-based µPADs were produced using the free Silhouette Studio® software and printed on both sides of the paper using the wax printer. The “Registration Marks” option in the software was also selected prior to printing to ensure alignment of the printed feature with the following deposition step [24]. As depicted in Figure S-2, the distance-based pattern (designed line width = 0.4 mm before wax melting) was composed of a circular sample zone (3.5 mm diameter) and a straight channel (1.2 × 25 mm) along with some scale bars, which were drawn at 1 mm intervals next to the channel for direct measurement of the colored band length. The scale bars were intentionally chosen to be red in color for clear identification of the band length when the µPADs were placed in the dark UV viewing cabinet required for the determination of aluminum (the red gave the highest contrast of the ten available colors). The sizes of both the sample zone and the channels were optimized for storage of the lowest possible volume of sample (4 µL), while at the same time

having a stable fluid flow and obvious color change. The traditional µPADs were comprised of simple circles with diameter of 3.4 mm and designed line width of 0.5 mm (before wax melting). In the next step, the technical pens were filled with the corresponding chemical reagents and then inserted into the plotter to deposit the reagents on the detection zones. Afterward, the sheet was laminated (165 °C) from the bottom side in order to melt the wax through the thickness of the paper and also to give a higher mechanical stability to the fabricated µPADs and preventing any fluid leakage during analysis. While laminating, the top side of the device was covered with a piece of copy paper to avoid contamination of the laminator rollers with the melted wax and also to limit overexposure of the printed features to heat.

3-3-4- Gravimetric analysis

Figure 1A shows a flow chart depicting the gravimetric approach proposed in this work to measure deposition volumes. First, a certain volume (1 mL taken by a micropipette) of the model chemical ink (rhodamine 6G, 0.1% w/v in water-ethanol mixture 50% v/v) was weighed (n = 10) using the analytical balance, to obtain the density of the ink. Then, the pen cartridge was filled with the ink, attached to the nib body, and shaken a few times to help the ink to reach the tip. Considering the working principles of technical pens (described in Supporting Information), the tip was drawn along the paper to trigger the ink flow. After that, the filled pen (excluding the pen holder) was weighed and the initial mass was recorded. To keep potential weighing errors to a minimum, the pen holder was not included in the gravimetric measurements since it is not engaged in the ink delivery process so does not need to be weighed, whilst all the other components of the pen (Figure S-3) were in contact with the ink so required weighing. After obtaining the initial mass, the pen was inserted into the plotter

and a large number (N = 400) of straight lines (30 mm length) were plotted on a sheet of filter paper (A4 size) to simulate a number of individual linear depositions. Next, the pen holder was detached, and the remainder reweighed to determine the final mass. The difference between the two measurements was equal to the consumed mass of ink (e.g. 0.14281 ± 0.00213 g for plotting speed = 5) under the given conditions. Subsequently the mass of consumed ink for each individual plotted line and every millimetre (mm) of each line was obtained through dividing the obtained total mass by the number of plotted lines (N = 400) and the length of each line (30 mm), respectively. This mass could then be converted to a volume (nL) by considering the measured density (0.88764 ± 0.00167 g) of the corresponding ink. Both the initial (e.g 5.84801 g) and final (e.g 5.70681 g) measured masses of the pen used for the gravimetric calculations, are very large numbers relative to the inherent error of the balance (0.01 mg). Therefore, the final calculated volume (nL) is reliable in terms of possible deviations resulting from weighing errors. The same procedure can be applied for circular deposition by plotting circles instead of lines and the deposition volume can be measured per unit of square millimetre (mm^2) of the paper. In this work, this was only performed with Morin solution as the chemical ink in order to quantify the deposition volume for color intensity based μPADs in the determination of Al(III).

3-3-5 Aluminum detection

The determination of Al(III) was based on the formation of a fluorescent coordination complex of this metal with Morin in a slightly acidic medium, resulting in an instantaneous color change [25-28]. Under UV radiation, Al gives an intense green fluorescence in reaction with Morin. The fluorescence-based reagent was prepared by mixing equal parts (%v/v) of acetate buffer solution (pH = 4, 0.2 M) with Morin solution (0.1% w/v in ethanol 50%). Then

the reagent was deposited over the detection zones of the µPADs using the pen-plotting approach (constant plotting speed = 4 cm/s) and allowed to dry (5 min) for further analysis.

3-4- Results and discussion

We have previously shown how the pen-plotting approach can be a viable method for deposition of chemical reagent inks on paper for development of µPADs. However, there were some additional challenges with this technique, such as the precise positioning of deposition on desired user selected spots. This issue was resolved using the optical scanning function of the plotter [24]. An existing challenge with the pen-plotting approach is the uncertainty associated with the volume of the deposited ink on the substrate and the inability to predict the deposited volume. In the present work, we resolved this issue by implementing an elegant gravimetric approach to measure the volume of deposited ink on the paper. This is very significant as it provides practical quantitative information about the volume of deposited reagents which can be then used when developing and optimizing new assays on paper or other media.

3-4-1- Gravimetric quantification of deposition volume

It is worthwhile mentioning that among all conventional automatic deposition techniques, only automatic dispensers (usually used for development of lateral flow immunoassays) can deposit a known volume of ink (µL/cm) upon a substrate [29]. However, these come at a considerable expense, require regular maintenance (e.g. unclogging and cleaning steps), and can deliver misalignment of ink deposition with wax printed features, etc. With inkjet printing, as the most reliable deposition technique for µPADs, the maximum ejected volume can only be estimated from the printer features via mathematical calculations [30].

The gravimetric approach taken here is based on measuring the amount (mg) of ink consumed whilst plotting a large number of patterns (lines or circles) on the paper and then dividing the mass by that number to obtain the volume consumed for each individual pattern. The effect of plotting speed on the deposited volume was also investigated and the results were compiled as a graph (volume versus plotting speed) depicted in Figure 1B. As anticipated, the higher the speed, the less the deposition volume per unit of length. The error bars indicate the standard deviations, which are higher for lower speeds (e.g. ±3.01 and ±1.20 nL/mm for the speed of 1 and 3 cm/s, respectively); however, for medium and high speeds (e.g. 5 cm/s and higher) the errors are lower and almost the same (≈ ±0.41 nL/mm) showing the high reproducibility of the pen-plotting approach for reagent deposition. These small errors also confirm that the proposed gravimetric approach is a reliable method to determine the deposition volume. In addition, these results demonstrate how small volumes of reagent, as low as 7.55 ± 0.37 nL/mm (with plotting speed of 10 cm/s), can be precisely deposited on paper, which is sufficient to perform an assay without any need for multi-pass printing (as is usually required in inkjet printing to deposit sufficient reagents to produce strong signals [30]). However, it should also be noted that the numerical results presented here are for deposition of this particular model ink (rhodamine 6G, 0.1% w/v in ethanol 50% v/v), and will of course vary slightly for other inks of different viscosity and surface tension.

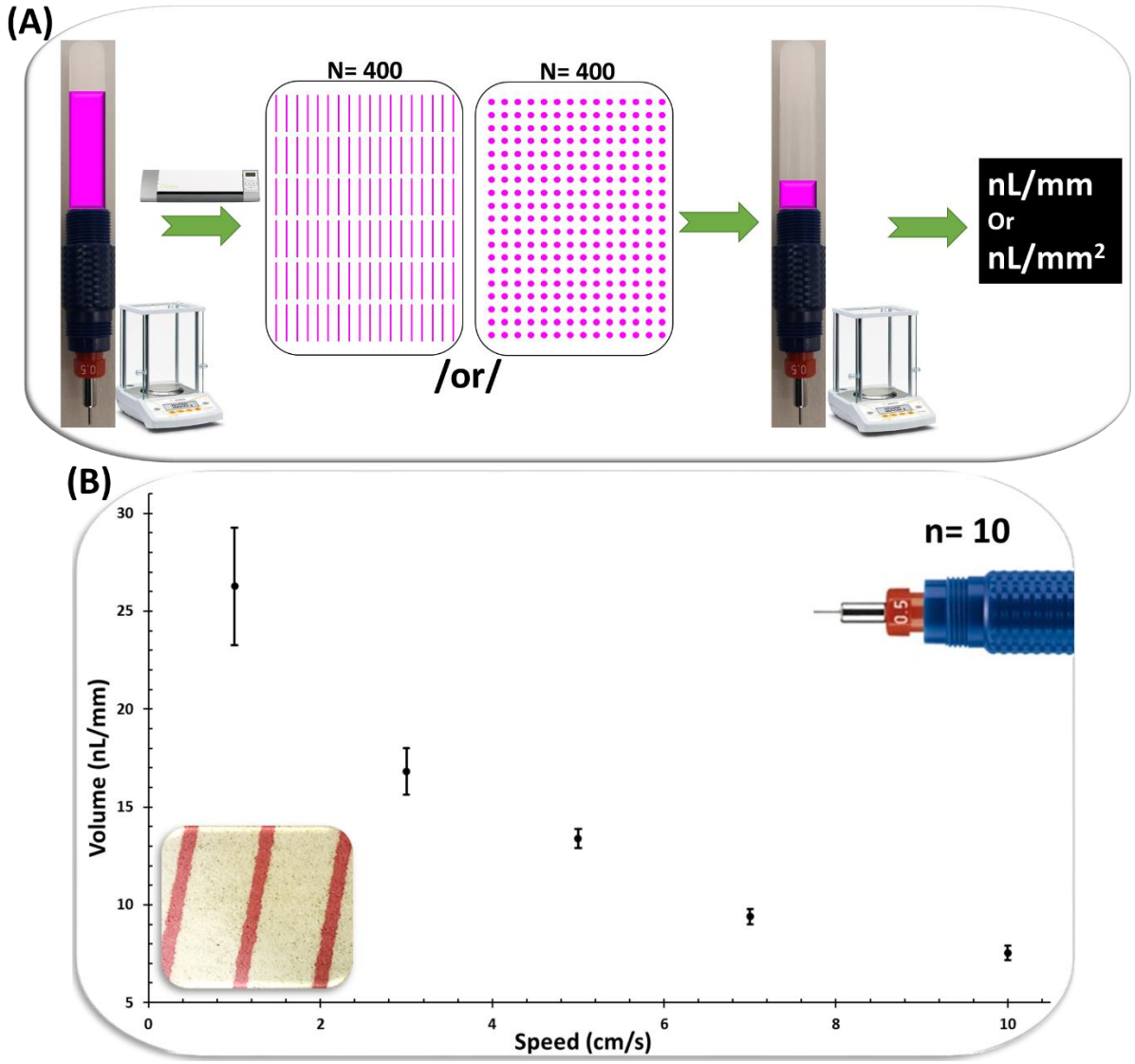

Figure 1. (A) Flow chart of the gravimetric approach used for the determination of deposition volume. N is the number of corresponding plotted patterns (lines or circles). (B) Graph obtained from performing the gravimetric approach in the linear manner (n = 10) with varying plotting speeds (cm/s). The higher the speed, the lower the deposition volume (nL/mm). Inset: photograph of the plotted straight lines.

3-4-2- Full coverage of the detection zones

3-4-2-1- Linear deposition

We have already demonstrated linear deposition of colorimetric reagents inside wax printed microfluidic channels in the form of very simple straight lines, which were then used within µPADs with distance-based detection [24]. Here the linear deposition is further

characterized and the effect of plotting speed on the width of plotted lines is investigated. This allows optimization of the plotting parameter settings for any particular application with specific device geometries. Technical pens were filled with the model ink (rhodamine 6G, 0.1% w/v in ethanol 50% v/v) and then straight lines (25 mm length) were plotted on the paper with different plotting speeds. Line width was measured by the fluorescence microscope at five points along the lines (at increments of 4 mm) and the results are shown in the graph in Figure 2. As expected, the higher the speed, the narrower the plotted lines, which signifies lower deposition volumes. This is also in agreement with the gravimetric measurements. These results indicate that by adjusting the plotting speed we can govern the width of the plotted lines across a relatively wide range of widths (≈ 628-1192 µm), which can be utilized later in the development of optimized µPADs designs. For instance, with this available line range, one single pass is enough to provide full coverage of a narrow detection zone, even for the narrowest reported wax printed channel used for distance-based measurements of ca. 900 µm [31]. For wider channels, the use of either lower plotting speeds or multiple linear deposition lines would be sufficient to cover the detection areas. The effect of reagent concentration on the width of plotted lines was also investigated; however, it was observed that the concentration had no significant effect on line width and only increased the color intensity of the plotted lines (Figure S-5). Detailed information about the microscopic measurements with a digital microscope used in this work is provided in the Supporting Information (Figure S-6).

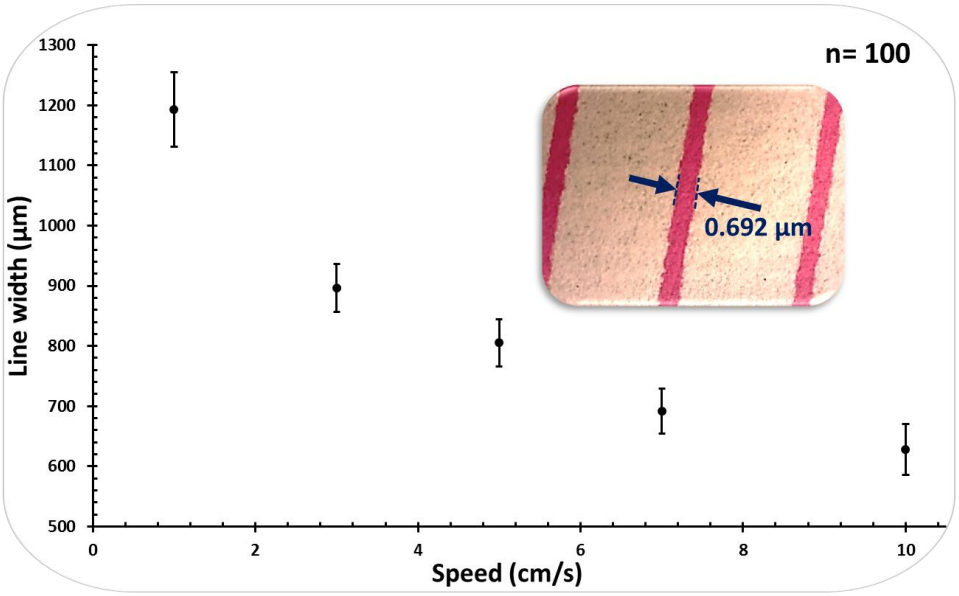

Figure 2. Linear deposition and the effect of plotting speed (cm/s) on the width of plotted lines. The higher the speed, the narrower the plotted lines. Inset: photograph of the plotted lines. The error bars represent standard deviations from average values.

3-4-2-2- Circular deposition

To further illustrate the applicability of the pen-plotting approach for deposition of reagents, we demonstrated a circular deposition of the model ink. This shows the suitability of this approach not only for distance-based µPADs, but also for traditional µPADs which are based on measurement of the color intensity in detection zones that typically have a circular shape. Circles with various diameters (0.25-4 mm) were designed by the Silhouette Studio® software and then plotted to emulate reagent deposition in circular detection zones within µPADs. The outer diameter of the plotted circles was measured by a fluorescence microscope and results are presented as a graph charting the measured diameter (M.D.) versus designed diameter (Figure 3A). Circle designs with diameter in the range of 0.25-2 mm resulted in fully filled plotted circles with diameters in the range of 2.44 ± 0.06 to 3.26 ± 0.09 mm, which is in the typical size range of detection zones used in traditional µPADs. Diameters larger than 2 mm produced circles with empty centers since the amount of deposited ink was not enough to fully cover that area via ink wicking with the aid of the capillary effect. Thus, in order to

fully cover detection zones larger than 3.26 mm, multiple circular deposition lines (Figure 3B,b) could be implemented. To further demonstrate the circular deposition, circles with different sizes (inner diameter, 1.5-7 mm) were wax printed on the paper simulating traditional µPADs and then the pen-plotting approach was successfully applied to fill the circles with the model ink (Figure 3B). Based on the obtained graph and also considering the constant line width of the plotted circles (≈ 1 mm), the required number of multiple deposition lines with given diameters could be designed to fully cover the corresponding regions (Figure 3B). In the case of the smallest wax printed circle (1.5 mm), a single deposition line (0.25 mm length) instead of a circle was used to ensure the deposition would take place inside the desired area. In this case, the pen tip makes a small semicircular trace (diameter ≈ 1 mm) which was the smallest possible trace created by this approach with this particular ink. These experiments are an illustration of the suitability of the pen-plotting approach for a wide variety of applications.

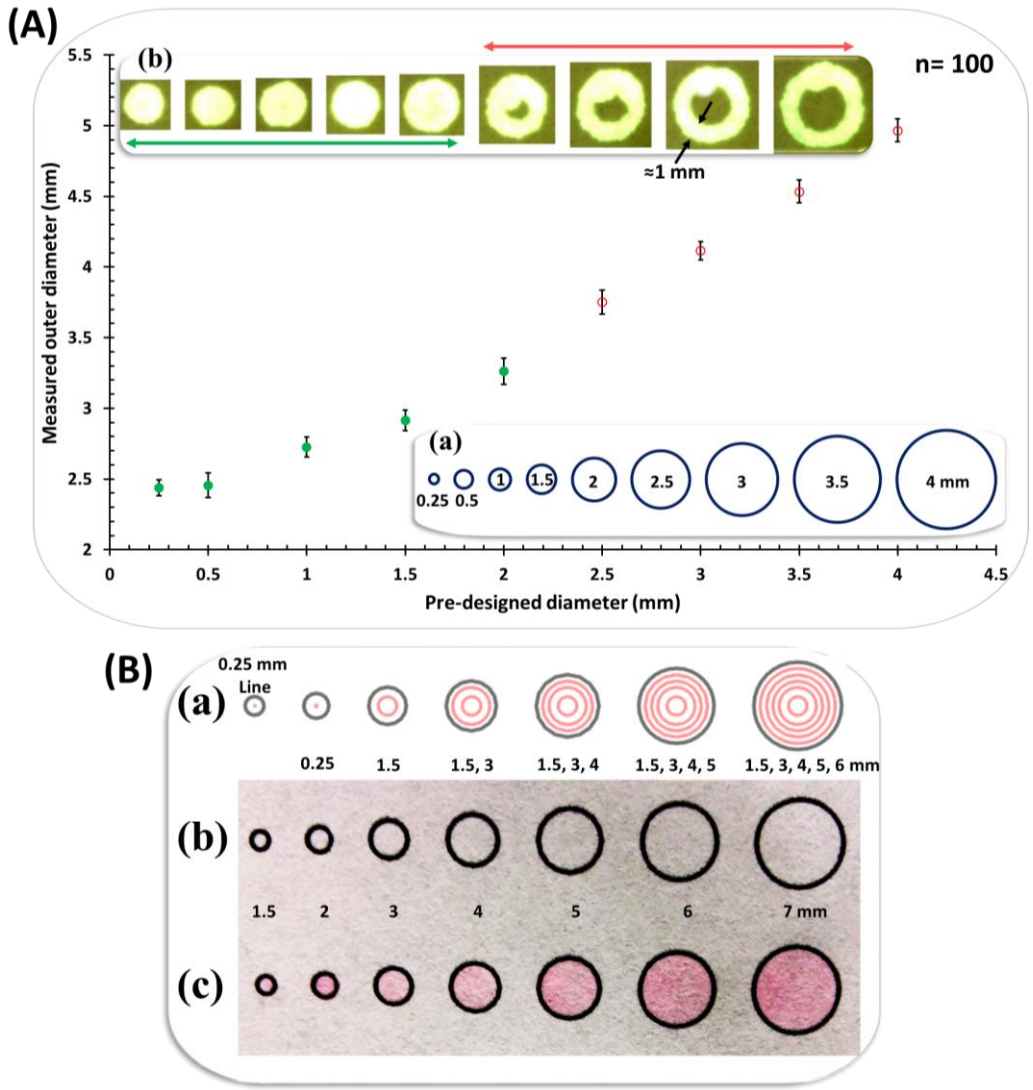

Figure 3. Circular deposition. (A) Graph showing the relationship between diameters of designed circles (theoretical) vs. plotted circles (experimental, n = 100). Markers indicate fully filled (●) and unfilled (○) circles. Inset: (a) computer designed circles with various sizes. (b) photograph of the plotted circles. The unfilled circles had almost identical line widths (≈ 1 mm). (B) Demonstration of circular deposition to fill up wax printed circles with different sizes. (a) computer designed circular deposition lines (red circles) with their corresponding diameters. In order to fill up wax printed circles larger than 4 mm, multiple deposition lines (more than one deposition line) were used. (b) Photograph of wax printed circles with their corresponding diameters. (c) Photograph of wax printed circles after being filled up by performing the circular deposition.

3-4-3- Determination of aluminum in natural waters

The association between aluminum toxicity and some neurological diseases such as Alzheimers, Parkinsons and dialysis encephalopathy in humans has been well documented. Therefore, determination of low concentrations of aluminum in natural waters and other

environmental samples is vitally important [32,33]. Currently, several conventional analytical techniques such as atomic absorption or emission, mass spectroscopic techniques, and electrochemical methods are used for determination of Al(III) in water samples. Despite their high sensitivity and precision, these methods are costly and time-consuming, and they need complex equipment and trained operators, which are all properties unsuitable for on-site analysis. Alternatively, µPADs can be utilized for rapid, low-cost, instrument-free, and portable analysis of the water samples.

To demonstrate the analytical potential of the technical concepts presented here, the fluorescence-based determination of aluminum was investigated using both distance-based and traditional µPADs. The gravimetrical approach was used (n= 4) to measure the deposition volume of the fluorescent reagent (Morin, 0.1% w/v in ethanol 50%) in various detection zones. Deposition volumes were 16.62 ± 0.38 nL/mm and 42.88 ± 2.15 nL/mm^2 for distance-based and traditional µPADs, respectively. Straight lines (line width = 748 ± 0.02 µm) and fully filled circles (outer diameter = 2.82 ± 0.07 mm) were used to cover the straight channel and circular shaped detection zones of the corresponding µPADs. The amount of reagent deposited in the detection zone was optimized (by changing the concentration) to create the best color contrast, along with the highest sensitivity on the µPADs.

3-4-3-1- Distance-based measurement

It is obvious that having reproducible linear deposition of the reagent over the detection channels in individual µPADs is essential for reproducibility and precision of the analysis. In the present work, this requirement was met by performing the linear deposition of reagents via the pen-plotting approach. The developed distance-based µPADs fabricated by linear homogenous deposition of a Morin solution over the straight channels, were successfully

applied for instrument-free quantification of aluminum in water samples. According to the Australian and New Zealand guidelines for fresh and marine water quality, the concentration of Al in irrigation waters should not be more than 5 mg/L (long-term use) or 20 mg/L (short-term use) [34]. In this work, distance-based determination of standard solutions of Al was investigated in the range of 2-30 ng (0.5-7.5 mg/L) and the calibration curve was obtained from the measured distance signals. For the detection of Al(III), the µPADs were exposed to UV light (λmax = 254 nm) for observation of the fluorescent emission from Morin-Al complex along the channels. The shortest visible length (average = 2.08 ± 0.38 mm) correlated to a sample containing 2 ng of Al, which was then considered as the detection limit (mass detection limit). The actual photograph of µPADs after loading 4 µL of standard Al(III) solutions with various concentrations into the sample inlets are depicted in Figure 4, along with the corresponding response curves. The standard deviations and error bars in the corresponding graph, represent excellent reproducibility (average RSD = 6.45%, n = 20) of analysis, which indirectly confirms the reliability of the pen-plotting approach for linear deposition of reagents.

The effect of possible co-existing interfering metal ions on the determination of Al was investigated by applying water samples containing Al (2.5 ppm) and different metal ions (Na(I), K(I), Pb(II), Ni(II), Zn(II), Mg(II), Mn(II), Ca(II), Co(II), Cd(II), Cr(II), Fe(II), and Hg(II)) with Al:metal ratio of 1:1. The formation of fluorescent Morin-metal (e.g. Al, Ca, Mg, Be, etc.) complexes is pH dependent and in the specified pH here (pH = 4) is highly selective for Al. In addition, the acetate used in the buffer composition can also function as a masking agent preventing many metal interferences. However, the major interference concern is Fe(III), which would interfere by quenching the fluorescent signal to some extent. The presence of

the metal ions did not have a significant impact on the distance signal; however, Fe(III) in Al:metal ratio of more than 1:0.5 caused some interference in the form of fluorescence quenching, which mostly affected the intensity of the formed color band rather than the distance signal. By depositing a mixture of hydroxylamine hydrochloride to reduce Fe(III) to Fe(II), and 1,10-phenanthroline as a masking agent for Fe(II) in the sample zone prior to analysis, an Al:Fe(III) ratio of more than 1:1 could be tolerated.

Real water samples were collected (Ringarooma, Tasmania, Australia), filtered, and spiked with a known concentration (2.5 ppm) of standard Al solution and then analyzed both with the distance-based µPADs and atomic absorption spectroscopy (AAS). Results indicated a good agreement (within 10% error) between these two techniques (Table S-1). The non-spiked water samples did not generate any distance signal on the µPADs indicating normal levels of the target metal in the water sample. This was further confirmed by AAS analysis which showed Al at trace levels and below the detection limit of the distance-based µPADs.

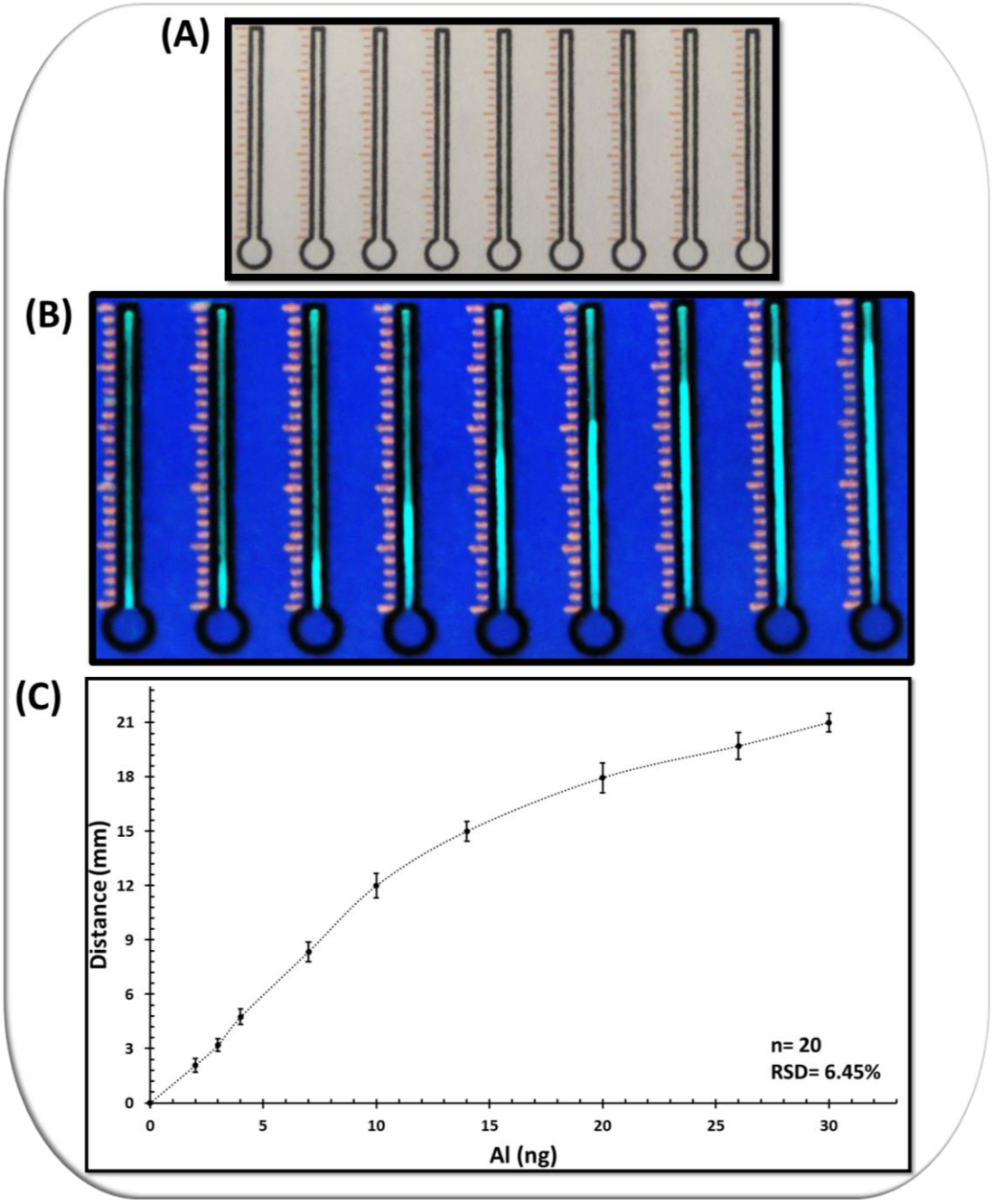

Figure 4. Distance-based determination of aluminum. (A) Photograph of distance-based µPADs at the end of analysis after pipetting 4 µL of Al standard solutions. No color change or distance signal is observable. (B) Photograph of distance-based µPADs after placing them in the UV viewing cabinet and exposing to 254 nm UV illumination. Contrast and brightness are modified for better observation. (C) Response curve of different concentrations of Al (2-30 ng) to the distance-based µPADs. Markers reflect the average of 20 repeated measurements. The error bars represent the standard deviations from the average values.

3-4-3-2- Color intensity-based measurement

Circular deposition was also utilized for the determination of Al based on traditional color intensity measurements by deposition of the fluorescent reagent in the well-shaped (circular) µPADs (Movie S-1). The µPADs were loaded with 2 µL of standard solutions of Al with various concentrations and then were allowed to dry (10 min) under ambient conditions. The color intensity-based determination was investigated in the range of 0.5-7 ng (0.25-3.5 mg/L) of Al and the calibration curve was obtained for different intensities of green fluorescence emission (G) recorded by fluorescence microscope (Supporting Information). The signals were plotted as ΔG (GSample - GBlank) versus Al concentrations (Figure 5). The mass limit of detection (LOD) was calculated to be 0.83 ng of Al, based on three times the standard deviation (3SD) of the signal (green intensity) of the blank. Above 7 ng of Al, the paper surface was saturated with fluorescence emission and no additional increase in green intensity could be measured.

Similar to the distance-based measurements, here the average RSD representing the reproducibility of all tests was 3.38% (n = 12) which indicates the reliability of the pen-plotting approach for circular deposition of reagents as well as for linear deposition. The traditional µPADs present a slightly lower detection limit of Al; however, the distance-based µPADs eliminate the need for external detectors and also enable a much wider dynamic range since detection in traditional µPADs faces color saturation at much lower concentrations compared to distance-based µPADs. A detailed comparison between traditional and distance-based µPADs for determination of Al is shown in Table S2 in the Supporting Information.

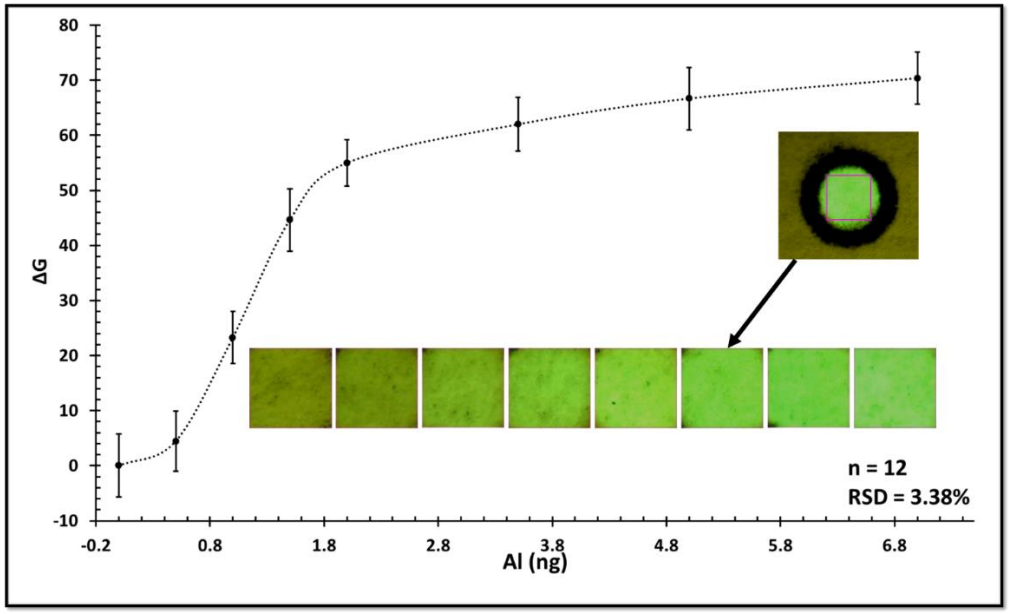

Figure 5. Color intensity-based determination of aluminum. Graph represents the calibration curve associated with Al analysis (1-7 ng) obtained from recorded green intensities (using a fluorescence microscope) at the detection zone of the µPADs. The markers and error bars reflect the average and standard deviations of 12 measurements. Inset: photographs of detection areas of paper after loading with various concentration of Al.

3-5- Conclusions

This study characterizes in detail the pen-plotting approach and documents it as a versatile, rapid, reproducible, and high-throughput method for deposition of chemical reagents on paper substrates for the development of µPADs. An accurate gravimetric method is introduced which can be readily used in order to determine the volume of deposited reagents and overcome the existing uncertainty in this regard. The versatility of this approach is further illustrated by demonstrating the reagent deposition in both linear and circular forms which can be later implemented in the fabrication of µPADs with a variety of designs and applications.

Traditional color intensity based µPADs utilized circular deposition, and distance-based µPADs utilized linear deposition of fluorescent reagent by pen-plotting for the determination of Al(III) in natural waters. The distance-based µPADs exhibited a much wider dynamic range

since detection in traditional µPADs faces color saturation at much lower concentrations. The low RSD values for all the measured parameters obtained from these µPADs indicate the reliability of this approach for reproducible deposition of reagents on µPADs of different designs and sizes. The controlled and reproducible nanolitre scale deposition of chemical inks along with good control over the size and shape of the plotted features may stimulate novel applications even in other research areas demanding localized delivery of chemical reagents.

3-6- References

[1] D.M. Cate, J.A. Adkins, J. Mettakoonpitak, C.S. Henry, Recent developments in paper-based microfluidic devices, Analytical Chemistry, 87 (2015) 19-41.

[2] Y. Yang, E. Noviana, M.P. Nguyen, B.J. Geiss, D.S. Dandy, C.S. Henry, Paper-based microfluidic devices: Emerging Ttemes and applications, Analytical Chemistry, 89 (2017) 71-91.

[3] M.M. Gong, D. Sinton, Turning the page: advancing paper-based microfluidics for broad diagnostic application, Chemical Reviews, 117 (2017) 8447-8480.

[4] K. Yamada, H. Shibata, K. Suzuki, D. Citterio, Toward practical application of paper-based microfluidics for medical diagnostics: state-of-the-art and challenges, Lab on a Chip, 17 (2017) 1206-1249.

[5] S. Ahmed, M.P.N. Bui, A. Abbas, Paper-based chemical and biological sensors: Engineering aspects, Biosensors and Bioelectronics, 77 (2016) 249-263.

[6] Y. He, Y. Wu, J.Z. Fu, W.B. Wu, Fabrication of paper-based microfluidic analysis devices: a review, RSC Advances, 5 (2015) 78109-78127.

[7] X. Jiang, Z.H. Fan, Fabrication and operation of paper-based analytical devices, Annual Review of Analytical Chemistry, 9 (2016) 203-222.

[8] Y. Xia, J. Si, Z. Li, Fabrication techniques for microfluidic paper-based analytical devices and their applications for biological testing: A review, Biosensors and Bioelectronics, 77 (2016) 774-789.

[9] D.M. Cate, W. Dungchai, J.C. Cunningham, J. Volckens, C.S. Henry, Simple, distance-based measurement for paper analytical devices, Lab on a Chip - Miniaturisation for Chemistry and Biology, 13 (2013) 2397-2404.

[10] Tian, J. Li, Y. Song, L. Zhou, Z. Zhu, C.J. Yang, Distance-based microfluidic quantitative detection methods for point-of-care testing, Lab on a Chip, 16 (2016) 1139-1151.

[11] X. Wei, T. Tian, S. Jia, Z. Zhu, Y. Ma, J. Sun, Z. Lin, C.J. Yang, Microfluidic distance readout sweet hydrogel integrated paper-based analytical device (μDiSH-PAD) for visual quantitative point-of-care testing, Analytical Chemistry, 88 (2016) 2345-2352.

[12] M. Srisa-Art, K.E. Boehle, B.J. Geiss, C.S. Henry, Highly sensitive detection of Salmonella typhimurium using a colorimetric paper-based analytical device coupled with immunomagnetic separation, Analytical chemistry, 90 (2017) 1035-1043.

[13] T. Tian, Y. An, Y. Wu, Y. Song, Z. Zhu, C. Yang, Integrated distance-based origami paper analytical device for one-step visualized analysis, ACS Applied Materials and Interfaces, 9 (2017) 30480-30487.

[14] R. Pratiwi, M.P. Nguyen, S. Ibrahim, N. Yoshioka, C.S. Henry, D.H. Tjahjono, A selective distance-based paper analytical device for copper (II) determination using a porphyrin derivative, Talanta, 174 (2017) 493-499.

[15] N. Komuro, S. Takaki, K. Suzuki, D. Citterio, Inkjet printed (bio)chemical sensing devices, Analytical and Bioanalytical Chemistry, 405 (2013) 5785-5805.

[16] B. Creran, X. Li, B. Duncan, C.S. Kim, D.F. Moyano, V.M. Rotello, Detection of bacteria using inkjet-printed enzymatic test strips, ACS Applied Materials & Interfaces, 6 (2014) 19525-19530.

[17] K. Yamada, T.G. Henares, K. Suzuki, D. Citterio, Paper-based inkjet-printed microfluidic analytical devices, Angewandte Chemie - International Edition, 54 (2015) 5294-5310.

[18] A. Apilux, Y. Ukita, M. Chikae, O. Chailapakul, Y. Takamura, Development of automated paper-based devices for sequential multistep sandwich enzyme-linked immunosorbent assays using inkjet printing, Lab on a Chip - Miniaturisation for Chemistry and Biology, 13 (2013) 126-135.

[19] J. Lessing, A.C. Glavan, S.B. Walker, C. Keplinger, J.A. Lewis, G.M. Whitesides, Inkjet printing of conductive inks with high lateral resolution on omniphobic “RF paper” for paper-based electronics and MEMS, Advanced Materials, 26 (2014) 4677-4682.

[20] T.G. Henares, K. Yamada, S. Takaki, K. Suzuki, D. Citterio, “Drop-slip” bulk sample flow on fully inkjet-printed microfluidic paper-based analytical device, Sensors and Actuators B: Chemical, 244 (2017) 1129-1137.

[21] C. Dixon, J. Lamanna, A.R. Wheeler, Printed microfluidics, Advanced Functional Materials, 27 (2017).

[22] N. Ruecha, O. Chailapakul, K. Suzuki, D. Citterio, Fully inkjet-printed paper-based potentiometric ion-sensing devices, Analytical Chemistry, 89 (2017) 10608-10616.

[23] N. Nuchtavorn, M. Macka, A novel highly flexible, simple, rapid and low-cost fabrication tool for paper-based microfluidic devices (µPADs) using technical drawing pens and in-house formulated aqueous inks, Analytica Chimica Acta, 919 (2016) 70-77.

[24] M. Rahbar, P.N. Nesterenko, B. Paull, M. Macka, Geometrical alignment of multiple fabrication steps for rapid prototyping of microfluidic paper-based analytical devices, Analytical Chemistry, 89 (2017) 11918–11923.

[25] K.L. Cheng, K. Ueno, T. Imamura, CRC handbook of organic analytical reagents, CRC press1992.

[26] J. Tria, E.C. Butler, P.R. Haddad, A.R. Bowie, Determination of aluminum in natural water samples, Analytica Chimica Acta, 588 (2007) 153-165.

[27] M.J. Ahmed, J. Hossan, Spectrophotometric determination of aluminum by morin, Talanta, 42 (1995) 1135-1142.

[28] H.-z. Lian, Y.-f. Kang, S.-p. Bi, A. Yasin, D.-l. Shao, Y.-j. Chen, L.-m. Dai, L.-c. Tian, Morin applied in speciation of aluminum in natural waters and biological samples by reversed-phase high-performance liquid chromatography with fluorescence detection, Analytical and Bioanalytical Chemistry, 376 (2003) 542-548.

[29] J. Credou, R. Faddoul, T. Berthelot, Photo-assisted inkjet printing of antibodies onto cellulose for the eco 2- friendly preparation of immunoassay membranes, RSC Advances, 5 (2015) 29786-29798.

[30] D.M. Cate, S.D. Noblitt, J. Volckens, C.S. Henry, Multiplexed paper analytical device for quantification of metals using distance-based detection, Lab on a Chip - Miniaturisation for Chemistry and Biology, 15 (2015) 2808-2818.

[31] K. Yamada, T.G. Henares, K. Suzuki, D. Citterio, Distance-Based Tear Lactoferrin Assay on microfluidic paper device using interfacial interactions on surface-modified cellulose, ACS Applied Materials and Interfaces, 7 (2015) 24864-24875.

[32] Sarkar, B. Heavy metals in the environment, CRC Press 2002.

[33] E. Underwood, Trace elements in human and animal nutrition, Elsevier 2012.

[34] ANZECC, ARMCANZ. (Australian and New Zealand Environmental and Conservation Council, Agriculture and Resource Management Council of Australia and New Zealand, Canberra) Australian and New Zealand guidelines for fresh and marine water quality. no. 4. Volume 3, Chapter 9, 2000.

3-7- Supplementary information for chapter 3

3-7-1- Working principle of technical pens

Nowadays, technical pens are available in the market in a wide range of brands, features, applications and tip sizes; however, in this work, we implemented a Staedtler technical pen for deposition of reagents. Different components of this pen along with a front view of the tip of the pen's nib are illustrated in Figure S-4. The ink transport mechanism of this pen is based on the ink flow from the cartridge through the feed and ending at the metal tip of the nib. The narrow delivery metal needle functions as a valve which allows the ink to be released once the pen tip comes in contact with the surface of the paper. Basically, the tip is usually closed and blocked by the needle and dragging the pen across the paper pushes the needle slightly upward and creates a tiny space for the ink to flow out (Figure S-4b). This results in a very precise and controlled ink flow pattern which consequently generates consistent and reproducible traces on the paper. Holding the tip perpendicular to the surface of paper will create more consistent traces which can be assured using an electronic plotter.

3-7-2- Optimization of plotting parameter settings

One of the most useful features of the Silhouette Studio® software and the Cameo plotter/cutter is that the cutting or plotting parameter settings (speed and applied force) can be set to optimal levels for different applications. By choosing the "cut settings" option in the software, we can access different settings for manipulation of the machine. According to information provided by the instrument manufacturer, the speed of plotting can be adjusted from 10-100 cm/s (represented in a range of 1-10 in the software) [1]. The applied force on the substrate by the pen's tip, can also be adjusted in 33 levels, represented as "Thickness"

in the software. Each level of the thicknesses is approximately equal to 7 grams force (gf) so it is possible to apply a range of 7-230 gf by this machine. “gf” is not an SI unit and is just an approximate unit given by the manufacturer, adjusting the applied force by the machine. Throughout this work, the minimum “Thickness” level (i.e. 1 = 7 gf) was used for all experiments to avoid any potential damage to the paper surface which might be caused by the pen tip. Moreover, it was observed that varying the “Thickness” has no significant effect either on deposition volume or on width of plotted lines (results not shown).

3-7-3- Microscopic measurements

The Dino-Lite microscope (AM4115T-GFBW) used in this work includes one white and seven blue LEDs with an emission filter of 510 nm which are useful for green fluorescing illumination. In addition, the DinoCapture 2.0 software controlling the microscope offers some practical features for accurate and precise measurement of different geometrical shapes and color analysis purposes [2]. The magnification of the microscope was locked on “30” throughout all these measurements.

3-7-3-1- Line width

The “Auto Distance Measurement” tool was used to measure the width of plotted lines (discussed in “linear deposition” section) by precisely detecting the edges of corresponding lines (Figure S-6A). A detection path was defined by setting the edge detection criteria (R, G, B color threshold in the range of 0-255), in a way to allow the highest possible measurement sensitivity.

3-7-3-2- Circle diameter

In order to measure the diameter of the plotted circles representing the circular deposition of the pen-plotting approach, the “Diameter Circle” tool (Figure S-6B) of the software was used. As illustrated in the Figure, the circumference, area, and radius of a circle can be readily measured simply by clicking and extending out the indicator circle to the desired diameter. Similar to the plotted lines in the previous section which were comprised of some rough edges, the plotted circles also did not have smooth edges. Thus, the diameter measurements were accomplished by extending out the indicator circle to an extent to which the plotted circles would be covered thoroughly.

3-7-4- Color intensity analysis

In this work, the digital image colorimetry (DIC) for color intensity based determination of Al, was performed in a rapid, and precise way using the digital microscope and the “DinoCapture” software. In other words, no camera or scanner was used to record images which would then be followed by image analyzing software such as ImageJ to process the color intensity. DinoCapture offers a very useful tool namely “Color Average” which automatically measures the average RGB color values within a selected region of the captured image. The color values are displayed in hexadecimal format (a hex triplet, e.g. 638B0F) which later can be easily converted into the RGB (i.e. 0-255) format. Herewith, after loading the Al sample and the drying step, the well shape traditional µPADs were placed under (with a certain distance, 4.5 mm) the microscope in ambient light to capture the images. A constant “Camera Adjustment” was used throughout all the image analysis (Figure S-6C). In order to select the desired regions of the µPADs for color intensity analysis, the indicator square of this tool with a constant dimension (1.45×1.45 mm) was used for all measurements (Figure S-

6D). The size of this square was selected in a way that its corners met exactly the inner edges of the wax printed µPADs and recorded the color intensities of the same regions of the µPADs in a reproducible manner. From the obtained hexadecimal values, only the converted green values were used for color intensity measurements.

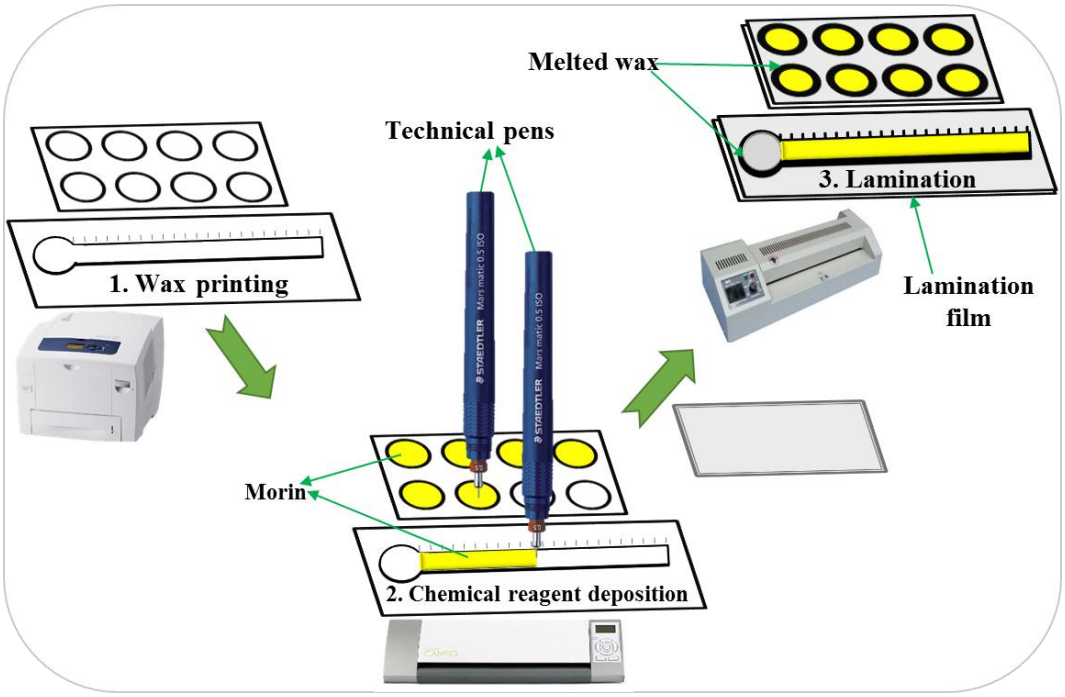

Figure S-1. Schematic representation of the fabrication process for both traditional well-shaped and distance-based µPADs.

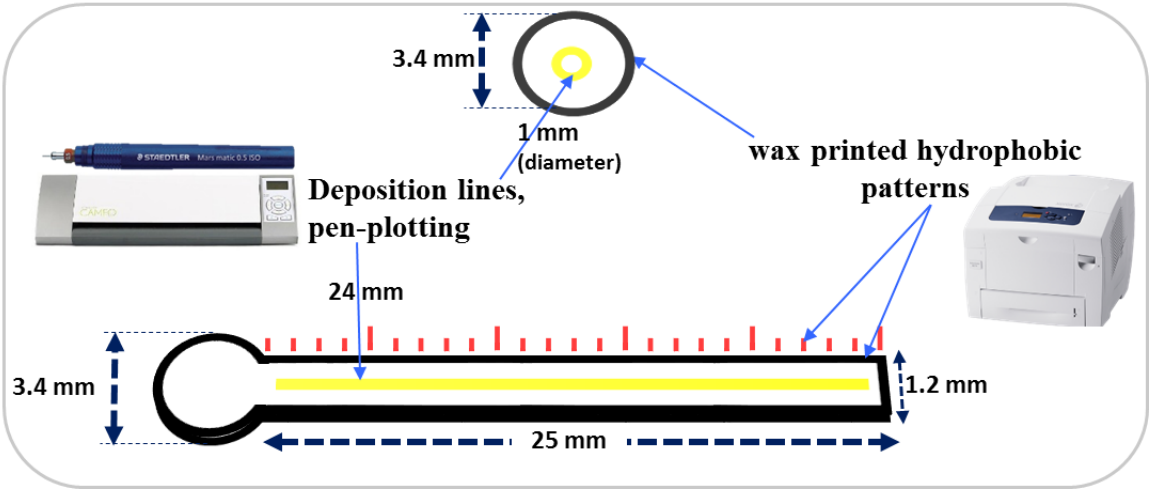

Figure S-2. Outline of single distance-based and well-shaped microfluidic patterns along with the corresponding linear and circular deposition lines. The indicated dimensions of wax printing features represent the values set in the Silhouette Studio software which will be enlarged after wax melting in the laminating step. In the distance-based pattern, the color of the scale bars has been set to red in order to be fluorescent under UV illumination.

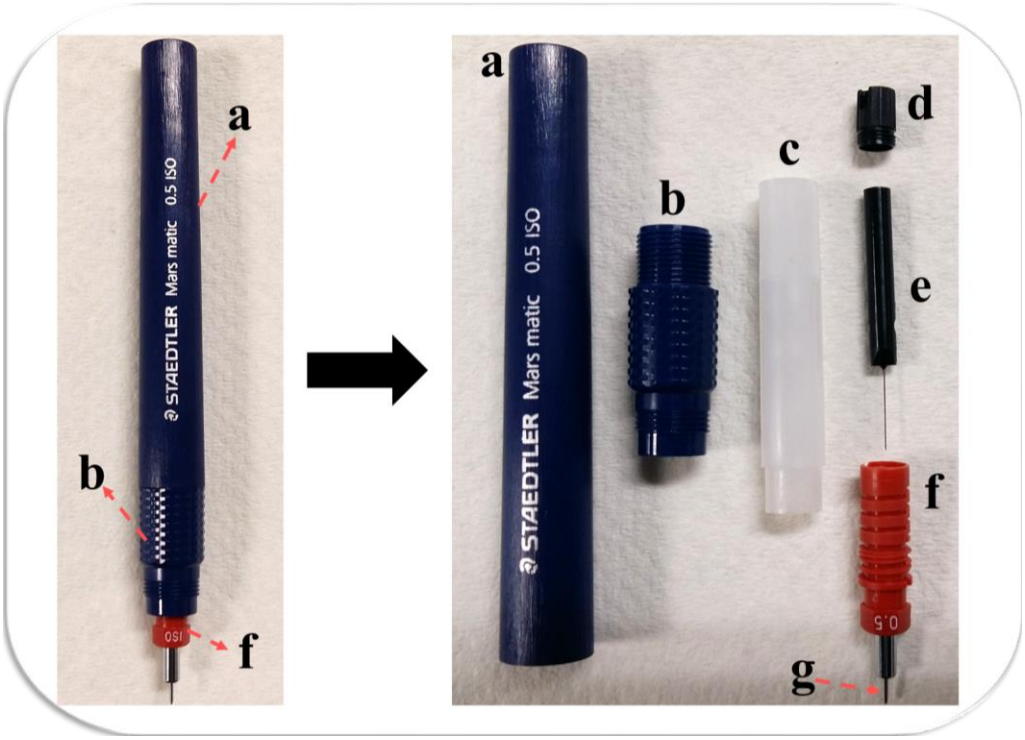

Figure S-3. Different components of a technical pen. a) Holder, b) Nib body, c) Cartridge, d) Feed cover, e) Delivery metal needle, f) Feed g) Metal nib.

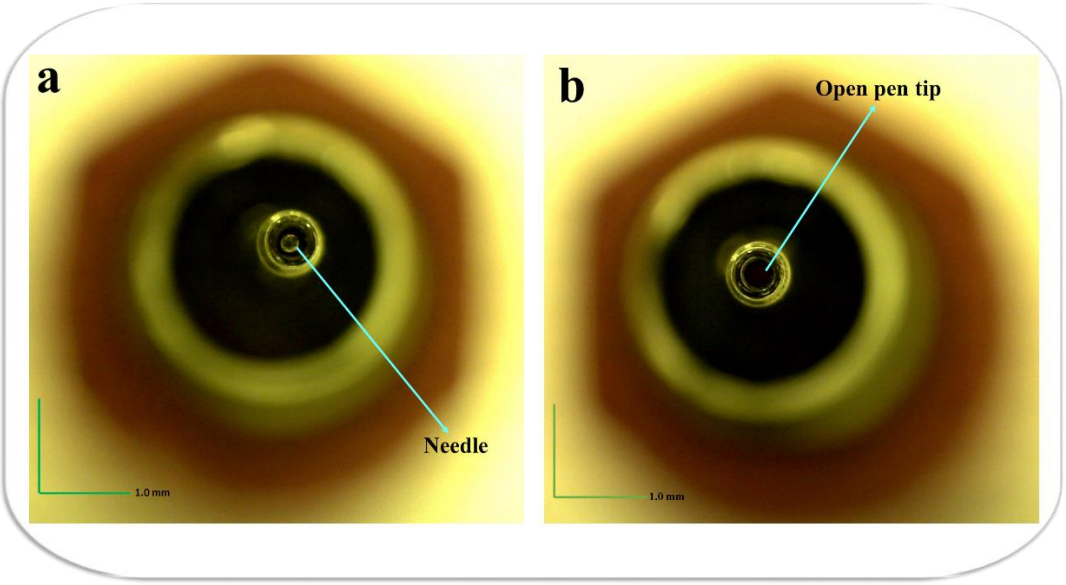

Figure S-4. A front view of the tip of the technical pen. a) The pen tip is blocked by the metal needle. b) The pen tip is open in the absence of the needle.

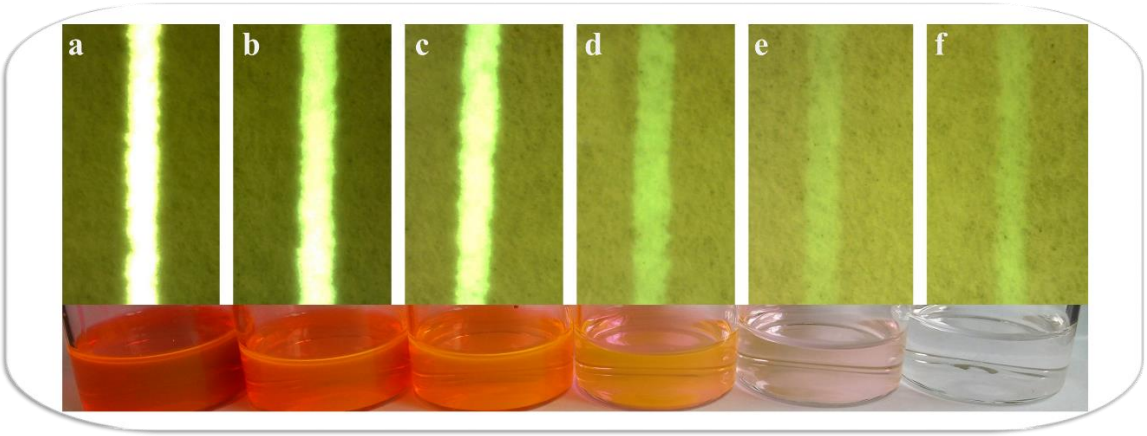

Figure S-5. The effect of reagent concentration on the width of plotted lines in a linear manner. Technical pens filed with different concentrations of rhodamine 6G (a-f, 2000, 500, 200, 20, 2, 0.2 µM) traced the straight lines with almost the same width but different fluorescent intensities.

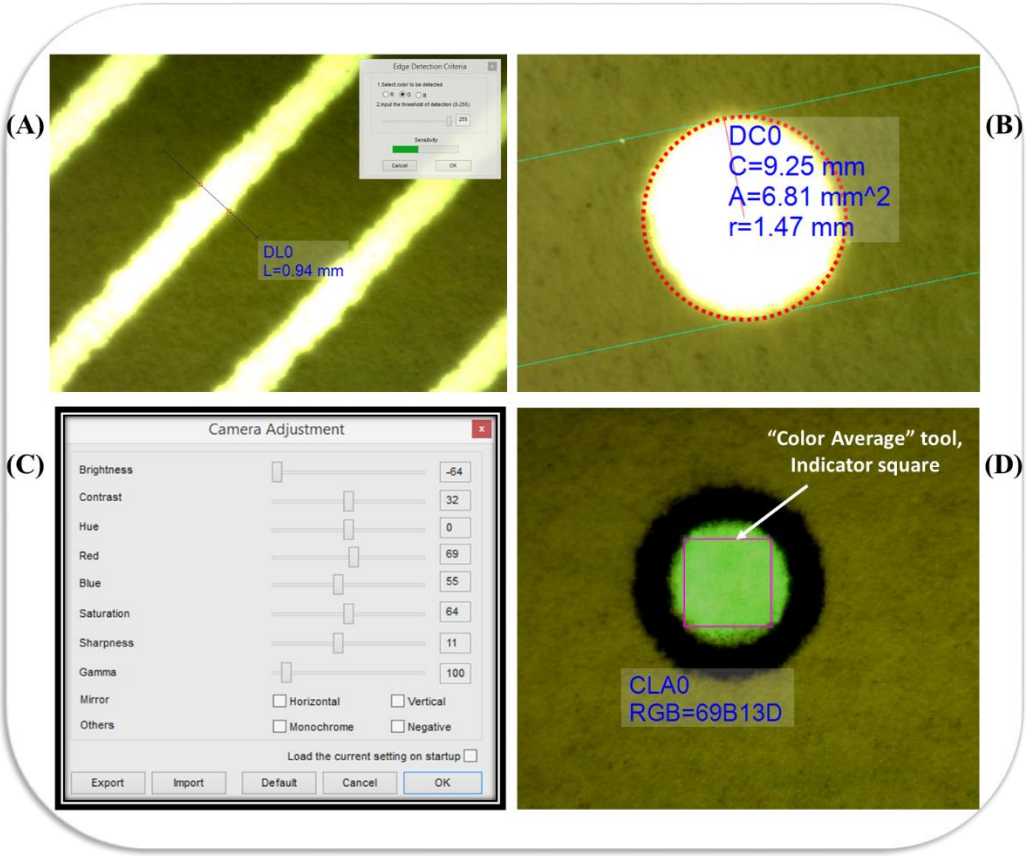

Figure S-6. Microscopic measurements. (A) "Auto Distance Measurement" tool determining the line width (B) "Diameter Circle" tool determining the diameter of plotted circles (C) "Camera Adjustment" set for recording images of traditional µPADs in determination of Al (D) "Color Average" tool used to measure the green intensity generated in the detection zone of µPADs due to formation of the Morin-Al fluorescent complex.

Table S-1. Real water sample determined by AAS and distance-based µPADs (n = 4).

Al	Added (ppm)	Found (ppm)	Recovery (%)
AAS	2.5	2.57 ± 0.26	102.8
µPADs	2.5	2.41 ± 0.74	96.4

Table S-2. Comparative illustration of the performance of traditional and distance-based µPADs in the determination of Al.

Al determination	Traditional µPADs	Distance-based µPADs
Instrument-free detection	No	Yes
Analytical dynamic range	0.5-7.0 ng (0.25-3.5 ppm)	2.0-30 ng (0.5-7.5 ppm)
LOD (ng)	0.5	2.0
Sample size (µL)	2.0	4.0

Movie S-1. Circular deposition of fluorescent reagent in traditional µPADs for color intensity-based determination of Al.

https://ars.els-cdn.com/content/image/1-s2.0-S000326701831064X-mmc2.mp4

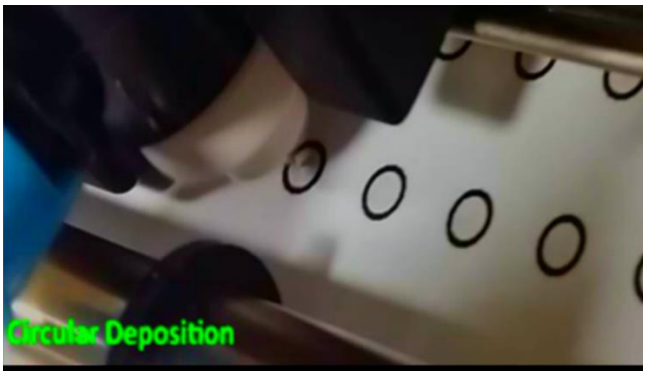

References for the supplementary information

[1] Silhouette Studio® V3 user's manual, https://cdn.silhouetteamerica.com/m/d/manual_silhouette-studio_v5.pdf, (accessed July 2017).

[1] DinoCapture 2.0 Users Guide, http://www.dino-lite.com/download03.php, (accessed November 2017).

Chapter 4- Effect of Device Geometry on Performance of Distance-Based µPADs

This chapter has been published as a research article in "Analytica Chimica Acta, 1063 (2019) 1-8." It is produced here with permission of the Elsevier. This article was also featured in the cover front of the journal.

4-1- Overview

Chloride (Cl^-) is an inorganic anion present in a broad range of samples (e.g. biological, environmental, food, water, etc.), the determination of which is of widespread significance. In this work, we translate the well-established traditional argentometric method (Mohr's precipitation titration) into a small, simple, portable, and low-cost paper-based microfluidic diagnostic device, which provides rapid and quantitative analysis. The developed device enables the determination of chloride sample volumes as small as 5 µL. A distance-based detection method is implemented providing fully instrument-free quantitation. The beneficial effects of channel geometry (variable widths with constant heights) on analytical parameters were investigated. Trapezoidal channels (channel width changes linearly with height) were used to create a gradient of paper surface (titrant) available for the reaction, compared to the typical uniform rectangular channels (constant channel width). The trapezoid with increasing width offered higher sensitivity and lower detection limits (i.e. 0.05 mM vs 0.1 mM from the rectangular channel) for chloride determination across the concentration range of 0.05-25 mM. In addition, the effect of concentration of the deposited reagent on the obtained distance signals was investigated using varying concentrations of titrant ($AgNO_3$), which allowed determination of chloride across a wider dynamic range (up to 200 mM). The utility of the paper devices was demonstrated by determination of chloride in a variety of matrices including body fluids (sweat, serum, and urine) and water samples (drinking, mineral, river water).

4-2- Introduction

The importance of chloride quantification, as a major anionic constituent of many environmental, food, health, and water samples, has been discussed and reported upon for over a century. Numerous analytical approaches have been introduced over this time for the determination of Cl^- delivering various levels of sensitivity and selectivity, according to need. Some of these methods, e.g. precipitation titrations, UV-Vis spectroscopy, potentiometry, and ion chromatography, are now well developed and have established themselves as standard laboratory-based techniques [1]. For instance, the precipitation titration is known to be a reliable and accurate classical technique, which measures the volume of the consumed titrant (e.g. $AgNO_3$ in the argentometric method) to determine the concentration of the target analyte (e.g. Cl^-), via the formation of insoluble products (e.g AgCl) during the titration. The Mohr method in particular, as one of the oldest (dating back to the mid-1800s), simplest, and most accurate argentometric titrations, is still commonly used as a reference technique today [2,3]. However, each of the above laboratory techniques has some disadvantages, including the cost and complexity of the required instrumentation, the need for skilled analysts, or the large volumes of samples and reagents required (e.g. for titrations). In isolation or in combination, these disadvantages exclude these standard approaches when rapid, low-cost, and 'point-of-care' or 'at-site' measurements are required.

Over the last decade, microfluidic paper-based analytical devices (µPADs) have emerged as a promising approach to address the growing demand for low-cost, rapid, portable, quantitative, disposable, and point-of-care analytical devices. In meeting some or all of these requirements, µPADs also offer other distinct inherent advantages, including ease of production, low sample and reagent consumption, and ease of use. In comparison to the

traditional microfluidic lab-on-a-chip platforms prepared from glass and PDMS etc., µPADs exploit the capillary forces within the paper substrate, which further eliminates the need for any mechanical or electrical power source to generate the liquid flow. Paper is typically compatible with most chemical and biological assays and has the added capability of being able to store the desired reagents for further analysis [4-7]. Microfluidic channels on µPADs are usually defined via creating hydrophobic barriers (using wax printing or other methods) on the paper surface which constrain the fluid flow [8-10].

Considering the critical detection step, over the years there have been several different detection techniques applied with µPADs, such as digital image colorimetry (DIC), electrochemistry, chemiluminescence, electrochemiluminescence, and fluorescence. Of these techniques, colorimetry has gained most popularity for simplicity reasons, and also due to its compatibility with a variety of portable and common low-cost detectors (e.g. modern smartphones, scanners, digital cameras, etc.), making the quantitative readout (color intensity measurement) relatively straightforward [11]. However, recently, distance-based detection methods have received increased attention, which eliminate the need entirely for any external detector/device and thus deliver instrument-free assays. In most distance-based µPADs, the sample flows along the microfluidic channels (rectangular) with the aid of the capillary action and consequently provides for interaction of the target solute present in the sample with the pre-deposited chromogenic reagents, resulting in the gradual depletion of the solute and the formation of a colored product zone. The color transition comes to a halt when the sample is completely depleted of all of the solute present. Finally, the length of the colored band measured against a calibrated scale, is proportional to the concentration of the target solute [12-21].

To-date very few µPADs based assays are commercially available, although some lateral flow test strips have emerged, e.g. test strips for chloride determination, based upon porous materials impregnated with chromogenic reagents and enclosed within plastic films, have been developed by Environmental Test Systems Inc. (Elkhart, Ind. U.S.A.), and are sold under the tradename “Quantab” [22]. However, little quantitative information on the performance of these strips has been published. Indeed, to-date and to the authors’ knowledge, there has not been any scientific article published that discusses in detail the performance of argentometric determination of chloride upon paper or other porous substrates. There are however reviews published detailing the advantages of µPADs over traditional dipsticks and lateral flow test strips to which the reader is directed [23,24].

Herein, we integrate the microfluidic distance-based concept and the chemistry from the Mohr titration to develop µPADs for instrument-free and single step quantification of chloride. The distance-based detection concept is further explored by investigating the effect of channel geometry on the analytical performance of µPADs. For the first time, trapezoidal shape detection channels are used for distance-based detection instead of typical rectangular channels. The mass transport along these asymmetrical microfluidic channels was investigated using a model fluid to mimic the distance-based detection. The effect of deposited reagent ($AgNO_3$) concentration on the obtained distance signals is also investigated by applying a higher level of titrant upon the detection channels. A proof-of-concept study was carried out using the developed µPADs for quantification of chloride in different media, including synthetic body fluid samples (sweat, serum, and urine) and also water samples (drinking, mineral, and river water). This extends the application of the fundamental

precipitation titrations further from only simple analysis (e.g. water samples) toward more significant biological and health-related analysis.

4-3- Experimental section

4-3-1- Chemicals and materials

All chemicals were of analytical reagent grade. Sodium chloride, sodium iodide, sodium bromide, potassium chromate, potassium di-chromate, silver nitrate, lactic acid, and ammonium hydroxide were purchased from Sigma-Aldrich. Nitric acid, hydrochloric acid, and isopropyl alcohol were supplied from Merck. Citric acid, sodium bicarbonate, urea, calcium chloride, magnesium sulfate, sodium sulfate, potassium dihydrogen phosphate, dipotassium hydrogen phosphate, glucose, ammonium chloride, and magnesium chloride were supplied from BHD Chemicals and used as received. In order to prepare the standard chloride solutions, sodium chloride was dried for 2 h in an oven at 120 °C and allowed to cool down in a desiccator. Water was treated with a Millipore (Bedford, MA, USA) Milli-Q water purification system and was used throughout. Whatman grade 1 qualitative filter paper with a pore size of 11 µm and thickness of 180 µm (GE Healthcare Australia Pty. Ltd, NSW, Australia) was used for fabrication of µPADs. Transparent laminating film (thickness of 125 µm, GBC, NSW, Australia) was used to laminate the µPADs.

4-3-2- Instrumentation

A wax printer (Colorqube 8870, Xerox, Norwalk, CT, USA) was utilized to print the microfluidic patterns upon the filter paper. The pen-plotting approach was used to deposit the chemical reagents over detection channels of the distance-based µPADs. The deposition was performed using Mars®matic 700 technical pens (STAEDTLER Mars GmbH & Co. KG,

Nuernberg, Germany, line width = 0.5 mm) filled with the reagents and inserted into the pen holder of a desktop electronic craft plotter/cutter (Silhouette CAMEO®, Kuluin, QLD, Australia). Silhouette Studio® (V4.1.156) free software was used to design the microfluidic layouts. The paper media was affixed on a Silhouette Cameo reusable cutting mat (12"×12" Cut12) and loaded into the plotter for the deposition step. The lamination step was carried out using an A3 laminator (LM330, Laminating Wholesalers, VIC, Australia) with adjustable lamination temperature. A potentiometric autotitrator (Metrohm, Model Titrando 905, Switzerland) along with an Ag Titrode electrode were employed to measure chloride content in unknown real samples.

4-3-3- Design and fabrication of µPADs

The detailed fabrication process of µPADs has been described previously [25,26]. Briefly, the distance-based microfluidic patterns were designed using the Silhouette Studio® and wax printed on both sides of the paper to ensure the complete confinement of the sample solution within the channels. The distance-based microfluidic patterns were composed of a sample zone and a straight detection channel. The outline and dimensions (before and after wax melting) of both rectangular and trapezoidal µPADs are illustrated in Figure S-1A. Scale bars were also designed at 1 mm intervals next to the channels for the naked eye reading of the length of the colored bands. The fabrication process was continued by deposition of the corresponding reagents upon the detection channels using multiple deposition lines [27]. In spite of different channel designs, the overall length of the deposition lines was kept the same (58 mm) for both trapezoidal and rectangular detection channels (Figure S-1B). This can ensure that the same amount of reagents (titrant) would be delivered to the detection channels which was a key point to support the comparative study performed in this work.

Afterward, the paper was laminated (165 °C) from both the top and bottom sides in order to melt the wax through the thickness of the paper. Photographs of µPADs through different steps of preparation are shown in Figure S-2.

4-3-4- Chloride determination

The distance-based chloride determination is based on the Mohr precipitation titration but in a reverse manner since herein the typical end-point product of the titration (i.e. brown Ag_2CrO_4 precipitate) was first formed upon the microfluidic channels resulting in formation of AgCl (white precipitate) after the sample (Cl^-) introduction. In the first step, the silver nitrate solution (50 mM) was deposited (plotting speed = 2 cm/s) over the channels and allowed to dry (2 min). In the second step, a chromate buffer solution was deposited over the channels resulting in formation of a brown silver chromate precipitate (Movie S1). The chromate buffer (pH = 7.2, 50 mM) was prepared via mixing the appropriate amount of potassium chromate and potassium di-chromate. These two steps were also performed in the reverse order (i.e. $AgNO_3$ on top of K_2CrO_4, result not shown); however, the first order created a better homogeneity and coverage of the chromate precipitate over the detection channels.

4-4- Results and discussion

4-4-1- Distance-based determination of chloride

Herein we utilized a variation of argentometric determination (Mohr titration method) where the silver chromate crystals were initially formed over the detection channels by depositing chromate solution over the silver layer. Here the brown colored silver chromate will function as the colorimetric indicator for the distance-based detection by turning to white color after loading the chloride sample onto the µPADs (Figure 1A). The main principle behind

this distance-based detection was the lower solubility of silver chloride compared to silver chromate which favours the formation of the chloride precipitate compared to its chromate counterpart. The chloride anions displace the chromate ions in the precipitate and form the white colored silver chloride crystals. This will result in the creation of a white colored band, the length of which can be correlated to the concentration of the chloride present in the sample. Figure 1B depicts the distance-based µPADs in different stages of their preparation and application.

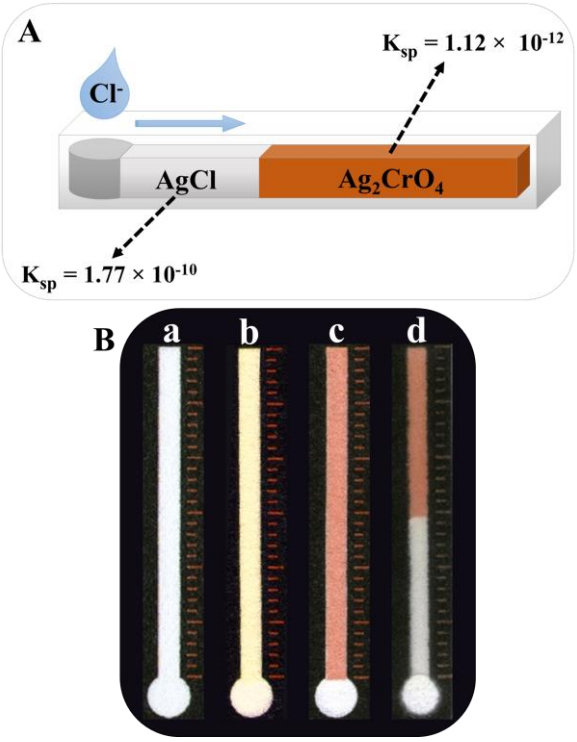

Figure 1. (A) Schematic representation of the argentometric distance-based determination of chloride on paper microfluidic channels. The difference in solubility value of silver chromate and silver chloride is the principle behind the observed phenomenon. (B) Photographs of µPADs in various stages of preparation and use: (a) Rectangular microfluidic pattern wax printed on paper. (b) Deposition of yellow color K_2CrO_4 solution upon the paper in the absence of $AgNO_3$ with no precipitate formation. (c) Deposition of chromate solution upon the channels which have already been subjected to $AgNO_3$ solution results in formation of the brown Ag_2CrO_4 precipitate. (d) Introduction of chloride sample into µPADs resulting in formation of the white AgCl colored band.

To acquire a distance signal upon the paper microfluidic channels, either the deposited reagents or the colored product of the reaction should be somehow (e.g. precipitation, aggregation, intermolecular interactions, etc.) immobilized on the paper. Otherwise, due to the washing away effect, the desired stable colored band with a sharp boundary defining the distance signal, cannot be created over the channels even if a visible color change occurs on the paper [12,28,29]. In the present case, both the indicating reagent (i.e. Ag_2CrO_4) and the product of the reaction (i.e. AgCl) are precipitated on the paper surface enabling formation of a stable colored band over the detection channels. Figure 2 shows SEM images of the paper substrates accommodating the crystals which are trapped throughout the paper fibers. SEM images of the plain filter paper are also shown in Figure S-3 for comparison. This was further confirmed (results not shown) by introducing water samples (6 µL, 3×) into the sample zone of the µPADs, before (only Ag_2CrO_4 on the channels) and after (including AgCl) being exposed to chloride samples. There was no washing away effect observed, which indicates the robust immobilization of the crystals upon the paper. In addition to the relatively large size of the crystals, which sees them captured within the paper pores, the results indicate the crystals may be also electrostatically attracted to the surface of the cellulose fibers.

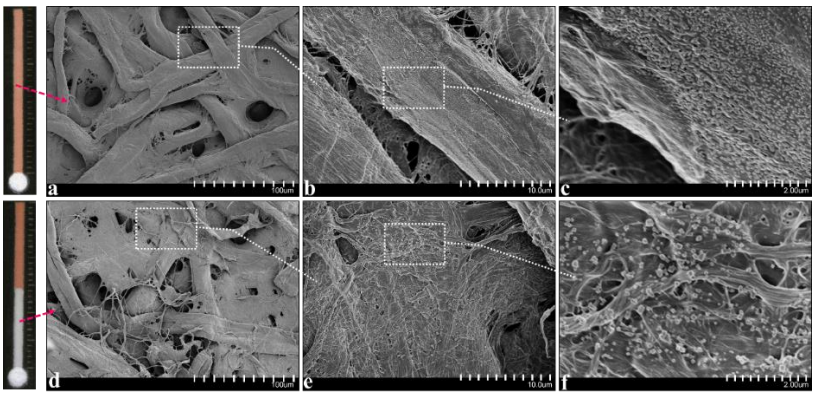

Figure 2. SEM images of the paper substrate in the detection channel area: (a-c) Silver chromate crystals immobilized in cellulosic network before loading the chloride sample into the µPADs. (d-f) Formation of silver chloride crystals trapped in paper fibers after introducing the chloride sample.

The fabricated distance-based µPADs were employed for instrument-free measurement of chloride by loading 5 µL of standard solutions (with varying concentrations) into the sample zones. Figure 3A shows the photograph of µPADs for determination of chloride over the range of 0.1-25 mM (3.5-886.25 mg/L). The calibration curve, determined from the measured distance signals, is also shown in Figure 3B. The shortest visible colored band (0.5 mm) from the beginning of the detection channel, was considered as the limit of detection which was obtained from the sample containing 0.1 mM of chloride. However, it is well known that in all argentometric methods the silver ion titrant forms precipitates not only with chloride, but also with bromide or iodide ions, essentially providing a total halide measurement in solutions where these interfering ions are present. However, in most of the target samples for this simple diagnostic (e.g. body fluids or natural waters) the level of bromide and iodide in relation to the target chloride ion is typically negligible and below the detection limit of the distance-based µPADs presented here, so they will not significantly affect the distance measured signals and quantitate performance of the assay. In cases where samples do contain significant amount of other halides, the total halide level can be considered, since the same distance signal can be correlated to the total halide value assuming that the distance-based µPADs respond to all halides in the same manner (i.e. producing the same distance signal individually). This was further verified by testing the distance-based µPADs with standard solutions of bromide, iodide, and also a mixture of all three halides and comparing that with the chloride sample. The distance signals obtained from all tested samples were the same (within 5% error) which confirms the viability of distance-based detection for the determination of total halide levels as well (Figure S-4). Since the herein used Mohr method is a very well established and accepted analytical method and also the mentioned commercial device uses the same principle in a distance-based format for chloride measurement, further

investigations regarding possible interferences from other anions or cations were deemed to be unnecessary. It is also well known that the normal level of coexisting ions in the target samples (especially the herein investigated body fluids and water samples) do not compromise the desired chloride measurements [30-33]. In addition, as will be presented in the following sections, the developed distance-based µPADs were successfully used for chloride measurement in several real samples presenting various matrixes where the results were further validated indicating the viability of the µPADs for chloride measurement not being affected by any interferences.

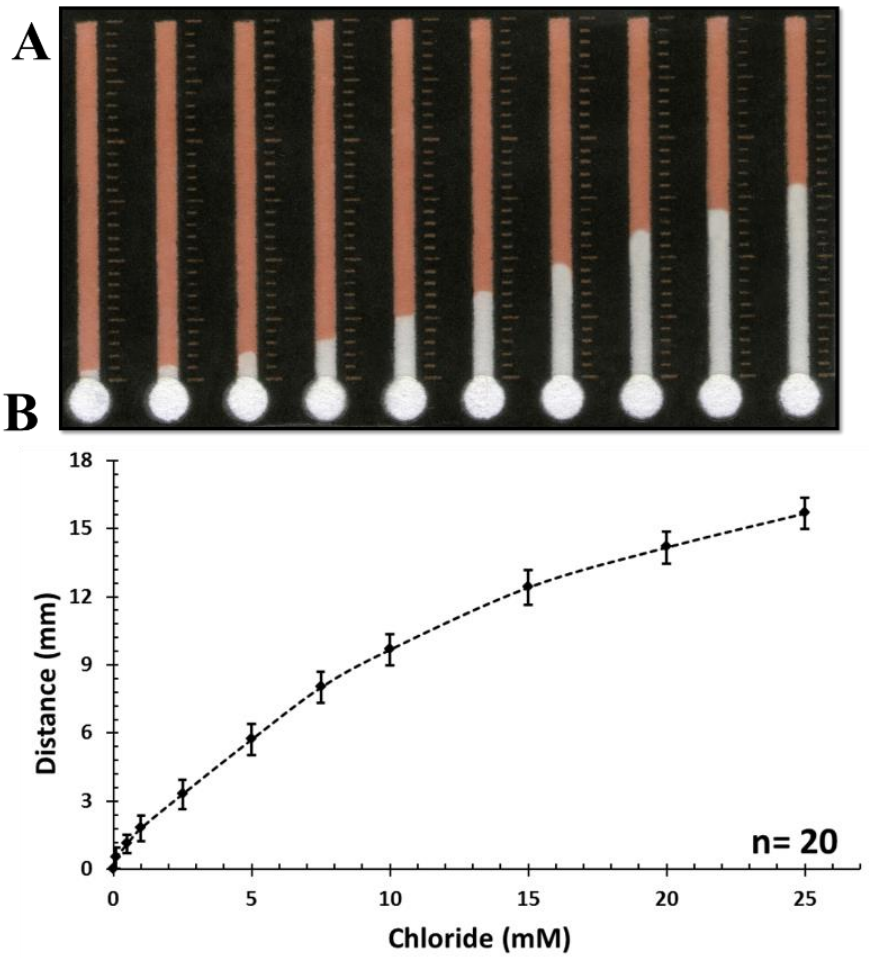

Figure 3. (A) Photograph of µPADs indicating the obtained distance signals after introducing 5 µL of standard chloride solutions in the range of 0.1-25 mM. (B) Corresponding response calibration curve acquired from distance-based detection of chloride. Markers reflect an average of 20 repetitive measurements. The error bars represent the standard deviations corresponding to the average values.

4-4-2- Mass transport along asymmetric channels

As mentioned earlier, distance-based µPADs with new channel designs (asymmetrical trapezoidal channels) were fabricated to investigate how channel geometry can improve the analytical performance by affecting the distance signal. However, before using the new channels for distance-based detection, the mass transport along them was investigated using a model ink. Two types of trapezoidal microfluidic channels with varying widths (Type A and B, Figure 4A) were designed to create a gradient of paper surface and deposited reagent (titrant) available along the detection channels, compared to the typical rectangular channels with constant width and uniform surface area. In spite of the different designs, the total surface area was kept exactly the same for all channels (Figure 4A, AA = AR = AB = 60 mm^2) in order to perform a valid comparison merely based on the differences in channel geometry. On the other hand, the channel length was also the same (30 mm) for all designs and was intentionally considered slightly longer than the solvent front (∽28 mm). This generates a fluid transport independent of the channel length. Capillary fluid transport along trapezoidal porous medium has been already studied in order to investigate the asymmetric fluid transport behavior, with results showing a flow pattern which does not follow the typical behavior predicted by the Washburn equation [34]. It was shown that the flow rate along the trapezoid with descending width along the channel (i.e. Type B in the present work) was faster than that on both the uniform channel (i.e. the Reference in here, Washburn flow profile) and also trapezoid channel with ascending width (i.e. Type A in here). We observed a similar flow pattern after introducing a dye solution (5 µL of eosin, 0.1% w/v in water) into the sample zone of µPADs and monitoring the solvent front (Figure 4B and Movie S2).

In spite of the reported work investigating the flow rate pattern along asymmetric microfluidic channels upon paper, there has not been any useful application shown for such designs. In this work, the flow rate patterns along the microfluidic channels were not reassessed, whereas the mass transport over the channels, as a crucial factor affecting the distance signals, was evaluated. Even though the solvent (water) front reaches almost to the end of all types of channels, the dye front stops before reaching to the end. This is due to the intermolecular interactions between the dye molecules and the paper surface, which see the dye molecules adsorbed and therefore retained on the paper. We used this phenomenon as a model to simulate distance-based detection by considering the paper surface itself as a deposited reactant and the dye as an analyte being captured along the detection channels by cellulosic fibers. Figure 4B depicts the time course of mass (dye) transport on paper channels with various channel geometries. In Type A the dye front traveled the longest distance although at the beginning it was lagging behind due to the lower flow rates compared to the other types. This reflects the fact that there is less paper surface available at the beginning of the channel to trap the dye, so there will be more free dye molecules remained traveling longer distances along the channel. Thus, Type A provides the highest mass transport among different designed paper microfluidic channels with the same total surface area.

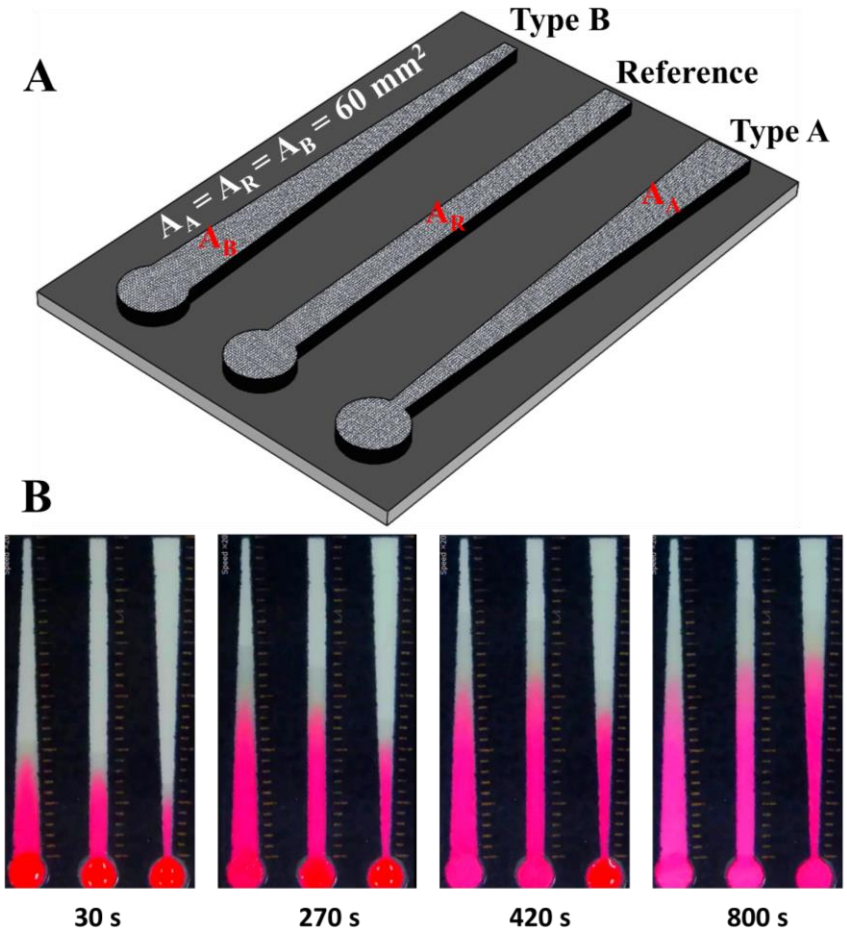

Figure 4. (A) Schematic representation of microfluidic channels designed with varying geometries. The length (30 mm) and also the overall surface area of all channel types are the same (AA = AR = AB = 60 mm^2). (B) Time course of mass transport on paper microfluidic channels with various geometries. A solution of eosin dye is used as a model illustrating the distance-based detection pattern over the channels. The photos were obtained from Movie S2.

4-4-3- The effect of channel geometry on distance signals

The effect of channel width on distance signals has been previously investigated on µPADs with constant channel width [26,27]. It was shown that wide channels produce shorter distance signals resulting in lower sensitivity and narrow channels produce longer distance signals which result in narrower dynamic range. Narrow channels also dramatically increase the assay time due to the low flow rates. Herein, we perform distance-based detection on channels with varying widths (gradient, 1-3 mm before lamination). After demonstrating the mass transport using the dye solution model, the trapezoidal channels were brought to use

in the here studied distance-based determination of chloride/halides. Photographs of both Type A and B trapezoidal µPADs for argentometric determination of chloride are depicted in Figure 5A and B, respectively. In colored bands which presented parabolic tips (especially for higher concentrations), the apexes were considered while reading the distance signals. Figure 5C represents the calibration curves obtained from the recorded distance signals from trapezoidal µPADs. The previously acquired curve from rectangular µPADs (Reference) is also shown for comparison.

Anticipated from the dye model experiment, Type A provides significantly higher sensitivity (slope of response curve) in the same concentration range (0-25 mM) in comparison to the other two types of channels. This improvement in sensitivity was more notable in lower levels of chloride which can be later useful when looking at samples containing very low concentrations of chloride. This is contributed with the asymmetrical shape of detection channels providing a gradient of paper surface which consequently generates an ascending gradient of titrant ($AgNO_3$) available to precipitate with the target chloride ions. This ascending gradient results in more unreacted analyte ions (chloride) which travel further along the channels and consequently create longer colored bands. A reverse effect was observed for Type B providing a descending gradient which causes higher depletion of analyte per distance unit along the channel. In addition to sensitivity, the LOD was also improved in Type A considering the LODs of 0.05, 0.1, and 0.5 mM for Type A, Reference, and Type B, respectively.

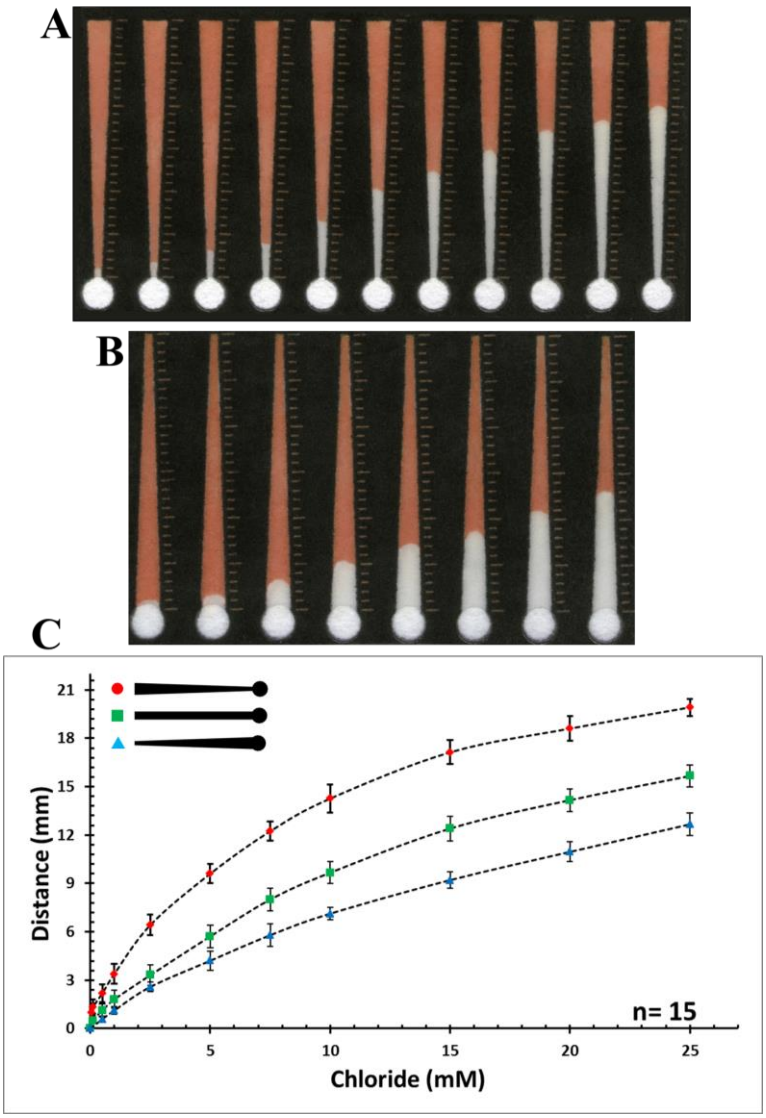

Figure 5. µPADs with trapezoidal detection channel geometries for determination of standard samples of chloride (5 µL) with different concentrations: (A) Type A, 0.05-25 mM. (B) Type B, 0.5-25 mM. (C) Response curves correlating the distance signals obtained from chloride measurement with trapezoidal µPADs. The response curve from the rectangular µPADs (showed previously in Figure 3B) is also shown as a reference for compression.

4-4-4- High range chloride determination

In order to achieve wider dynamic ranges for distance-based determination of chloride, the concentration of deposited titrant (AgNO3) was increased up to five times (250 mM vs 50 mM for low range). As expected, the color of silver chromate precipitate formed over the channels was darker which is due to higher level of AgNO3. It was observed that the higher the concentrations of titrant, the shorter the distance signals. This experiment was carried out

using only Type A distance-based µPADs which exhibited the best analytical performance. The distance-based determination of chloride was performed over the range of 2.5-200 mM. Photographs of high range µPADs along with the obtained calibration curve, are shown in Figure 6. This enables determination of chloride across wider concentration ranges, which can be used for samples containing a high level of chloride without any need for sample dilution.

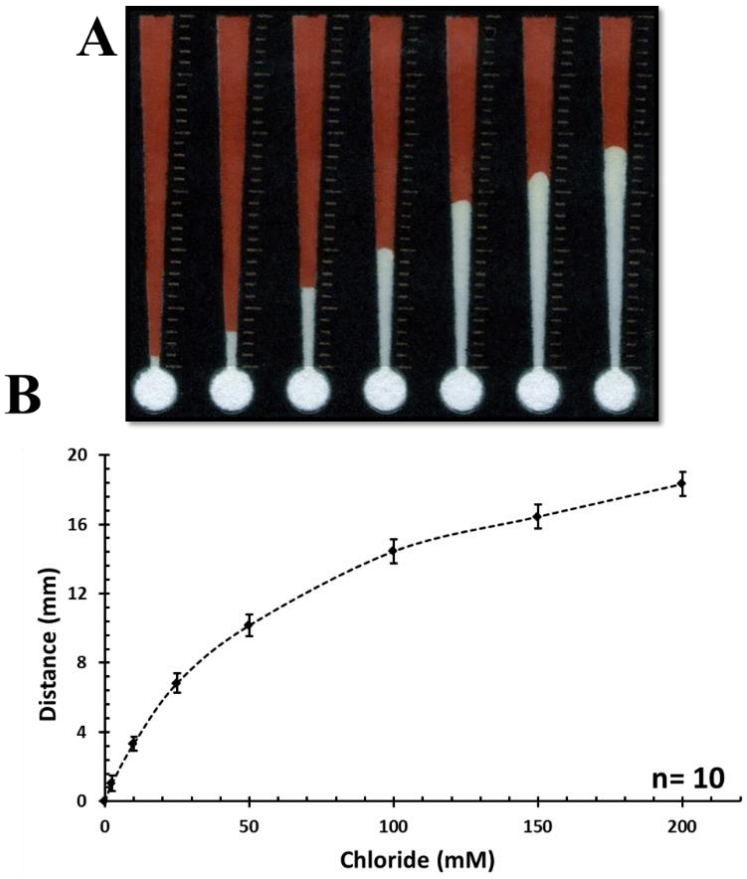

Figure 6. High range µPADs for chloride determination. (A) Photograph of Type A µPADs indicating the distance signals acquired from chloride samples with concentrations ranging in 2.5-200 mM. (B) Calibration curve of the corresponding distance-based measurements.

4-4-5- Quantification of chloride in real samples

Chloride is the most common anion in the body fluids (e.g. sweat, tear, urine, and serum) involved in many physiological functions. A number of diseases are diagnosed by monitoring the excessive or deficient level of chloride in different biological fluids. For instance, the

normal level of chloride in serum is in a range between 97-107 mM and the chloride level out of this range can be a symptom of some disorders such as Hyperchloraemia and Hypochloraemia. Cystic Fibrosis (CF) is another disease affecting multiple organs including the lungs and the intestines (especially in infants) which is diagnosed by high chloride level in sweat. Chloride level higher than 60 mM indicates a CF positive and according to Cystic Fibrosis Foundation (CFF) a sweat chloride sensor should be able to operate in a dynamic range of 10-160 mM. Monitoring urinary chloride is also crucial in evaluation of kidney's function diagnosing disorders such as volume depletion and metabolic alkalosis [35-37]. Nonetheless, the currently available techniques for determination of chloride extensively rely upon trained operators, expensive instruments, and relatively high volume of sample, which is a critical point when it comes to analysing some biological samples such as tear, sweat, and serum. The microfluidic instrument-free determination of chloride presented here, resolves all these issues and is a viable alternative for the current methods (e.g. Wescor Macroduct sweat check system [38]).

The Type A distance-based µPADs were employed for determination of chloride in various real samples to verify their viability for various matrices (n= 6). Artificial sweat, serum, and urine samples were prepared according to standard recipes (details in Supporting Information). In order to further investigate the performance of µPADs, some water samples, including river estuary water (River Derwent, Tasmania, Australia, diluted 10×), drinking water, and mineral water (Icelandic Water Holdings, Ölfus, Iceland) were also analysed. Chloride levels in these unknown water samples were also validated using a potentiometric autotitrator. The results of all real sample analysis are summarized in Table 1 indicating that

µPADs can be a reliable, practical, instrument-free, and easy to use alternative for conventional methods in chloride determination.

In particular, compared to the commercial test strips (i.e. Quantab), the presented microfluidic paper-based format is simpler to fabricate. These µPADs are simply produced using wax printing and pen-plotting methods followed by a finishing lamination step which makes this approach ideal for rapid bench-top prototyping. The µPADs can be used for a wide range of samples (e.g tear, serum, and sweat) due to the microscale sample volumes (e.g. 5 µL vs milliliter scale for test strips) which permits direct analysis of samples without any initial dilution. The dimension of µPADs can be scaled down further to allocate even smaller volumes of sample (e.g. 1 µL). As demonstrated in this work, the geometry and design of µPADs can be also optimized in order to improve analytical parameters such as sensitivity.

Table 1. Measurement of chloride level (mM) in various real samples

Samples	Expected value/Auto titrator[a]	µPADs
Sweat	18.5	17.8±1.57
Serum	111.8	119.3±2.37
Urine	117.5	115.3±4.62
Mineral water	0.35±0.03	0.39±0.07
Tap water	0.27±0.01	0.33±0.06
River estuary water	497.8±8.05	544.1±14.1

[a]For the body fluid samples the expected Cl^- concentration was considered and the water samples were validated using autotitrator (n= 4).

4-5- Conclusions

For the immobilized assay, the traditional argentometric titration has been converted into distance-based detection format on µPADs for instrument-free quantification of chloride.

Herein we have demonstrated the applicability of the distance-based µPADs by successfully utilizing them for chloride measurement in a variety of complex biological media and water samples. This could easily be even further extended to chloride determination in other complex samples for medical, food, agricultural, environmental, and industrial point-of-need analysis. The distance-based detection principle has been further developed by introducing new detection channel geometries in order to improve the analytical performance of the µPADs. It is also shown that increasing the concentration of the reagent deposited over the channels, results in wider dynamic ranges enabling detection of higher levels of the target analyte. This work distinctly illustrates that incorporation of classical well-established analytical concepts within current microfluidic paper-based platforms yields modern miniaturized analytical approaches leading to numerous advantages. Finally, considering precipitation titration as a fundamental analytical technique whereas paper-based microfluidic as an emerging modern analytical technique, the simplicity and accessibility of the presented integrated paperfluidic concept can be even used for teaching purposes.

4-6- References

[1] T.R. Crompton, Determination of anions in natural and treated waters, CRC Press, 2014.

[2] W.E. Federation, A.P.H. Association, Standard methods for the examination of water and wastewater, American Public Health Association (APHA): Washington, DC, USA, (2005).

[3] D.C. Harris, Quantitative chemical analysis, Macmillan, 2010.

[4] P.N. Nge, C.I. Rogers, A.T. Woolley, Advances in microfluidic materials, functions, integration, and applications, Chemical Reviews, 113 (2013) 2550-2583.

[5] D.M. Cate, J.A. Adkins, J. Mettakoonpitak, C.S. Henry, Recent developments in paper-based microfluidic devices, Analytical Chemistry, 87 (2015) 19-41.

[6] Y. Yang, E. Noviana, M.P. Nguyen, B.J. Geiss, D.S. Dandy, C.S. Henry, Paper-based microfluidic devices: emerging themes and applications, Analytical Chemistry, 89 (2017) 71-91.

[7] M.M. Gong, D. Sinton, Turning the page: advancing paper-based microfluidics for broad diagnostic application, Chemical reviews, 117 (2017) 8447-8480.

[8] Y. He, Y. Wu, J.Z. Fu, W.B. Wu, Fabrication of paper-based microfluidic analysis devices: a review, RSC Advances, 5 (2015) 78109-78127.

[9] Y. Xia, J. Si, Z. Li, Fabrication techniques for microfluidic paper-based analytical devices and their applications for biological testing: A review, Biosensors and Bioelectronics, 77 (2016) 774-789.

[10] X. Jiang, Z.H. Fan, Fabrication and operation of paper-based analytical devices, Annual Review of Analytical Chemistry, 9 (2016) 203-222.

[11] G.G. Morbioli, T. Mazzu-Nascimento, A.M. Stockton, E. Carrilho, Technical aspects and challenges of colorimetric detection with microfluidic paper-based analytical devices (μPADs)-a review, Analytica chimica acta, 970 (2017) 1-22.

[12] D.M. Cate, W. Dungchai, J.C. Cunningham, J. Volckens, C.S. Henry, Simple, distance-based measurement for paper analytical devices, Lab on a Chip, 13 (2013) 2397-2404.

[13] X. Wei, T. Tian, S. Jia, Z. Zhu, Y. Ma, J. Sun, Z. Lin, C.J. Yang, Target-responsive DNA hydrogel mediated stop-flow microfluidic paper-based analytic device for rapid, portable and visual detection of multiple targets, Analytical Chemistry, 87 (2015) 4275-4282.

[14] T. Tian, J. Li, Y. Song, L. Zhou, Z. Zhu, C.J. Yang, Distance-based microfluidic quantitative detection methods for point-of-care testing, Lab on a Chip, 16 (2016) 1139-1151.

[15] X. Wei, T. Tian, S. Jia, Z. Zhu, Y. Ma, J. Sun, Z. Lin, C.J. Yang, Microfluidic distance readout sweet hydrogel integrated paper-based analytical device (μDiSH-PAD) for visual quantitative point-of-care testing, Analytical Chemistry, 88 (2016) 2345-2352.

[16] Y. Zhang, D. Gao, J. Fan, J. Nie, S. Le, W. Zhu, J. Yang, J. Li, Naked-eye quantitative aptamer-based assay on paper device, Biosensors and Bioelectronics, 78 (2016) 538-546.

[17] M. Srisa-Art, K.E. Boehle, B.J. Geiss, C.S. Henry, Highly sensitive detection of salmonella typhimurium using a colorimetric paper-based analytical device coupled with immunomagnetic separation, Analytical chemistry, 90 (2017) 1035-1043.

[18] T. Tian, Y. An, Y. Wu, Y. Song, Z. Zhu, C. Yang, Integrated distance-based origami paper analytical device for one-step visualized analysis, ACS Applied Materials and Interfaces, 9 (2017) 30480-30487.

[19] C.W. Quinn, D.M. Cate, D.D. Miller-Lionberg, T. Reilly III, J. Volckens, C.S. Henry, Solid-phase extraction coupled to a paper-based technique for trace copper detection in drinking water, Environmental science & technology, 52 (2018) 3567-3573.

[20] Y. Chen, W. Chu, W. Liu, X. Guo, Distance-based carcinoembryonic antigen assay on microfluidic paper immunodevice, Sensors and Actuators B: Chemical, 260 (2018) 452-459.

[21] C.T. Gerold, E. Bakker, C.S. Henry, Selective distance-based k+ quantification on paper-based microfluidics, Analytical chemistry, 90 (2018) 4894-4900.

[22] Terry, Carol Ann. Test devices and methods for determining halides in aqueous samples. U.S. Patent 5,229,299, July 20, 1993.

[23] A.K. Yetisen, M.S. Akram, C.R. Lowe, Paper-based microfluidic point-of-care diagnostic devices, Lab on a Chip, 13 (2013) 2210-2251.

[24] K. Yamada, H. Shibata, K. Suzuki, D. Citterio, Toward practical application of paper-based microfluidics for medical diagnostics: state-of-the-art and challenges, Lab on a Chip, 17 (2017) 1206-1249.

[25] N. Nuchtavorn, M. Macka, A novel highly flexible, simple, rapid and low-cost fabrication tool for paper-based microfluidic devices (µPADs) using technical drawing pens and in-house formulated aqueous inks, Analytica chimica acta, 919 (2016) 70-77.

[26] M. Rahbar, P.N. Nesterenko, B. Paull, M. Macka, Geometrical alignment of multiple fabrication steps for rapid prototyping of microfluidic paper-based analytical devices, Analytical chemistry, 89 (2017) 11918-11923.

[27] M. Rahbar, P.N. Nesterenko, B. Paull, M. Macka, High-throughput deposition of chemical reagents via pen-plotting technique for microfluidic paper-based analytical devices, Analytica Chimica Acta, 1047 (2019) 115-123.

[28] D.M. Cate, S.D. Noblitt, J. Volckens, C.S. Henry, Multiplexed paper analytical device for quantification of metals using distance-based detection, Lab on a Chip, 15 (2015) 2808-2818.

[29] K. Yamada, T.G. Henares, K. Suzuki, D. Citterio, Distance-based tear lactoferrin assay on microfluidic paper device using interfacial interactions on surface-modified cellulose, ACS Applied Materials and Interfaces, 7 (2015) 24864-24875.

[30] P.J. Sloan, G. Beevers, F.E. Baxter, The Quantab strip in the measurement of urinary chloride and sodium concentrations, Clinical chemistry, 30 (1984) 1705-1707.

[31] R.W. Jeffery, V.A. Mullenbach, W.M. Bjornson-Benson, R. J. Prineas, J.L. Forster, D. G. Schlundt, Home testing of urine chloride to estimate dietary sodium intake: evaluation of feasibility and accuracy, Addictive behaviors, 12 (1987) 17-21.

[32] D.C. Harris, Quantitative Chemical Analysis. Macmillan, 2010.

[33] H.T. Sheen, H.L. Kahler, Effect of ions on Mohr method for chloride determination, Industrial & Engineering Chemistry Analytical Edition, 10 (1938) 628-629.

[34] D. Shou, L. Ye, J. Fan, K. Fu, M. Mei, H. Wang, Q. Chen, Geometry-induced asymmetric capillary flow, Langmuir, 30 (2014) 5448-5454.

[35] H.S. Toh, C. Batchelor-McAuley, K. Tschulik, R.G. Compton, Electrochemical detection of chloride levels in sweat using silver nanoparticles: a basis for the preliminary screening for cystic fibrosis, Analyst, 138 (2013) 4292-4297.

[36] N.A. Brunzel, Fundamentals of urine and body fluid analysis, Elsevier Health Sciences, 2016.

[37] K. Berend, L.H. van Hulsteijn, R.O. Gans, Chloride: the queen of electrolytes? European journal of internal medicine, 23 (2012) 203-211.

[38] A. Lynch, D. Diamond, M. Leader, Point-of-need diagnosis of cystic fibrosis using a potentiometric ion-selective electrode array, Analyst, 125 (2000) 2264-2267.

4-7- Supplementary information for chapter 4

4-7-1- Preparation of artificial test solutions

Sweat sample was produced based on a British Standard (BS EN1811-1999) [1] and by mixing 18.5 mM sodium chloride, 2.1 mM urea, 1.3 mM lactic acid in Milli-Q water (18.2MΩ cm^{-1}). The pH of the solution was adjusted to 6.5 using ammonium hydroxide and nitric acid.

Serum sample was modeled by mixing 111 mM sodium chloride, 0.8 mM magnesium chloride, 29 mM sodium bicarbonate, 2.2 mM dipotassium hydrogen phosphate, 2.5 mM urea and 4.7 mM glucose in Milli-Q water (18.2MΩ cm^{-1}) [2].

Urine solution was prepared according to a previous report [3] and comprised of 90 mM sodium chloride, 25 mM ammonium chloride, 2.5 mM calcium chloride, 1.1 mM lactic acid, 2.0 mM citric acid, 25 mM sodium bicarbonate, 170 mM urea, 2.0 mM magnesium sulfate, 10 mM sodium sulfate, 7.0 mM potassium dihydrogen phosphate, and 7.0 mM dipotassium hydrogen phosphate in Milli-Q water (18.2MΩ cm^{-1}). The pH of the solution was adjusted to 6.0 by addition of 1.0 M hydrochloric acid. This solution was kept in the refrigerator until use.

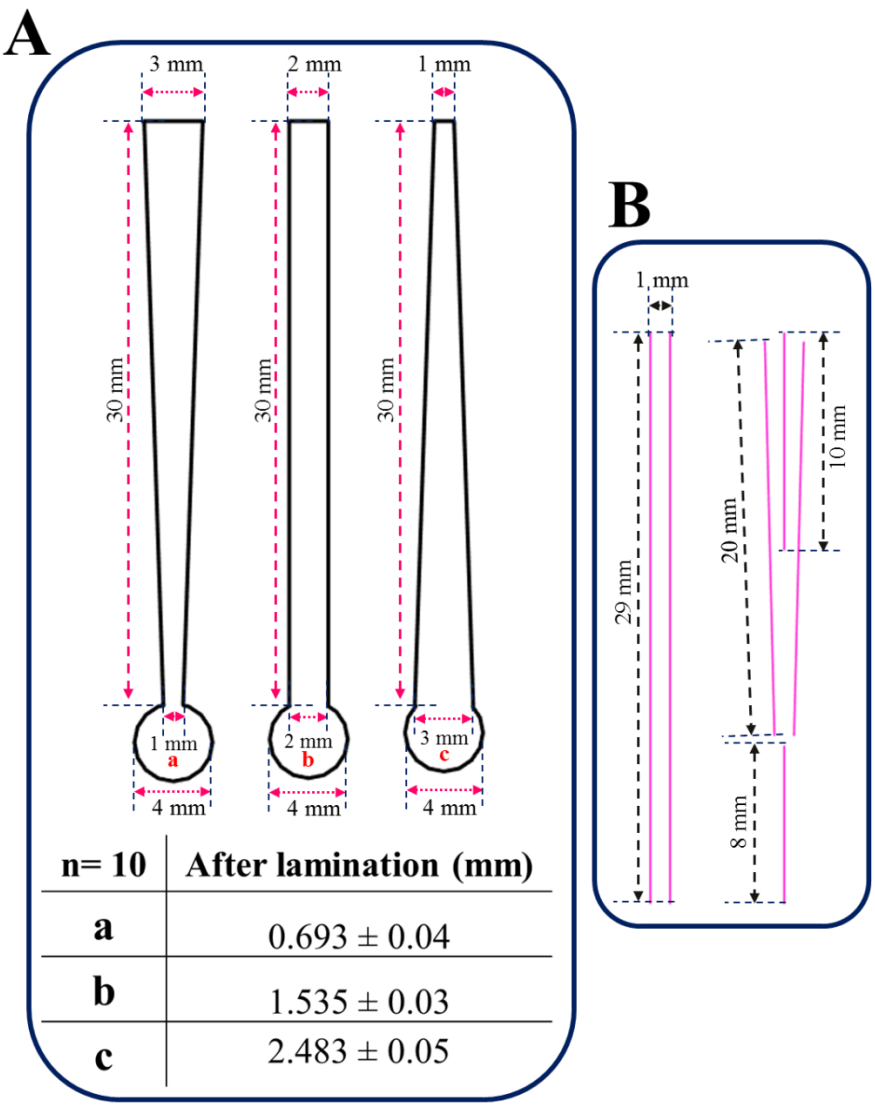

n= 10	After lamination (mm)
a	0.693 ± 0.04
b	1.535 ± 0.03
c	2.483 ± 0.05

Figure S-1. (A) Outline of distance-based microfluidic patterns. The presented dimensions correspond to the values set in the Silhouette Studio software for wax printing step. The corresponding table illustrates values regarding the actual sizes of bases (i.e. a, b, and c) of the rectangular and trapezoidal detection channels after lamination step and wax melting. (B) The dimensions and orientations of deposition lines designed within both the rectangular and trapezoidal detection channels for deposition of reagents via the pen-plotting method. The overall length of both designed deposition patterns (comprising distinct lines) is the same (58 mm) to ensure delivering the same amount of reagent into the detection channels of distance-based µPADs with different geometries.

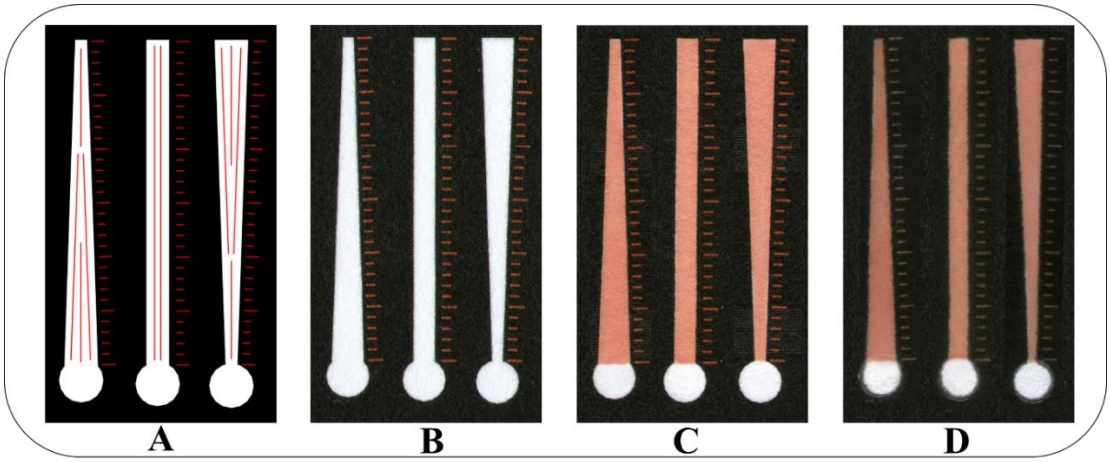

Figure S-2. Distance-based µPADs in different steps of preparation. (A) Computer design layout. The position of multiple deposition lines within the detection channels are also depicted. (B) Wax printed patterns on filter paper. (C) Deposition of reagents via the pen-plotting approach and formation of brown silver chromate precipitate upon the detection channels. The reagent concentration was optimized to produce the lowest detection limit in the widest possible dynamic range while having a stable, reproducible, and obvious colored band with well-defined end points formed over the channels. Both the silver and chromate solutions were mixed with isopropanol (20% v/v) before filling the technical pens. This facilitates the chemical ink flow from the pens and ensures a more homogeneous deposition over the paper. (D) Lamination of the devices from both top and bottom sides in order to melt the wax. Lamination also provides the µPADs with other benefits including a higher mechanical stability, prevention of any fluid leakage or evaporation during the assay, and protecting the detection channels from any possible cross contamination.

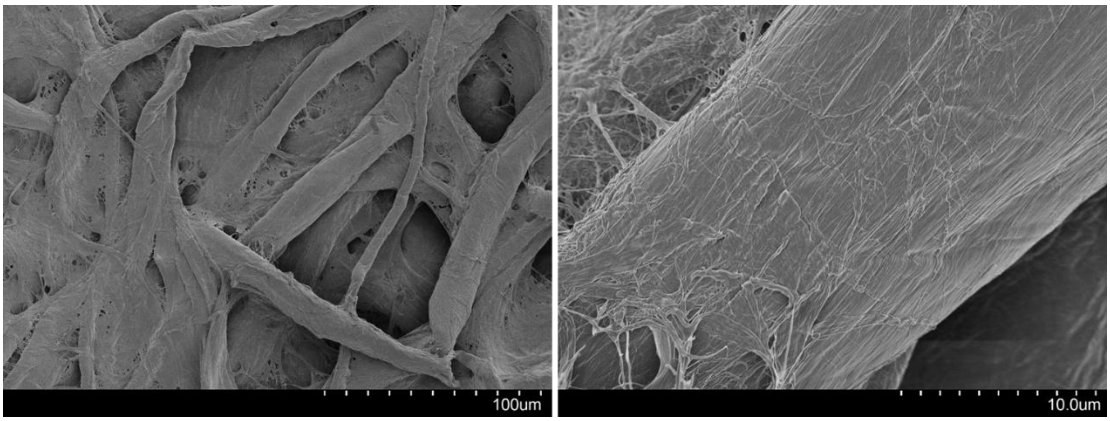

Figure S-3. SEM images of plain filter paper before deposition of any reagent. This is for comparison with images showed in Figure S-3.

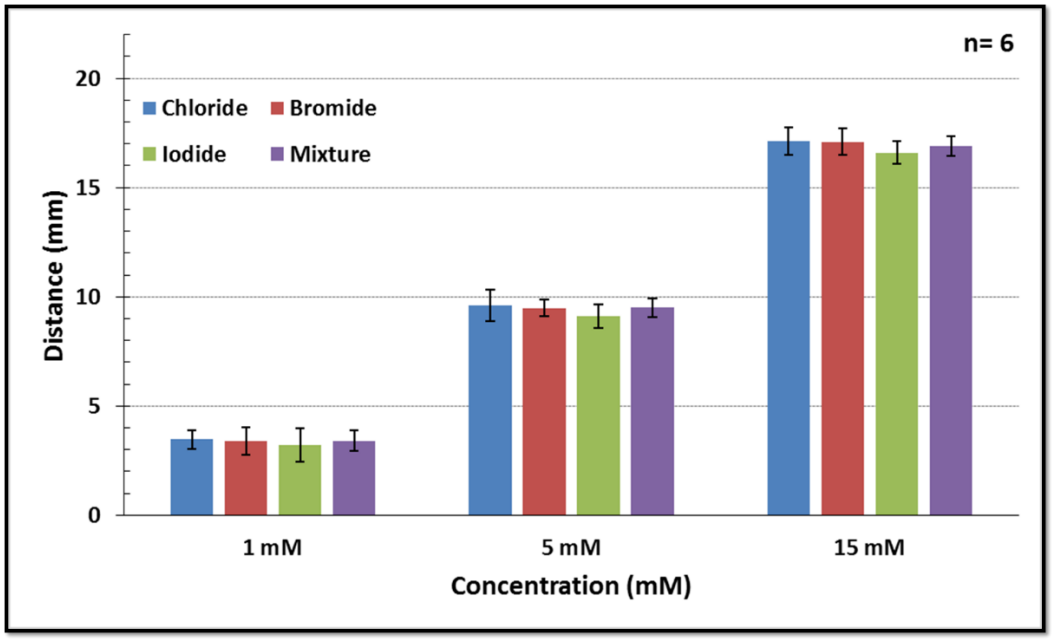

Figure S-4. Distance-based detection of halides. Standard solutions of three different halides individually and also a mixture of all of them were analysed with the distance-based µPADs (only rectangular one). Three different concentrations were tested. The distance signals obtained for all four different types of tested solutions, were identical (within 5% error) verifying the equal response of distance-based µPADs to different halides. This is important when looking at the total halide level.

Movie S-1. Deposition step of µPADs fabrication via the pen-plotting approach. The following reaction was performed by depositing yellow color potassium chromate solution upon the microfluidic channels which were initially impregnated with silver nitrate. This movie is only for demonstration purposes illustrating how the chromate crystals form on the paper surface. Herein, the microfluidic designs are intentionally printed upon the paper with a white surrounding which improves the visibility while video recording the formation of the brown silver chromate requiring preferably a white background for obvious illustration of the generated color. The original patterns used in this work for chloride detection were printed in an offset format giving each design a black surrounding not suitable for recording purposes.

$$2AgNO_3 + K_2CrO_4 \longrightarrow \underset{\text{(Brown)}}{Ag_2CrO_4\downarrow} + 2KNO_3$$
(Yellow)

https://ars.els-cdn.com/content/image/1-s2.0-S0003267019302375-mmc1.mp4

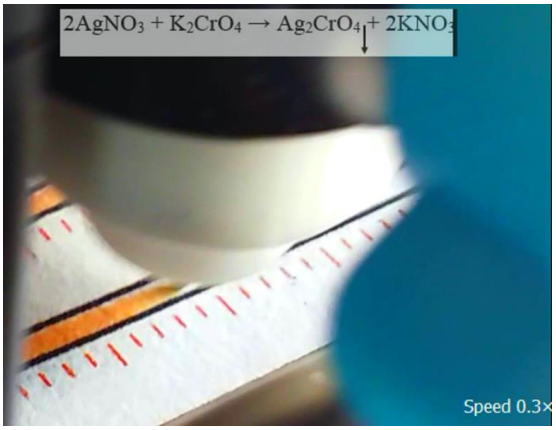

Movie S-2. Mass transport on microfluidic channels with different geometries. Eosin dye solution (5 µL, 0.1% w/v in water) is used as a model solution to demonstrate the mass transport phenomenon along the paper microfluidic channels with varying geometries.

https://ars.els-cdn.com/content/image/1-s2.0-S0003267019302375-mmc2.mp4

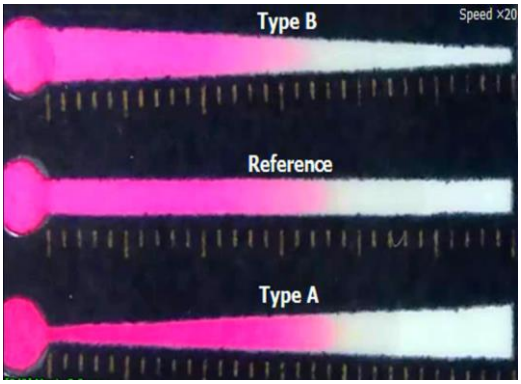

References for the supplementary information

[1] K. Kulthong, S. Srisung, K. Boonpavanitchakul, W. Kangwansupamonkon, R. Maniratanachote, Determination of silver nanoparticle release from antibacterial fabrics into artificial sweat, Particle and fibre toxicology, 7 (2010) 1.

[2] M. Novell, T. Guinovart, P. Blondeau, F.X. Rius, F.J. Andrade, A paper-based potentiometric cell for decentralized monitoring of Li levels in whole blood, Lab on a Chip, 14 (2014) 1308-1314

[3] T. Brooks, C. Keevil, A simple artificial urine for the growth of urinary pathogens, Letters in applied microbiology, 24 (1997) 203-206.

Chapter 5- Ion-Exchange Based Immobilization of Colorimetric Reagents on Distance-Based µPADs

This chapter has been published as a research article in “Analytical Chemistry, 91(14) (2019) 8756-8761.” It is produced here with permission of the American Chemical Society.

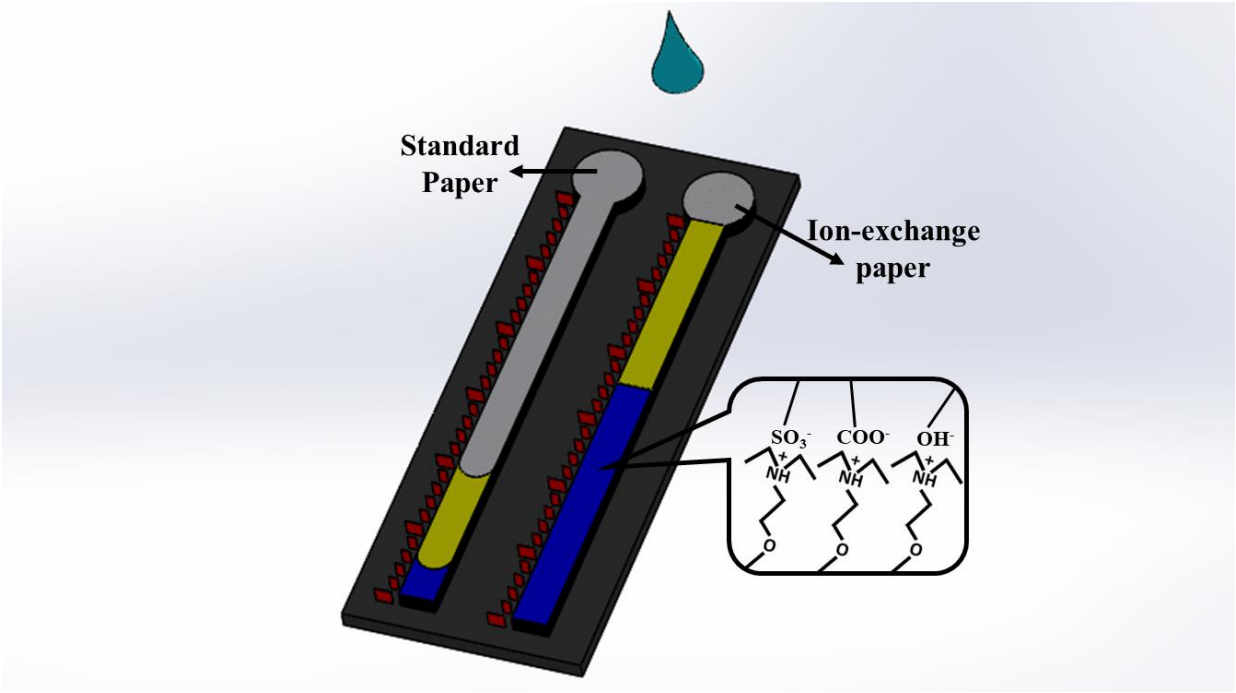

5-1- Overview

Distance-based detection methods, as used in development of microfluidic paper analytical devices (µPADs), rely on the dynamic formation of a colored band along the length of paper microfluidic channels. The color change is driven by the reaction of chromogenic reagents (typically water-insoluble) that are bound to the paper, thus not subject to being washed away by the sample flow along the detection channel. Here, we introduce the use of an anion-exchange filter paper (as a replacement for standard, unmodified filter paper) for distance-based detection in µPADs, in order to immobilize the water-soluble anionic reagents upon the paper detection channels based on ion-exchange interactions of the oppositely charged paper (protonated tertiary amine groups) and the anionic groups of the reagents. The ion-exchange (IE) paper was initially characterized and its properties were compared with standard cellulose paper. The IE paper was shown to be capable of strong retention of anionic reagents exhibiting acidic functional groups (carboxylic, sulfonic), which become deprotonated and negatively charged when in contact with the IE paper. The effect of the ionic strength (10-250 mM Cl^-) and pH (1-13) on the immobilization of the investigated reagents were also determined. The IE-µPADs were then modified with anionic chromogenic reagents and applied to distance-based determination of total calcium (LOD = 0.03 mM) and total acidity (LOD = 2.5 mM) content in serum and wine samples, respectively. The detailed mechanisms of the developed assays on the IE paper are also discussed. We propose that IE-µPADs represent a useful new addition to the distance-based detection toolbox and considerably enhance the applicability of such detection method.

5-2- Introduction

Microfluidic paper-based analytical devices (µPADs) have evolved in the last decade to respond to the growing need for low-cost, rapid, portable, and accessible point-of-care diagnostics. The detection step in such devices is typically based on a colorimetric reaction in which a reagent bound to the paper produces a colored product after reacting with target analyte present in the sample. In traditional µPADs, quantitative analysis requires digital image colorimetry (DIC), in which color and intensity are related to analyte concentration via a camera and image-processing software [1,2]. Unfortunately, there are some issues and concerns associated with color development in µPAD analysis, including the 'coffee-ring effect' [3] which compromises the homogeneity and intensity of the color pattern, consequently affecting the analytical parameters obtained from DIC. The coffee-ring effect is caused by the fact that there are typically weak attractive forces between the chromogenic reagents (or the colored products of the reaction) and the paper fibers, such that the developed color pattern becomes washed away and/or shifts toward the edges of the detection zone as sample flows through the device [3-5]. There is great interest in solving this problem by modification of the paper surface by functionalized nanomaterials or oxidizing agents to create attractive forces (e.g. electrostatic interactions) between the reagents (or colored products) and the paper fibers. These efforts have been relatively satisfactory, resulting in more uniform color patterns and consequently better analytical performance [5-12]. However, these approaches are not universal and often require relatively tedious preparation steps for each particular assay. Moreover, multiple exposures to different solutions throughout the modification process can deteriorate the mechanical stability and wicking properties of the filter paper (because of the limited wet strength of paper).

A promising alternative to quantitation on µPADs is the use of "distance-based" detection, in which the amount of analyte is converted into a distance signal on a channel, allowing for analysis by eye (with no external instrumentation) [13-17]. But these methods typically require continuous flow of sample or other solvent through the channel, which exacerbates the challenge of weak interactions between the reagents (or the colored products) and the paper fibers. This challenge is especially problematic at the beginning of the detection channel because of the higher flow rates in this region [18]. This limits the applicability of the distance-based detection to a limited number of colorimetric reactions, specifically those that rely on water-insoluble chromogenic reagents or colored products that form precipitates or large crystals that can become trapped within the 3D structure of the cellulose [19-26]. It has been shown that in order to develop distance-based assays which do not necessarily rely on precipitation reactions but rather involve water-soluble chromogenic reagents, the paper must be extensively modified to retain the reagents and thus to allow formation of a stable distance signal [14].

In response to the challenges described above, we introduce a new suite of methods for immobilizing chromogenic reagents on distance-based µPADs. The new methods rely on anion exchange filter paper (instead of conventional, unmodified filter paper) to allow for convenient electrostatic immobilization of anionic chromogenic reagents (as the most widely used in (bio)chemical assays), such that they will not be washed away by the sample fluid flow. The IE paper used here is modified to present pH-buffered weakly basic constituents, which can cause deprotonation and thus immobilization of acidic reagents such that they become affixed within the paper in the detection channels. This represents a simple, straight-forward, and comprehensive approach to immobilization which can be applied to a wide

variety of reagents without specific modification, functionalization, or preparation process for different assays. Herein we describe experiments evaluating the fluidic properties of the IE paper, as well as the effect of pH and ionic strength on displacement of deposited reagents. Most importantly, we evaluate the applicability of the new technique for distance-based µPAD measurements applied to quantifying Ca^{2+} in serum and total acidity in wine.

5-3- Experimental section

5-3-1- Chemicals and materials

Unless otherwise specified, reagents were purchased from Sigma-Aldrich (Oakville, ON, Canada), and all aqueous solutions were prepared in deionized water (DI water) with a resistivity >18 MΩ•cm obtained from a Millipore (Bedford, MA, USA) Milli-Q water purification system. All chromogenic reagents were in their acid form except 2,6-Dichlorophenolindophenol (DCPIP) which was in its sodium salt form. Whatman grade 1 and DE81 ion-exchange filter papers (GE Healthcare Australia Pty. Ltd, NSW, Australia) were used for fabrication of the µPADs. Transparent laminating film (thickness of 125 µm, GBC, ON, Canada) was used to laminate the µPADs.

5-3-2- Measurement of total calcium and acidity

The chromogenic detection reagent solution for the determination of Ca^{2+} comprised arsenazo III (1 mM), TBE (5×) buffer, and isopropanol (10% v/v). For the determination of total acidity, bromothymol blue (1 mM in 20% v/v ethanol) was used as the colorimetric reagent. In both cases, reagents were deposited upon the detection channels using the pen-plotting approach [17,27] (plotting speed = 1 cm/s) and were allowed to dry (2 min) before the final

lamination step. Further details regarding instrumentation and fabrication of µPADs can be found in the Supporting Information.

5-4- Results and discussion

5-4-1- Characterization of the IE paper

The DE81 anion exchange filter paper used here comprises a cellulose substrate that is modified with diethylaminoethyl (DEAE) functional groups (pKa= 9.5) [28] which are protonated and therefore positively charged at neutral pH. This type of IE paper has been traditionally used in enzyme assays, DNA polymerase tests, and for separation of anions, nucleotides, and amino acids. Here we introduce the use of DEAE paper as a substrate for fabrication of µPADs to immobilize the anionic colorimetric reagents.

The DEAE paper used here was initially characterized and compared with conventional filter paper for use as a substrate for µPADs. First, SEM images revealed no obvious differences between the morphology of the IE paper relative to conventional paper (Figure S-1). Then, the new substrates were evaluated for printability, an important property for paper substrates used in the fabrication of µPADs. As shown in Figure S-2, the IE paper was found to be print compatible, and (most importantly) was capable of supporting printed-wax structures that could confine aqueous solutions within them. Finally, flow rate in µPADs formed from both types of paper was measured. It was found that the IE paper presented a slightly lower flow rate than conventional filter paper (Figure S-3), but one that is well within the range of utility for distance-based detection. This also indicates that the IE paper has similar pore size in relation to the pore size of the standard paper (11 µm).

After demonstrating utility for µPAD functionality, attention was turned to evaluating the anion exchange properties of the IE paper. Being aware that the IE paper used in the present work was a weakly basic anion exchanger, an experiment was designed to measure the effective basicity (pKa) of the paper. A series of pH indicators (pKa ranging 7.1-11.2) were selected and their dilute solutions (0.1% w/v in 20% v/v ethanol) were pipetted onto the paper (Figure S-4). Starting from low pH and moving to high pH, the pKa of the first indicator for which the IE paper was not able to convert to its basic form (as realized via a lack of color change), was considered as the effective pKa of the paper. As reported by the manufacturer, this value was found to be approximately 9.4. This is important to know, as the pKas of the paper, the chromogenic reagents, and the analytes must be considered when designing distance-based assays. Further details regarding characterization of the IE paper can be found in the Supporting Information.

5-4-2- Immobilization tests

Fluorescein was selected as a model anionic analyte to evaluate the capability of the IE paper for electrostatic immobilization. Two spots of fluorescein (0.1 µL, 0.1 mM in water) were pipetted on the paper channels in IE-µPADs and after drying, water was introduced (10 µL- 3×) into the inlets. Importantly, the spots remained intact and no elution was observed, indicating a strong interaction between fluorescein and the IE paper surface (Figure 1A). This was further confirmed by keeping a paper strip impregnated with a spot of fluorescein in water for 2 hours (Figure S-5), followed by continuously flushing it with water, where no visible change was observed (Movie S1). However, when chloride (200 mM NaCl) was applied as an eluent to the µPADs, the spots were eluted, which confirms the immobilization is based on a simple and reversible ion-exchange mechanism. As a comparison, the same experiment

was performed on devices formed from standard filter paper, and the analyte was observed to elute in water even after a single wash (Figure 1B).

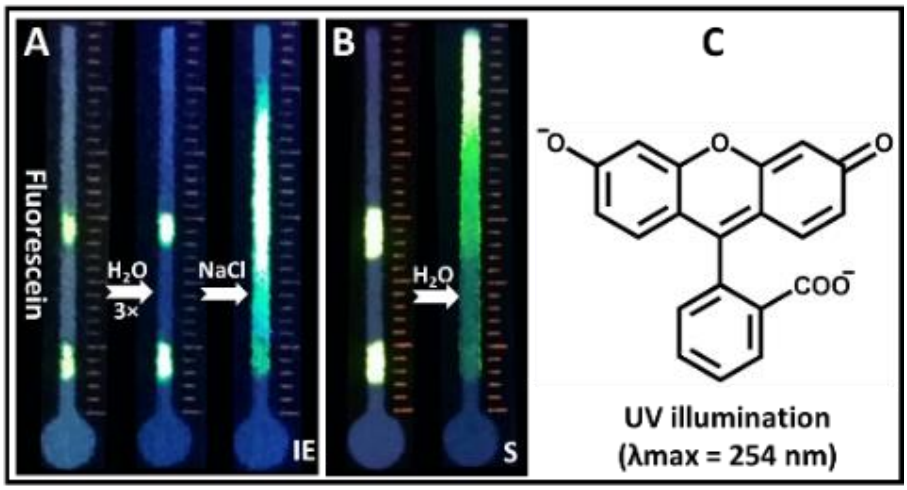

Figure 1. Immobilization test using fluorescein as a model anionic reagent on IE µPAD devices. (A) Representative photographs of fluorescein spots (under UV illumination) on an IE-µPAD device after spotting and drying (left), after rinsing with water (3× 10 µL) (middle) and after rinsing with aqueous NaCl (200 mM, 1× 10 µL) (right). (B) Representative photographs of fluorescein spots (under UV illumination) on a conventional µPAD device after spotting and drying (left) and after rinsing with water (1× 10 µL) (right). (C) The ionized structure of fluorescein comprising two anionic functional groups anchoring the dye on the positively charged IE paper.

The same tests were then applied to another common anionic dye, bromothymol blue (Figure S-6 and Movie S2), which showed the same behavior as fluorescein. Identical tests were applied to other reagents [including arsensazo III, calcein, 2,6-dichlorophenolindophenol (DCPIP), and thymol blue] with a range of different functional groups (Figure S-7), demonstrating the suitability of the IE paper for immobilization of a wide variety of anionic (acidic) reagents. Note that the amount of deposited reagents per unit area (mol/mm^2) in these tests was always negligible compared to the nominal IE capacity reported by the manufacturer (0.017 µmol/mm^2), which consequently provides complete immobilization of the dye molecules [e.g. ~5 pmol/mm^2 for the fluorescein spots in Figure 1 (~2 mm^2)]. The immobilization tests were also carried out with some cationic dyes (results

not shown) such as methylene blue, rhodamine 6G, toluidine blue, neutral red, and nile red where all were retained on both standard (as expected) and IE paper. It is worth noting that cellulose naturally presents a strong affinity to cationic dyes due to various interactions, including electrostatic (via the anionic carboxyl and hydroxyl groups of cellulose fibers), hydrogen bonding (through the amino, azo, and amide groups of the typical cationic dyes), Van der Waals, and hydrophobic [29].

5-4-3- Effect of ionic strength and pH on immobilization

IE effects can be changed by sample properties such as ionic strength and pH; thus, we studied the effects of these variables on the immobilization of indicator dyes. The effect of ionic strength on immobilization was studied by spotting fluorescein (0.1 µL) at the beginning of paper channels in IE-µPADs and then applying aliquots (10 µL) of different concentrations (10-250 mM) of aqueous chloride ion solution. Chloride was chosen for this demonstration, as it is the primary anion present in many biological samples (e.g. ~100 mM in serum). In these experiments, the distance the dye travelled along the channels was considered as the displacement distance [i.e., dye front – 1.5 mm (the initial length of the spot)], which was plotted against the concentration of chloride. As is shown in Figure 2A, there is a strong correlation between chloride concentration and the displacement distance. As shown in the inset images, despite the observed elution, the dye is not completely displaced from its origin, and there is a gradient formed along the channel. This result is useful, as if the reagent is not entirely washed away (with some remaining in the channel), even a gradient of immobilized reagent might be used (upon some tuning) for development of a distance-based assay.

The effect of pH on immobilization was investigated for sample pH effects using methods similar to those described above – i.e., depositing and drying a spot of fluorescein on an IE-

µPADs, followed by delivery of aliquots (10 µL) of different concentrations of HCl or NaOH at a range of different pH (1-13). The displacement distances for each condition were measured and plotted against the pH (Figure 2B). As expected, at high pH (i.e., over 11) the dye was displaced, caused by the titration and deprotonation of the ion-exchange sites (tertiary amine groups) by the sample. For acidic conditions, only pH 1 resulted in displacement, which is likely associated with both the high level of chloride ion (100 mM) present in this (HCl) sample, and also the protonation of the carboxyl group of fluorescein that is involved in the ion-exchange interaction. Note that the lower intensity of the eluted fluorescein band formed along the channel in this experiment is caused by the diminished fluorescence quantum yield (Φ) at low pH [30]. These observations provide a general framework for predicting how the immobilized reagents might be affected in extreme conditions. In addition to the investigated parameters, there might be some other factors playing a role in this context such as the number, pKa, and type of anionic functional groups anchoring the dye molecule on the surface of the IE paper. For instance, as shown in the following section, arsenazo III, which contains six anionic functional groups, is retained upon the paper so securely, that even samples containing high levels of competing anions do not cause elution.

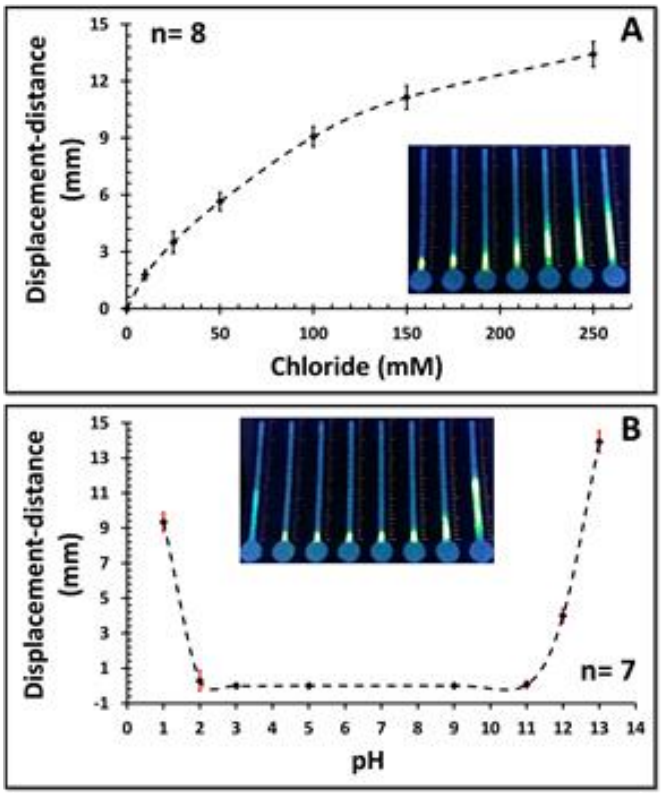

Figure 2. Effect of (A) ionic strength (chloride ion concentration) and (B) pH (1-13) on the immobilization of fluorescein on IE paper. The error bars represent the standard deviations from the average values. Insets are representative photographs (under UV illumination) of µPADs used in these experiments (each image corresponds to a data point on the relevant graph).

5-4-4- Distance-based µPAD assays

As proof of concept, two distance-based assays were developed for implementation on IE-µPADs, for determination of calcium and total acidity. The former (Ca^{2+}) was selected as one of the most prevalent cations in mammals —for example, human serum contains an average [Ca^{2+}] = 2.4 mM. The determination of Ca^{2+} level in serum is important because the deficiency and excessive concentrations are associated with the medical disorders, Hypocalcemia and Hypercalcemia, respectively [30]. Conventional methods for serum Ca2+ measurement (e.g. photometric methods, atomic absorbance spectroscopy, precipitation techniques, etc.) require multiple preparation steps, large volumes of sample and reagent, and/or bulky instrumentation, which limits their suitability for point-of-care analysis. We propose that IE-

µPADs with distance detection of Ca^{2+} offers an instrument-free, low-cost, rapid, and simple alternative that may be appropriate for application at the point-of-care. For distance-based determination of Ca^{2+}, arsensazo III was immobilized upon the IE paper channels. The immobilized dye is purple when not bound to calcium, but becomes blue upon exposure to Ca^{2+} containing sample in the µPADs, as depicted in Scheme 1. After introduction of Ca^{2+} ions, the arsonous and phenolic groups in the dye can complex with Ca^{2+}, while the sulfonate groups (which are not get involved in the complex formation), remain free to keep the dye immobilized. As shown in Figure 3A, this system was useful for distance-based determination of Ca^{2+} in standard solutions of Ca^{2+} (0.03-2.5 mM). The shortest discernible visible colored band formed at the beginning of the detection channel corresponds to 0.03 mM, which is comparable to or better than the limits of detection reported previously for Ca^{2+} in other types of µPADs [32,33].

The second application explored here was motivated by the need for measurements of total or titratable acidity (TA) in the quality assurance of drinks and beverages. TA is the measure of all the various acids present in the sample; however, tartaric acid is the primary acid in grape juices and wines and is often measured as a marker to represent all of the acids that are present. In particular, winemakers strive to maintain a balance between the concentration of acid (normally ~4-10 g/L or ~27-67 mM) and those of other components to reach the desired quality and taste [34]. TA is typically measured by traditional acid-base titrations relying on pH indicators or via digital auto-titrators with potentiometric detection. Here, we introduce distance-based µPADs as an alternative for rapid, simple, and instrument-free at-site measurement of total acidity. This assay relies on immobilized bromothymol blue (BTB) in IE-µPADs. In this case, the IE paper functions not only as an immobilizer, but also as

a titrant for the distance-based acid-base titration within the paper microfluidic channels. Specifically, as illustrated in Figure S-8, BTB is initially anchored on the IE paper via sulfonate and phenolic groups. In this state it is colored blue. After introduction of the acid sample, the phenolic group becomes protonated and is released from the paper; however, the sulfonate group is still bonded to paper allowing formation of a stable yellow-colored band on the paper. In tartaric acid experiments, it was found to be beneficial to cut out the IE-paper in the sample inlets in the µPADs. This has the effect of removing the extra IE groups that react with (titrate) the target acids (anions) present in the sample; this results in higher sensitivities (Figure S-9). As shown in Figure 3B, upon optimization, standard solutions (2.5-150 mM) of tartaric acid were loaded (10 µL) into the sample zone of the µPADs for distance-based signals. The shortest discernible visible colored band formed at the beginning of the detection channel corresponds to 2.5 mM, which is considerably better than the previous report on acid content measurement via µPADs [35]. Note that improved sensitivity for the IE-µPAD should be achievable by pre-acidifying the immobilized BTB reagent, which would result in lowering the basicity of the IE paper, resulting in longer distances.

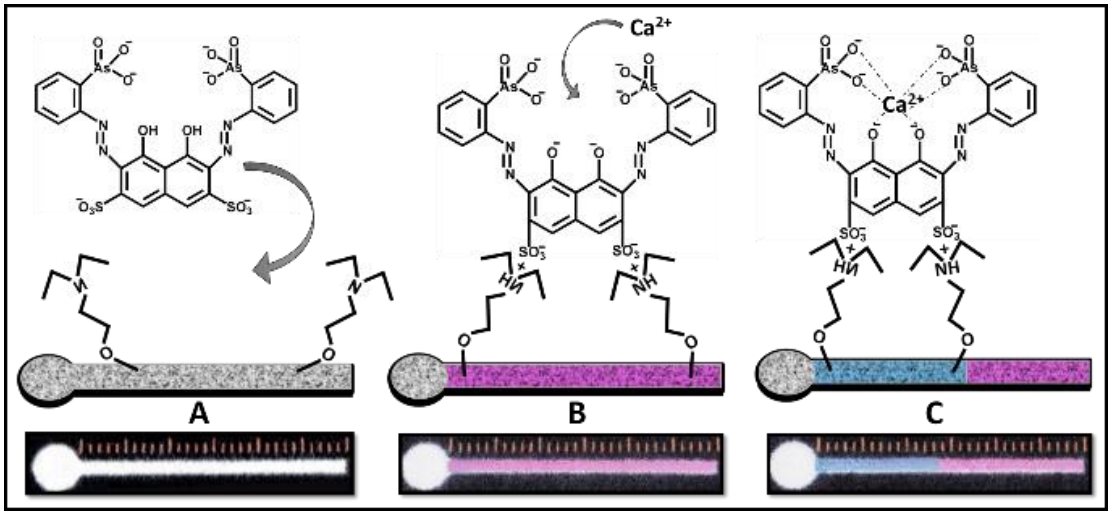

Scheme 1. Mechanism (top) and representative photographs (bottom) of Ca^{2+} assay performed on IE paper. (A) Wax printed IE-µPADs. (B) Non-complexed Arsenazo III (pink) is immobilized in the detection channel via its sulfonate groups (pKa= -2.5 and 0) [36]. (Note that the arsonous and phenolic groups might also be involved in the immobilization (due to the low pKa values35), but they are not shown in this manner for simplicity.) (C) Ca^{2+} containing sample is loaded and wicked from left to right; upon complexation with Arsenazo, the dye appears blue.

After developing IE-µPAD assays for calcium and acid, the tests were applied to determine the total calcium and acid in serum and wine samples, respectively. Specifically, calcium was measured in sheep serum (Quad Five, Ryegate, Mont.) known to contain 2.5 mM Ca^{2+} (according to the vendor, Figure S-10). The serum sample (diluted by water, 10×) was applied (10 µL) on the distance-based µPADs and the concentration of Ca^{2+} was found to be 0.31±0.08 mM (n= 4). The total acid assay was tested with white wine samples (Silver Fox Vineyards, Mariposa County, California), in which 10 µL of the neat sample was loaded into the inlet of µPADs and the total acid was determined to be 52.3±1.36 mM (n= 4). These measurements were consistent (within 10% error) with orthogonal measurements of the same samples using a potentiometric auto-titrator (Metrohm, Titrando 905), with the total acid determined to be 57.6 mM (n=4).

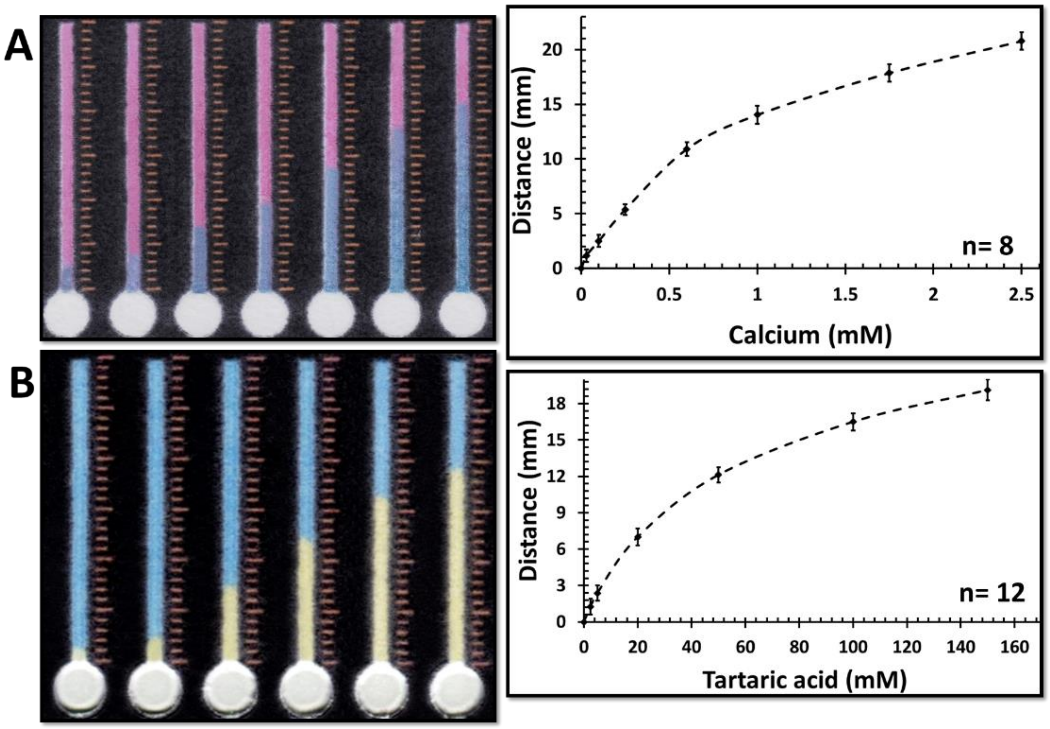

Figure 3. Distance-based measurements on IE-µPADs – left: representative photographs of devices after exposure to standard solutions with increasing concentration of analyte (left-to-right); right: plots of measured distance as a function of concentration. (A) Aqueous solutions of calcium (0.03-2.5 mM) (B) aqueous solutions of tartaric acid (2.5-150 mM). The error bars represent the standard deviations from the average values.

5-5- Conclusions

Herein we report the suitability of using ion-exchange filter paper for immobilizing anionic chromogenic reagents through ion-exchange interactions. The immobilization was demonstrated with various reagents comprising different ionizable (acidic) functional groups. The IE paper shows a similar morphology to standard cellulose paper and is printable using standard techniques used to fabricate µPADs. The effect of pH and ionic strength on the displacement of the immobilized reagents were investigated, providing understanding of the nature of the IE paper used for distance-based assays based on IE immobilization of chromogenic reagents. The immobilization concept was demonstrated by development of distance-based IE-µPADs for instrument-free determination of total calcium (cation) and acid (anion) with reasonable analytical performance. This new immobilization concept extends the

applicability of distance-based detection to a wider range of chemistries and assays by eliminating the necessity for water-insoluble chromogenic reagents or precipitated products. In addition, distance-based IE-µPADs have the potential to be useful for more complex assays. For instance, in future assays, the sample zone might also function as a sample prep zone, separating (filtering out) anionic interferences, resulting in higher sensitivities.

5-6- References

[1] Y. Yang, E. Noviana, M.P. Nguyen, B.J. Geiss, D.S. Dandy, C.S. Henry, Paper-based microfluidic devices: emerging themes and applications, Analytical Chemistry, 89 (2017) 71-91.

[2] K. Yamada, H. Shibata, K. Suzuki, D. Citterio, Toward practical application of paper-based microfluidics for medical diagnostics: state-of-the-art and challenges, Lab on a Chip, 17 (2017) 1206-1249.

[3] S.V. de Freitas, F.R. de Souza, J.C. Rodrigues Neto, G.A. Vasconcelos, P.V. Abdelnur, B.G. Vaz, C.S. Henry, W.K. Coltro, Uncovering the formation of color gradients for glucose colorimetric assays on microfluidic paper-based analytical devices by mass spectrometry imaging, Analytical Chemistry, 90(20) (2018) 11949-11954.

[4] G.G. Morbioli, T. Mazzu-Nascimento, A.M. Stockton, E. Carrilho, Technical aspects and challenges of colorimetric detection with microfluidic paper-based analytical devices (µPADs)-a review, Analytica chimica acta, 970 (2017) 1-22.

[5] L. McCann, T.E. Benavidez, S. Holtsclaw, C.D. Garcia, Addressing the distribution of proteins spotted on µPADs, Analyst, 142 (2017) 3899-3905.

[6] P. De Tarso Garcia, T.M. Garcia Cardoso, C.D. Garcia, E. Carrilho, W.K. Tomazelli Coltro, A handheld stamping process to fabricate microfluidic paper-based analytical devices with chemically modified surface for clinical assays, RSC Advances, 4 (2014) 37637-37644.

[7] E. Evans, E.F. Moreira Gabriel, T.E. Benavidez, W.K. Tomazelli Coltro, C.D. Garcia, Modification of microfluidic paper-based devices with silica nanoparticles, Analyst, 139 (2014) 5560-5567.

[8] A. Kumar, A. Hens, R.K. Arun, M. Chatterjee, K. Mahato, K. Layek, N. Chanda, A paper based microfluidic device for easy detection of uric acid using positively charged gold nanoparticles, Analyst, 140 (2015) 1817-1821.

[9] N. Pourreza, H. Golmohammadi, Application of curcumin nanoparticles in a lab-on-paper device as a simple and green pH probe, Talanta, 131 (2015) 136-141.

[10] F. Figueredo, P.T. Garcia, E. Cortón, W.K.T. Coltro, Enhanced Analytical Performance of Paper Microfluidic Devices by Using Fe3O4 Nanoparticles, MWCNT, and Graphene Oxide, ACS Applied Materials and Interfaces, 8 (2016) 11-15.

[11] X. Zhu, S. Xiong, J. Zhang, X. Zhang, X. Tong, S. Kong, Improving paper-based ELISA performance through covalent immobilization of antibodies, Sensors and Actuators B: Chemical, 255 (2017) 598–604.

[12] J.P. Devadhasan, J. Kim, A Chemically Functionalized Paper-based Microfluidic Platform for Multiplex Heavy Metal Detection, Sensors and Actuators B: Chemical, 273 (2018) 18-24.

[13] D.M. Cate, W. Dungchai, J.C. Cunningham, J. Volckens, C.S. Henry, Simple, distance-based measurement for paper analytical devices, Lab on a Chip - Miniaturisation for Chemistry and Biology, 13 (2013) 2397-2404.

[14] K. Yamada, T.G. Henares, K. Suzuki, D. Citterio, Distance-Based Tear Lactoferrin Assay on Microfluidic Paper Device Using Interfacial Interactions on Surface-Modified Cellulose, ACS Applied Materials and Interfaces, 7 (2015) 24864-24875.

[15] T. Tian, J. Li, Y. Song, L. Zhou, Z. Zhu, C.J. Yang, Distance-based microfluidic quantitative detection methods for point-of-care testing, Lab on a Chip, 16 (2016) 1139-1151.

[16] M. Rahbar, P.N. Nesterenko, B. Paull, M. Macka, Geometrical alignment of multiple fabrication steps for rapid prototyping of microfluidic paper-based analytical devices, Analytical Chemistry, 89 (2017) 11918–11923.

[17] M. Rahbar, P.N. Nesterenko, B. Paull, M. Macka, High-throughput deposition of chemical reagents via pen-plotting technique for microfluidic paper-based analytical devices, Analytica Chimica Acta, 1047 (2019) 115-123.

[18] R.B. Channon, M. Nguyen, A. Scorzelli, E. Henry, J. Volckens, D. Dandy, C. Henry, Rapid Flow in Multilayer Microfluidic Paper-Based Analytical Devices, Lab on a Chip, 18 (2018) 793-802.

[19] D.M. Cate, S.D. Noblitt, J. Volckens, C.S. Henry, Multiplexed paper analytical device for quantification of metals using distance-based detection, Lab on a Chip - Miniaturisation for Chemistry and Biology, 15 (2015) 2808-2818.

[20] X. Wei, T. Tian, S. Jia, Z. Zhu, Y. Ma, J. Sun, Z. Lin, C.J. Yang, Target-responsive DNA hydrogel mediated “stop-flow” microfluidic paper-based analytic device for rapid, portable and visual detection of multiple targets, Analytical Chemistry, 87 (2015) 4275-4282.

[21] X. Wei, T. Tian, S. Jia, Z. Zhu, Y. Ma, J. Sun, Z. Lin, C.J. Yang, Microfluidic Distance Readout Sweet Hydrogel Integrated Paper-Based Analytical Device (μDiSH-PAD) for Visual Quantitative Point-of-Care Testing, Analytical Chemistry, 88 (2016) 2345-2352.

[22] Y. Zhang, D. Gao, J. Fan, J. Nie, S. Le, W. Zhu, J. Yang, J. Li, Naked-eye quantitative aptamer-based assay on paper device, Biosensors and Bioelectronics, 78 (2016) 538-546.

[23] T. Tian, Y. An, Y. Wu, Y. Song, Z. Zhu, C. Yang, Integrated distance-based origami paper analytical device for one-step visualized analysis, ACS Applied Materials and Interfaces, 9 (2017) 30480-30487.

[24] C.W. Quinn, D.M. Cate, D.D. Miller-Lionberg, T. Reilly III, J. Volckens, C.S. Henry, Solid-phase extraction coupled to a paper-based technique for trace copper detection in drinking water, Environmental science & technology, 52 (2018) 3567-3573.

[25] Y. Chen, W. Chu, W. Liu, X. Guo, Distance-based carcinoembryonic antigen assay on microfluidic paper immunodevice, Sensors and Actuators B: Chemical, 260 (2018) 452-459.

[26] M. Rahbar, B. Paull, M. Macka, Instrument-free argentometric determination of chloride via trapezoidal distance-based microfluidic paper devices, Analytica Chimica Acta, 1063 (2019) 1-8.

[27] N. Nuchtavorn, M. Macka, A novel highly flexible, simple, rapid and low-cost fabrication tool for paper-based microfluidic devices (μPADs) using technical drawing pens and in-house formulated aqueous inks, Analytica Chimica Acta, 919 (2016) 70-77.

[28] Hettiarachchy, N. S., Ziegler, G. R. Protein functionality in Food Systems. CRC Press, 1994.

[29] Roberts, J. C., Paper Chemistry. Glasgow and London: Blackie, 1991.

[30] Martin, M. M., Lindqvist, L. J. Lumin., The pH dependence of fluorescein fluorescence, 10 (1975) 381-390.

[31] Rifai, N., Horvath, A. R., Wittwer, C. T. Tietz Textbook of Clinical Chemistry and Molecular Diagnostics. 6th ed.; Elsevier, 2018.

[32] Ostad, M. A., Hajinia, A., Heidari, T. Microchem. J., A novel direct and cost-effective method for fabricating paper-based microfluidic device by commercial eye pencil and its application for determining simultaneous calcium and magnesium 133 (2017) 545-550.

[33] S. Karita, T. Kaneta, Chelate titrations of Ca^{2+} and Mg^{2+} using microfluidic paper-based analytical devices, Analytica Chimica Acta, 924 (2016) 60-67.

[34] Mato, I., Suárez-Luque, S., & Huidobro, A review of the analytical methods to determine organic acids in grape juices and wines, J. F. Food Res. Int. 38 (2005) 1175-1188.

[35] S. Karita, T. Kaneta, Acid-base titrations using microfluidic paper-based analytical devices, Analytical Chemistry, 86 (2014) 12108-12114.

[36] Rowatt, E., Williams, R. J. P., The interaction of cations with the dye arsenazo III Biochemical Journal, 259 (1989) 295-298.

5-7- Supplementary information

5-7-1- Instrumentation

A wax printer (Colorqube 8870, Xerox, Norwalk, CT, USA) was used to print the microfluidic patterns upon the filter papers. A Silhouette CAMEO® 3 desktop craft plotter/cutter (Silhouette America®, Lindon, Utah, USA) along with the Mars® matic 700 technical pens (STAEDTLER Mars GmbH & Co. KG, Nuernberg, Germany, line width = 0.5 mm) were used for deposition of chemical reagents on the detection zones of the distance-based µPADs. Silhouette Studio® (V4.1.479) free software was used to design the µPADs patterns. A UV lamp (Spectroline®, XX-15NF, USA) was used to observe the fluorescence emission developed upon the paper.

5-7-2- Design and Fabrication of µPADs

The µPADs were fabricated according to the previous reports with a few minor changes [1-3]. Briefly, the microfluidic patterns were designed using the Silhouette Studio® and wax printed upon the paper. The distance-based microfluidic design comprised of a circular sample zone (5 mm) and a straight detection channel (30 mm). Scale bars were also printed at 1 mm intervals next to the channels for naked-eye measurement of distance signals. For distance-based µPADs used in total calcium and acid measurements, the corresponding chemical reagents were deposited over the detection channels via the Cameo plotter. Finally, the paper was placed on a hot plate (130 °C- 5 min) to melt the wax and then laminated (80 °C) from both sides.

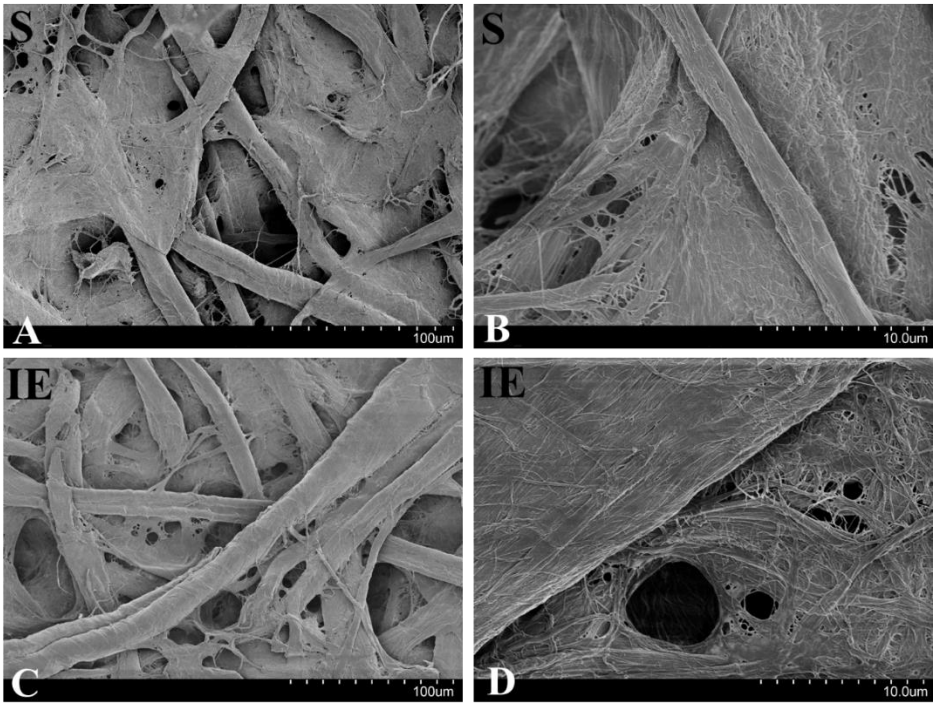

Figure S-1. SEM images of filter papers. (A, B) Standard Whatman paper, grade 1. (C, D) DE81 anion-exchange filter paper.

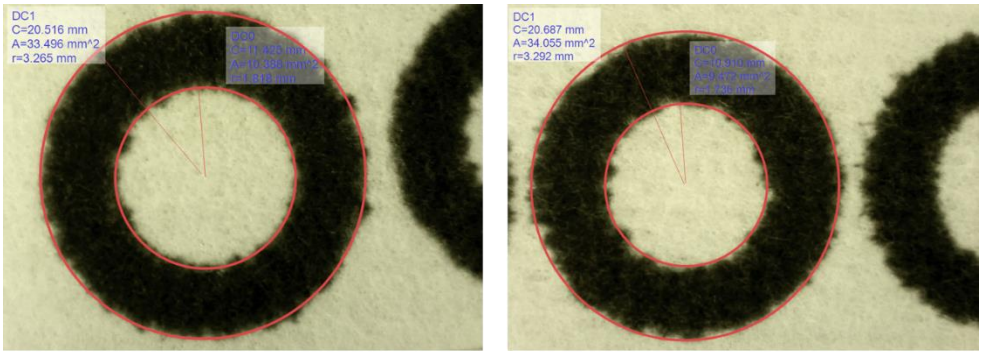

Figure S-2. Printability of IE paper. Circles were wax printed on both standard and IE paper and then after wax melting step (on a hot plate, 130 °C- 5 min), the line width was measured (using Dino-Lite digital microscope) which was found to be almost the same (~1.5 mm) for both types of papers, indicating similar behavior of papers toward the wax printing and melting processes. The wax printed circles on the IE paper were also able to confine the loaded liquids without any leakage.

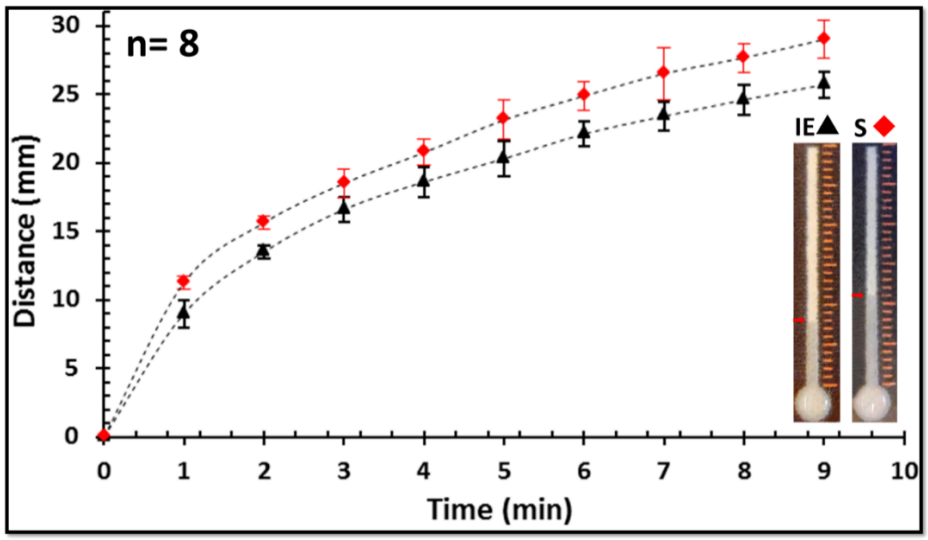

Figure S-3. Comparison of the flow rate between IE (▲) and standard (◆) paper. Water was loaded (10 µL) into the sample inlets of the distance-based µPADs and the sample flow through the microfluidic channels was recorded using a digital camera. Later the solvent front was monitored to measure the flow rate. The error bars represent the standard deviations from the average values. Insets are representative photographs of µPADs used in this experiment.

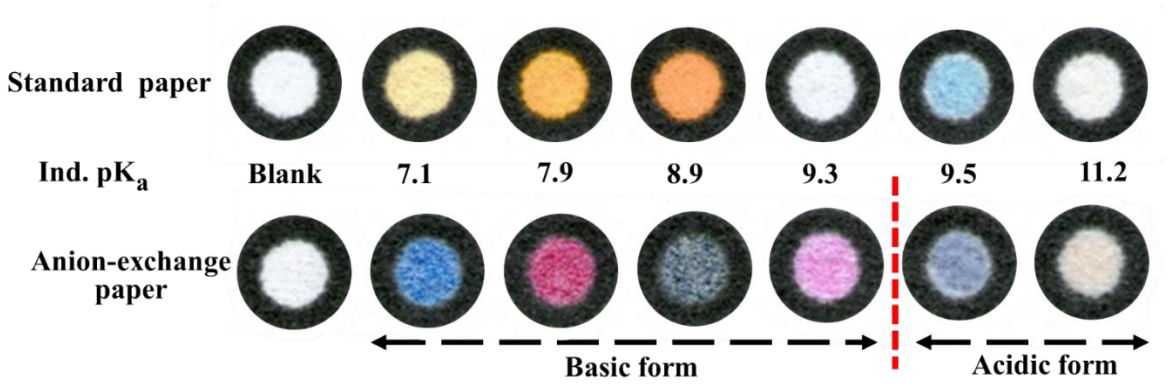

Figure S-4. Determination of the basicity (pKa) of the IE paper. The pH indicators (bromothymol blue (pKa=7.1), phenol red (7.9), thymol blue (8.9), phenolphthalein (9.3), nile blue A (9.5), alizarin yellow (11.2)) were prepared as 0.1% w/v in 20% v/v ethanol. The pH of each solution was adjusted (using NaOH and HCl, 100 mM) to the pKa of that particular indicator in order to provide the highest possible sensitivity to the pH changes. In other words, the pH of the indicator solution was kept exactly on the border of the acidic and basic range, ready to react to the slight changes of pH. The solutions were pipetted (1.5 µL) into the wax-printed wells, and the color change was observed (scanned after 1 min).

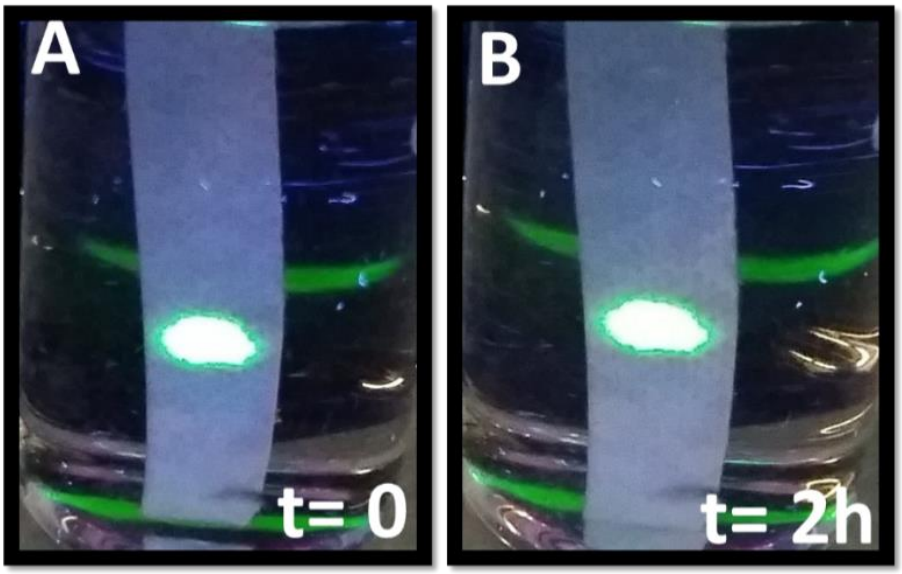

Figure S-5. Immobilization test continued. Fluorescein spot (1 µL- 0.1 mM) on IE paper strip was kept in water for 2h. No elution was observed, and the spot was absolutely intact indicating the strong interaction force between the ionized dye molecule and the IE paper.

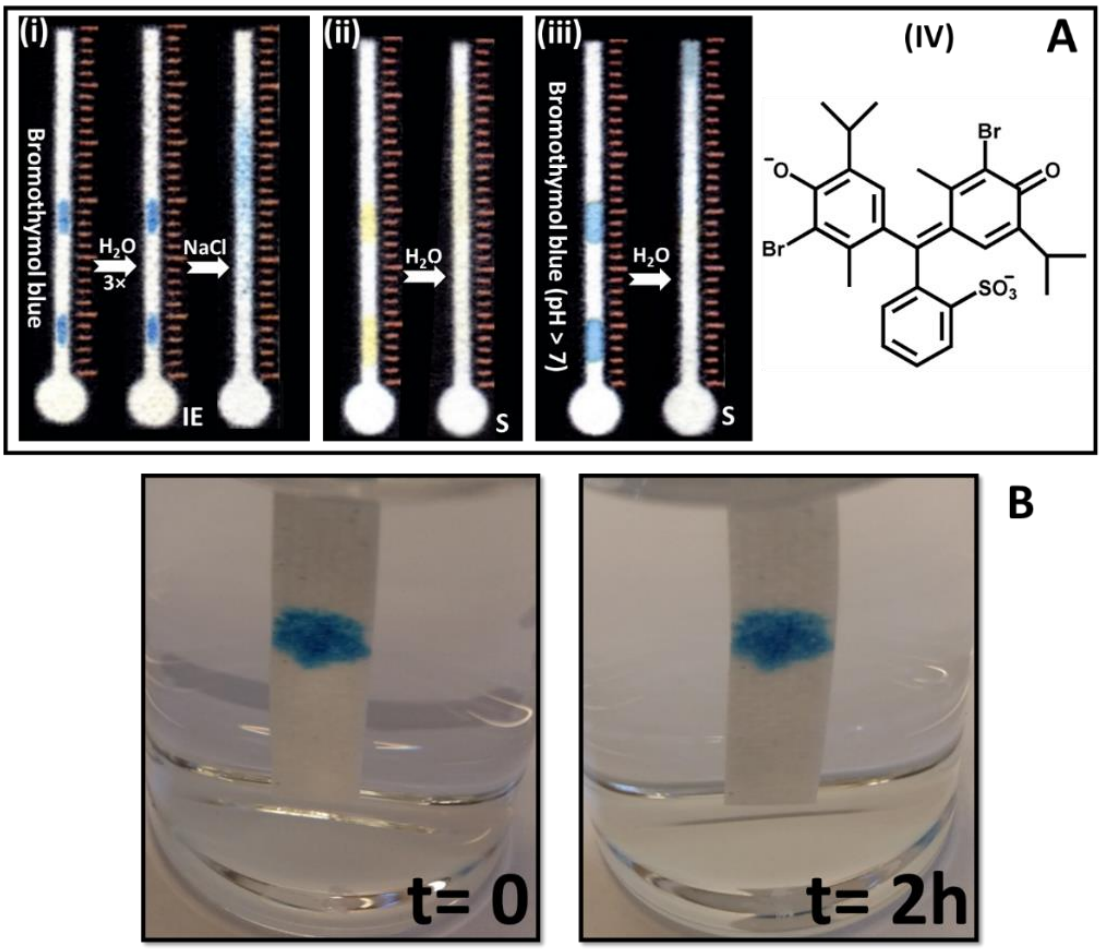

Figure S-6. (A) Immobilization test using bromothymol blue (BTB- 0.1 µL- 0.1% w/v in ethanol 20% v/v) on IE µPAD devices. (i) Representative photographs of BTB spots on an IE-µPAD device after spotting and drying (left), after rinsing with water (3× 10 µL) (middle) and after rinsing with aqueous NaCl (200 mM, 1× 10 µL) (right). (ii) Representative photographs of BTB spots on a conventional µPAD device after spotting and drying (left) and after rinsing with water (1× 10 µL) (right). (iii) Representative photographs of basic form (pH adjusted to 9 using NaOH) of BTB on a conventional µPAD device after spotting and drying (left) and after rinsing with water (1× 10 µL) (right). (IV) The ionized structure of BTB comprising two anionic functional groups anchoring the dye on the positively charged IE paper. (B) IE paper strip were spotted with BTB and kept in water for 2h, indicating strong attraction force between the dye and the paper surface, without any elution happening.

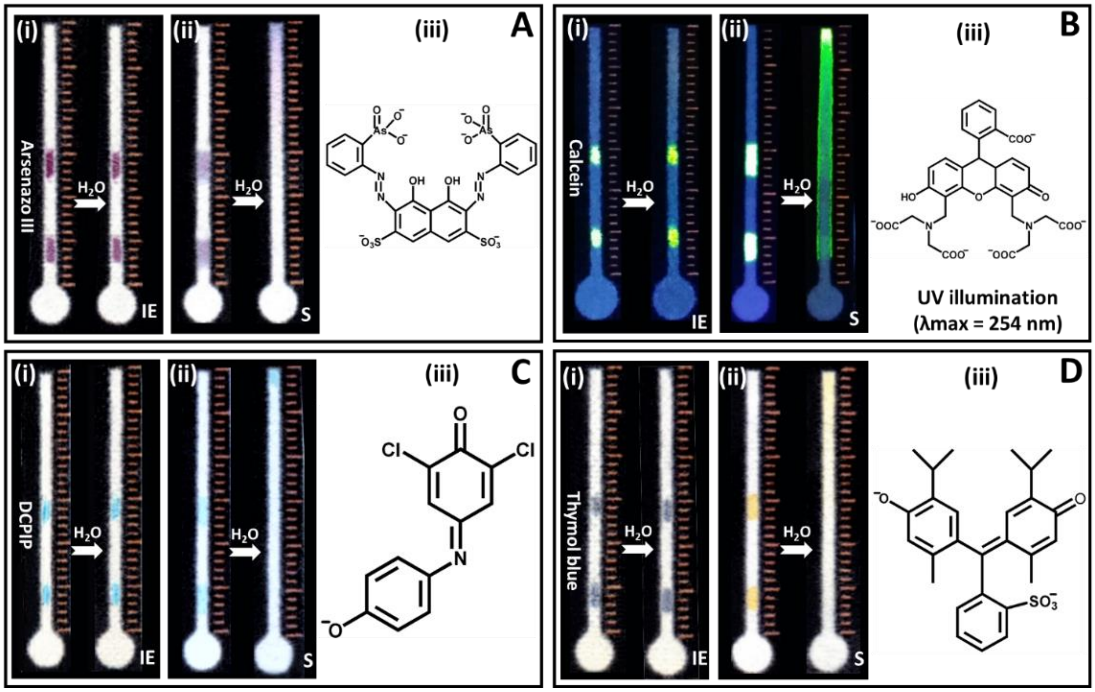

Figure S-7. Immobilization test using (A) Arsensazo III (1 mM in TBE buffer (5×)) (B) Calcein (0.1 mM in water) (C) 2,6-Dichlorophenolindophenol (DCPIP) sodium salt (0.1 mM in water) (D) Thymol blue (0.1% in ethanol 20% v/v) on IE µPAD devices. (i) Representative photographs of spots on an IE-µPAD device after spotting and drying (left), after rinsing with water (3× 10 µL) (right). (ii) Representative photographs of spots on a conventional µPAD device after spotting and drying (left) and after rinsing with water (1× 10 µL) (right). (iii) The ionized structure of dyes comprising anionic functional groups anchoring them on the positively charged IE paper.

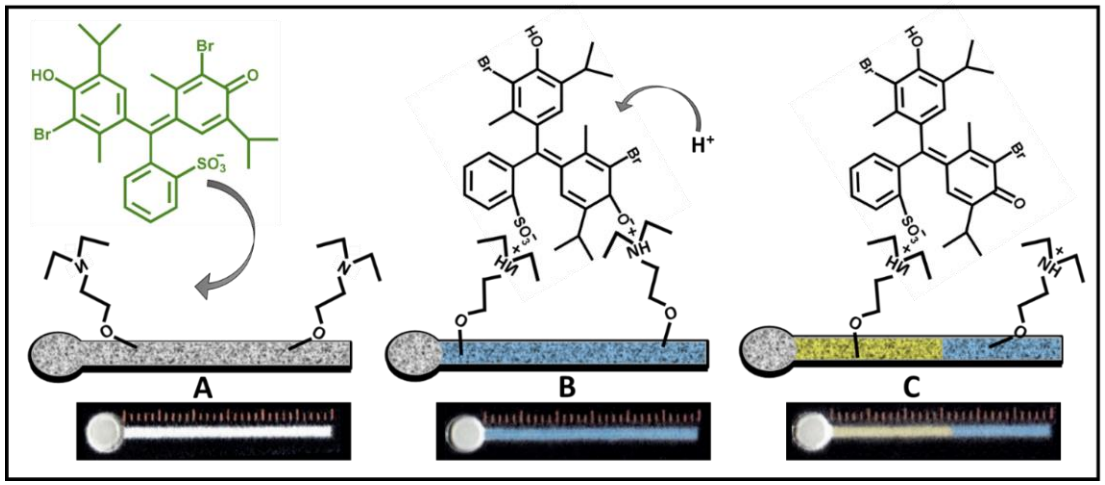

Figure S-8. Mechanism (top) and representative photographs (bottom) of total acid assay performed on IE paper. (A) Wax printed IE-µPADs. (B) Deprotonated bromothymol blue (BTB) (blue) is immobilized in the detection channel via its sulfonate and phenolic groups. (C) Acid containing sample is loaded and wicked from left to right; upon reaction with BTB, the dye protonates and appears blue.

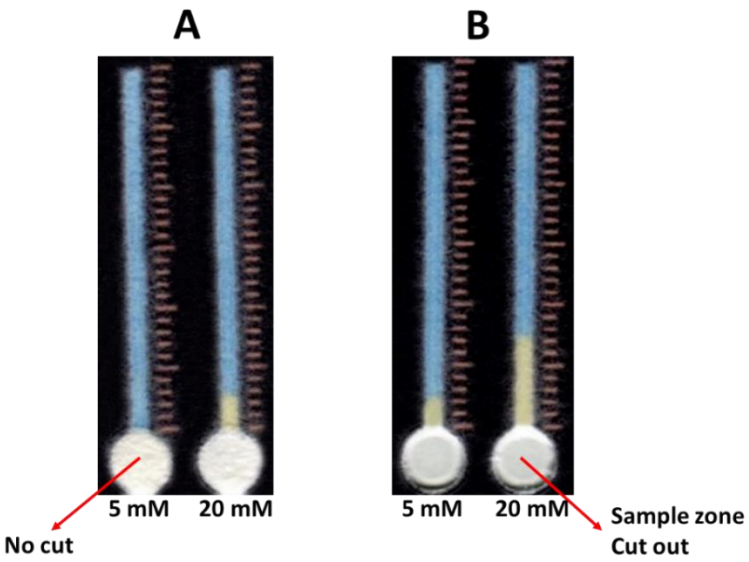

Figure S-9. Effect of sample zone removal on the distance signal obtained in the total acid assay (n= 5). The distance signal for the applied tartaric acid samples with two different concentrations (5 and 20 mM) on the IE-µPADs were A) 0 and 2.31±0.53 mm, sample inlets not cut out (B) 2.37±0.63 and 7.11±0.70 mm, sample inlets cut out. Removing the extra paper (titrant) in the sample zone is basically reducing the amount of titrant available on the IE-µPADs, resulting in longer distance signals (i.e. higher sensitivity).

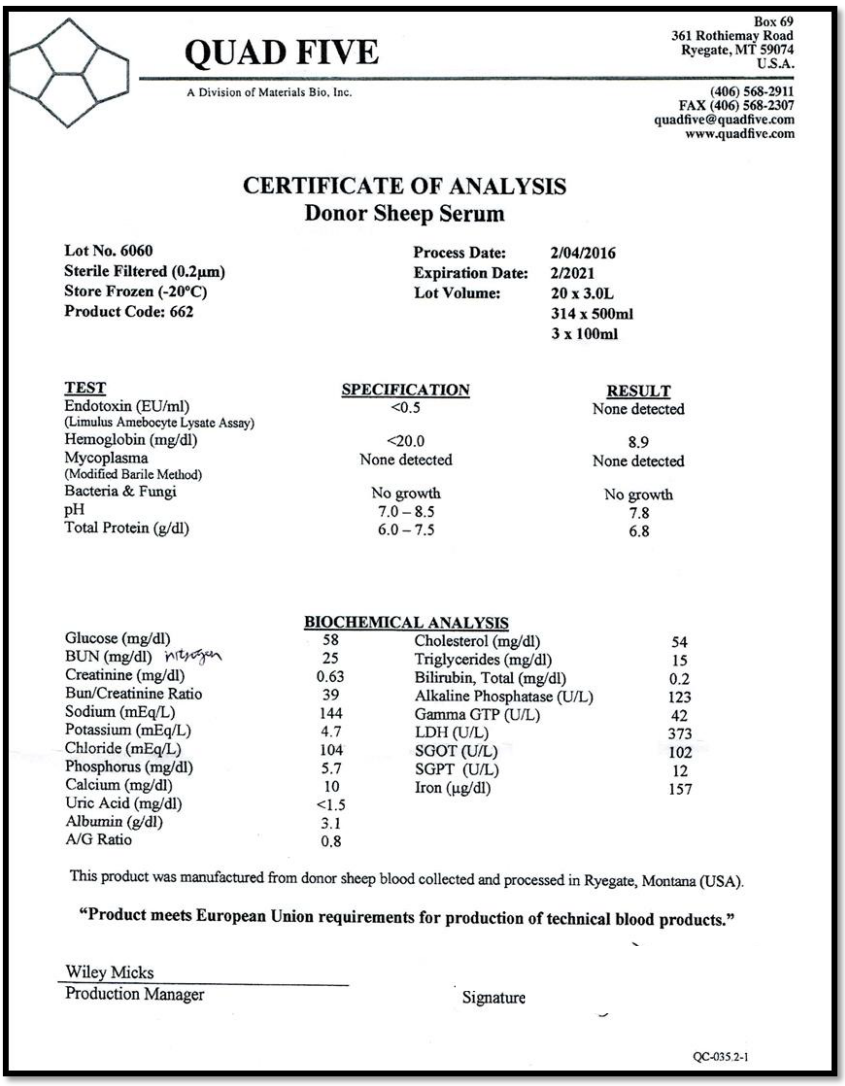

QUAD FIVE

A Division of Materials Bio, Inc.

Box 69
361 Rothiemay Road
Ryegate, MT 59074
U.S.A.

(406) 568-2911
FAX (406) 568-2307
quadfive@quadfive.com
www.quadfive.com

CERTIFICATE OF ANALYSIS
Donor Sheep Serum

Lot No. 6060
Sterile Filtered (0.2µm)
Store Frozen (-20°C)
Product Code: 662

Process Date: **2/04/2016**
Expiration Date: **2/2021**
Lot Volume: **20 x 3.0L**
314 x 500ml
3 x 100ml

TEST	SPECIFICATION	RESULT
Endotoxin (EU/ml) (Limulus Amebocyte Lysate Assay)	<0.5	None detected
Hemoglobin (mg/dl)	<20.0	8.9
Mycoplasma (Modified Barile Method)	None detected	None detected
Bacteria & Fungi	No growth	No growth
pH	7.0 – 8.5	7.8
Total Protein (g/dl)	6.0 – 7.5	6.8

BIOCHEMICAL ANALYSIS

Glucose (mg/dl)	58	Cholesterol (mg/dl)	54
BUN (mg/dl) nitrogen	25	Triglycerides (mg/dl)	15
Creatinine (mg/dl)	0.63	Bilirubin, Total (mg/dl)	0.2
Bun/Creatinine Ratio	39	Alkaline Phosphatase (U/L)	123
Sodium (mEq/L)	144	Gamma GTP (U/L)	42
Potassium (mEq/L)	4.7	LDH (U/L)	373
Chloride (mEq/L)	104	SGOT (U/L)	102
Phosphorus (mg/dl)	5.7	SGPT (U/L)	12
Calcium (mg/dl)	10	Iron (µg/dl)	157
Uric Acid (mg/dl)	<1.5		
Albumin (g/dl)	3.1		
A/G Ratio	0.8		

This product was manufactured from donor sheep blood collected and processed in Ryegate, Montana (USA).

"Product meets European Union requirements for production of technical blood products."

Wiley Micks
Production Manager

Signature

QC-035.2-1

Figure S10. Certificate of analysis of the sheep serum sample used in this work to demonstrate the performance of the IE-µPADs for distance-based determination of calcium.

Movie S-1. Immobilization test: Flushing fluorescein spot (1 µL) with water.

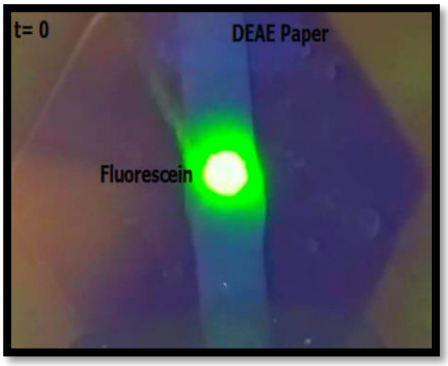

Movie S-2. Immobilization test: Flushing BTB spot (1 µL) with water.

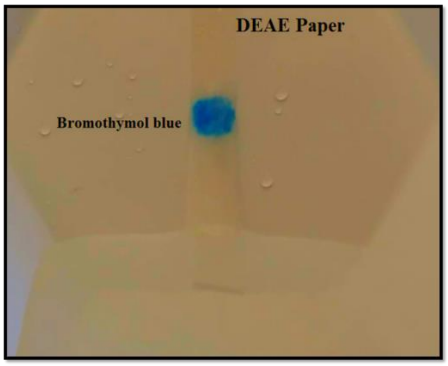

References for the supplementary information

[1] N. Nuchtavorn, M. Macka, A novel highly flexible, simple, rapid and low-cost fabrication tool for paper-based microfluidic devices (µPADs) using technical drawing pens and in-house formulated aqueous inks, Analytica Chimica Acta, 919 (2016) 70-77.

[2] M. Rahbar, P.N. Nesterenko, B. Paull, M. Macka, Geometrical alignment of multiple fabrication steps for rapid prototyping of microfluidic paper-based analytical devices, Analytical Chemistry, 89 (2017) 11918–11923.

[3] M. Rahbar, P.N. Nesterenko, B. Paull, M. Macka, High-throughput deposition of chemical reagents via pen-plotting technique for microfluidic paper-based analytical devices, Analytica Chimica Acta, 1047 (2019) 115-123.

Chapter 6- Concluding Remarks and Future Perspectives

In the past decade, there have been extensive efforts dedicated to the development of microfluidic paper-based analytical devices (µPADs) in order to provide a viable platform for the growing needs of point-of-care biomedical, environmental, food, and water safety monitoring, especially in remote and resource-limited regions. To date, significant progress has been made in making µPADs more practical for the real-time analysis; however, there are still some issues that remain regarding the practicability of µPADs, which hinder their transition from academic research into real-life applications. In particular, the reported techniques for µPAD fabrication still involve some time-consuming manual operating steps, impeding rapid, low-cost, and robust benchtop prototyping of µPADs. The second and third chapter of this thesis addressed this fabrication issue by introducing an integrated approach for facile and high-throughput fabrication of µPADs. This novel fabrication approach used a low-cost desktop electronic craft plotter/cutter coupled with a wax printer for rapid and automated prototyping of µPADs. This enabled the typical cutting and reagent deposition steps involved in fabrication of µPADs, being performed in an aligned manner with the wax printed features. The accuracy and precision of alignment was quantified (in chapter two) indicating the reliability of this technique for robust fabrication of µPADs. Furthermore, the fabricated µPADs using this method was demonstrated several times for determination of various analytes throughout this thesis and in all cases the obtained RSD values were relatively low, indicating the reproducibility of the implemented fabrication process. Chapter three extended this fabrication technique further by investigating the deposition feature of this approach and demonstrating deposition of reagents upon µPADs with various designs (linear and circular forms), while the deposition volume was quantified gravimetrically. This

resolved the issue regarding the uncertainty of the amount of deposited reagents upon paper which can be useful while designing different assays on µPADs.

The other problem restricting µPAD development is the signal interpretation (detection) methods which are mostly based on the digital image colorimetry (DIC), requiring the end-users to capture an image using typically uncalibrated and non-optimized instruments such as smartphones, dependent on a light-controlled environment for reproducible imaging. This makes it complicated to use µPADs for POC applications. However, semi-quantitative readout techniques, such as the distance-based detection method, have been developed to simplify result reading for end-users. The fourth and fifth chapters of this thesis studied the distance-based detection further in order to improve the analytical performance and also the practicability of this detection approach. The effect of device geometry on the performance of distance-based µPADs was investigated in chapter four. A new device geometry (a trapezoidal detection channel) was introduced which improved analytical parameters significantly. This was demonstrated with the instrumentation-free determination of chloride via trapezoidal distance-based µPADs. In chapter five, the immobilization of chromogenic reagents upon paper, was addressed. An anion exchange filter paper was introduced as a new substrate for fabrication of µPADs, allowing immobilization of water-soluble anionic reagents upon the paper surface and preventing the reagents being washed away by the sample fluid flow along the detection channels of distance-based µPADs. This extended the applicability of the distance-based detection method to assays which involved water-soluble anionic chromogenic reagents, which was not doable on the standard filter paper due to the washing away effect.

Overall, this thesis has addressed to some extent the existing challenges facing the current fabrication and detection methods used in the space of µPADs and has made progress in these regards. However, there are still some issues that need to be covered in future investigations. The design of the distance-based µPAD can be further developed in order to provide a more versatile platform for instrument-free determination of more complicated (bio)chemical assays. For example, there might be some extra components added to the typical thermometer shaped distance-based µPADs, which would provide features for required sequential reactions or sample pretreatment steps that need to be done prior to the final detection step. Another limitation of distance-based µPADs is the sampling (pipetting) step where usually a defined volume of sample must be pipetted into the µPADs for reproducible quantitative measurements. But when it comes to real public use, accurate micro-pipetting might not be a feasible sampling approach, so more practical methods need to be introduced to resolve this problem. Stability is considered another serious concern that needs to be taken into account, especially for biological assays, when mass producing µPADs for commercialization purposes. Modification of the paper substrate, implementation of reliable packaging strategies, and treatment of the reagents with compatible preservatives might be some possible solutions, enhancing the shelf life of the µPADs to allow consistent results and long-term use.